SUPRAMOLECULAR HYALURONIC ACID HYDROGEL FIBERS FOR TRANSLATIONAL TISSUE ENGINEERING APPLICATIONS

A Dissertation

Presented to

the faculty at the School of Engineering and Applied Science

University of Virginia

In partial fulfillment

of the requirements for the degree of

Doctor of Philosophy in Chemical Engineering

By

Beverly J. Miller

December 2022

APPROVAL SHEET

This

Dissertation

is submitted in partial fulfillment of the requirements for the degree of

Doctor of Philosophy

Author: Beverly J. Miller

This Dissertation has been read and approved by the examining committee:

Advisor: Steven R. Caliari, PhD

Advisor:

Committee Member: Matthew J. Lazzara, PhD

Committee Member: Rachel A. Letteri, PhD

Committee Member: George J. Christ, PhD

Committee Member: Monique H. Vaughan, MD

Accepted for the School of Engineering and Applied Science:

Jennifer L. West, School of Engineering and Applied Science

December 2022

ABSTRACT

Tissue engineering has emerged as an impactful multidisciplinary field harnessing the expertise of medicine, biology, and engineering to create various tools for fabricating tissue-like constructs. However, when it comes to fibrous tissue injuries, such as volumetric muscle loss (VML) or pelvic organ prolapse (POP), current tissue engineering treatment strategies fail to restore the structural or functional properties required for adequate repair. There is tremendous demand to produce biomaterials, namely hydrogels, capable of mimicking the structure and function of the native tissue microenvironment of fibrous tissues. Hydrogels offer many advantages including biodegradability, easy processing, and minimally invasive delivery along with controllable structural properties that enhance material similarity to the ECM. While there have been significant advancements in the design of hydrogel biomaterials for tissue engineering, there is an unmet need to develop mechanically robust hydrogels mimicking the nanofibrous tissue topography of skeletal muscle, tendon, and ligamental tissue types. To address this need, we have designed a fibrous hydrogel with supramolecular shear-thinning and self-healing mechanical properties that enable injectability for the augmentation of tissue repair following POP and VML injuries.

The following dissertation focuses on the development and characterization of a hydrogel biomaterial system to promote fibrous tissue repair following complex POP and VML injuries. The studies here use hyaluronic acid (HA) scaffolds as this biocompatible and hydrophilic polymer has become increasingly employed as a biomaterial in both clinical and research applications. In Chapter 2, we developed a supramolecularly modified fibrous HA scaffold for fibrous tissue engineering. Through the addition of guest (adamantane) and host (β-cyclodextrin) molecules to electrospun HA fibers, we were able to mimic the native fibrous tissue microenvironment and facilitate cell proliferation and elongation *in vitro* following injectable delivery. Next, Chapter 3 describes the development of the first uterosacral ligament suspension (USLS) model in rodents, thereby addressing an urgent need for biologically relevant animal models related to POP repair. In Chapter 4, we tuned the fibrous hydrogel formulation described in Chapter 2 for augmentation of the USLS procedure developed in Chapter 3. We tracked scaffold degradation *in vivo* and then evaluated functional recovery of the prolapse repair procedure using our recently developed *in situ* mechanical pull-off test. Last, Chapter 5 describes the use of a tibialis anterior (TA) VML model to assess the *in vivo* efficacy of fibrous HA scaffolds following skeletal muscle injury. Scaffolds were administered to the surgically created defect site with the functional recovery of the injured muscle assessed via maximal force production over time. Altogether, these studies present a fibrous hydrogel biomaterial platform with great potential to improve regenerative outcomes following POP, VML, and other fibrous tissue injuries.

ACKNOWLEDGEMENTS

First, I would like to thank my PI, Steven Caliari. I feel very fortunate to have been part of his lab these last five and a half years as he provided me with the opportunity to succeed and become a more independent scientist. His encouragement allowed for the collaboration between our lab and clinician Monique Vaughan and the following women's health research that pushed the boundaries of the types of human health challenges that our lab addressed. I am very proud of the resulting women's health research that we accomplished and would like to acknowledge that none of it would have been possible without Steven's support.

Thank you also to all the members of the Caliari lab who I have had the privilege of working with. I would like to particularly thank Erica Hui for her steadfast leadership as the most senior lab member throughout my time, Jenna Sumey for sanity coffee breaks, and Mackenzie Grubb for the mountain get aways. Also, Audrey Hansrisuk and Austin Amacher for agreeing to work with me and for pushing me both as a mentor and a scientist. You both brought such great energy to the lab and it made it easier to come to work each day. Last, I would like to thank Kelly Bukovic, Leilani Astrab, James Gentry, Geshani Bandara, Ryann Boudreau and all others in the Caliari lab for always having my back, providing great lab entertainment, helping me troubleshoot experiments, providing feedback on research and conference talks, loving food as much as I do, and creating a welcoming and safe space to work. The people of the Caliari lab, and honorary lab member Greg Grewal, have had such a positive impact on my time at UVA and I cannot thank you all enough.

Next, I would like to specifically thank urogynecological surgeon Dr. Monique Vaughan. Starting with a cold email in 2019, Monique has been an invaluable addition to my committee and to the research team. Her clinical expertise and hand-on assistance in the lab made the women's health content in this dissertation possible. Beyond her expert knowledge, she has been incredibly encouraging and has been a wonderful mentor to have in the latter half of my PhD journey. I know I am incredibly lucky to have had support from both Steven and Monique throughout this journey.

I was also fortunate to be mentored by many other talented scientists here at UVA. Rachel Letteri, George Christ, and Matt Lazzara as part of my committee have all provided impactful guidance and expertise to support me during this process. Additionally, I would like to thank both Kyle Lampe and Chris Highley who were always willing to listen and through our encounters have provided meaningful support in my time at UVA. Last, I would like to thank Barry Hinton from the department to Biology as his encouragement and expertise in reproductive biology allowed me to attend the Frontiers in Reproduction course in 2019.

Beyond UVA, I would like to thank the other fantastic scientists who have contributed to my journey. All the faculty and staff from the Frontiers in Reproduction course, along with the brilliant scientists of my cohort, were so welcoming and provided a thorough introduction into the field of reproductive biology. Next, Ariella Shikanov from the University of Michigan and Michelle Oyen from Washington University in St. Louis were both incredibly generous with their time and helping me navigate the interdisciplinary space of bioengineering for women's health. Last, Kyoko

Yoshida and Samantha Zambuto for their enthusiasm, willingness to share about their own engineering and women's health journeys, and ongoing friendship.

Outside of the time spent in lab, there was dancing, travel, and time outdoors thanks to my wonderful friends. My friends from UVA, Saringi Agata and Ashley Conley, were my go-to people to discuss all the woes of earning a PhD, while my friends outside of the university provided a space to forget about work for a while. From undergrad, Calder Dorn and Justine Feist, have always cheered me on and encouraged silly Portland adventures. And in Cville, I am truly thankful for Gabby Marolf and Nate Glenister who have always opened their home to me and made me feel cared for. Likewise, I am thankful for Macee Feeser, Chelsea Chambers, Will Stowe, Catie Payne, Morgan Hatfield, Shawn Clement, Jeff McDougal, Addie McMurty, Hudson Smith and others around Charlottesville who have made the East Coast feel like home. Thank you for showing me new places, the fun at Fridays after five, taking me camping and hiking, introducing me to new music and local concert venues, and for many fun game nights. I am so grateful to have everyone in my life and I am excited for all our future shenanigans.

In addition to my amazing friends, I need to thank my partner, Wiley, and his amazing family for their support over the years. Ever since junior year of undergrad, Wiley's parents Joyce and Wes have been a boon in my life. From big group dinners to providing a comforting space to relax and recoup after hard months, I am thankful for their open arms and open hearts. Also, the cousins, long time family friends, aunts, uncles, and grandparents who have all been so welcoming and supportive of both my and Wiley's grad school endeavors. And of course, Wiley, thank you for being my emotional support human from the end of undergrad all the way through grad school. Thank you for encouraging me when therapy was hard or when my research caused a mental breakdown. Between the countless plane rides, dinner dates, hiking and camping trips, and international travel that has kept us close throughout grad school, I am deeply grateful to have you in my life and I look forward to all our adventures to come.

Finally, I would like to thank my family for their love and support in all my endeavors. My sisters, Anna and Desiree, who have simultaneously been excellent role models and now wonderful friends in my life. My brother, Glenn, for his companionship both growing up and as roommates at Oregon State. I am thankful to have such a competitive and fun brother to both confide in and to go out dancing with. Next, I would like to thank my parents for their wisdom and support for me whatever challenge came my way. Last, I would like to thank my grandparents, my aunts, uncles, and cousins for continuing to encourage and support me through life. Overall, I am grateful to have a wonderful family that I can rely on and celebrate hard earned milestones with.

LIST OF SYMBOLS AND ABBREVIATIONS

Abbreviations	Term
2D	2 dimensional
3D	3 dimensional
Ad	Adamantane
ANOVA	Analysis of Variance
BOP	Benzotriazole-1-yloxytris-(dimethylamino)
C2C12s	Mouse myoblast cells
CD	β-cyclodextrin
DI	Deionized
E	Elastic modulus
ECM	Extracellular matrix
EDL	Extensor digitorum longus
EHL	Extensor hallucis longus
G’	Storage modulus
G”	Loss modulus
HA	Hyaluronic acid
HA-TBA	Hyaluronic acid *tert*-butyl ammonium salt
hMSCs	Human mesenchymal stromal cells
LAP	Lithium acylphosphinate
MALDI	Matrix-assisted laser desorption/ionization
MMP	Matrix metalloproteinases
NIH	National institutes of health
NorHA	Norbornene modified hyaluronic acid
NR	No repair
PBS	Phosphate buffered saline
POP	Pelvic organ prolapse
SD	Standard deviation
SEM	Scanning electron microscopy
TA	Tibialis anterior
USLS	Uterosacral ligament suspension
UV	Ultraviolet
UVA	University of Virginia
VML	Volumetric Muscle Loss

TABLE OF CONTENTS

CHAPTER 1: INTRODUCTION

1.1 Overview

Tissue engineering has emerged as an impactful multidisciplinary field harnessing the expertise of medicine, biology, and engineering to create various tools for fabricating tissue-like constructs (Mao & Mooney, 2015; Tamayol et al., 2013). Construct design takes into consideration the physiological environment including the structural, physical, and topographical features of native tissue (Khademhosseini et al., 2009). These tissue-like engineered scaffolds, or biomaterials, are broadly used to replace diseased and damaged tissue with the potential to be used for diagnostic and therapeutic research as well. Recently, there has been a growing interest in investigating new treatment options for fibrous tissue types, such as skeletal muscle (Kwee & Mooney, 2017; Mertens et al., 2013; Pollot & Corona, 2016), tendon (Chainani et al., 2013), and ligament (Kuo et al., 2010; Lim et al., 2019), due to the low success rates of current therapeutics. Engineered biomaterials, especially hydrogels (Caliari & Burdick, 2016; Slaughter et al., 2009), offer a promising platform for developing alternative treatment options for fibrous tissue damage. This dissertation focuses on the design and implementation of tunable fibrous hyaluronic acid (HA) hydrogels for the augmentation of fibrous tissue repair. In this section, the benefits of using hydrogels in tissue engineering will be discussed as well as design strategies specific to fibrous tissue types. Next, current treatment options for pelvic organ prolapse (POP) and volumetric muscle loss (VML) injuries will be discussed in addition to the shortcomings of current treatment methods for pelvic floor ligaments and skeletal muscle, respectively. Overall, this dissertation focuses on the gaps in clinical treatment options for POP and VML and how biomaterials can be leveraged (i.e., designed, characterized, and administered) to augment fibrous tissue repair.

1.2 Tissue engineered biomaterials for fibrous tissue repair

Scaffold design has historically focused on recapitulating the biochemical cues present in native tissue (Caliari et al., 2016; Tibbitt & Anseth, 2009), but increasing evidence illustrates the importance of also capturing the dynamic biophysical features of the three-dimensional extracellular matrix (ECM) when designing tissue-like materials (B. M. Baker et al., 2015; Davidson et al., 2019; Engler et al., 2006). Complexity in tissue-like material design only intensifies as tissue heterogeneity creates site-specific biochemical and biophysical cues unique to each tissue type, creating constantly shifting environmental cues for the resident cells (Rose & De Laporte, 2018; Wade & Burdick, 2012; Wolf & Kumar, 2019). In addition to the cellular scale, the ECM facilitates hierarchical tissue organization where cell-matrix interactions maintain homeostasis in healthy conditions or initiate an inflammatory feedback loop in wound healing conditions (Kuo & Tuan, 2003; Mahdy, 2019; C. J. Mann et al., 2011). Innovative approaches have emerged to improve engineered materials for non-fibrous tissues, but approaches for skeletal muscle, tendon, and ligament have lagged. Here, we discuss aspects of designing biomaterials, particularly hydrogels, for fibrous tissue applications.

1.2.1 ECM mimicking scaffolds for fibrous tissue types

From an engineering standpoint, the fibrous tissues of the body, such as skeletal muscle, tendons, and ligaments, have key functional similarities stemming from similar biomechanical properties (Kuo et al., 2010). These tissues experience complex loading during even simple everyday activities and therefore biomaterial mechanical integrity is of great interest to tissue engineers. Additionally, stiffness in tissues varies between homeostasis and wound healing (Cosgrove et al., 2016) therefore changing how the tissue experiences stress and strain. However, increased understanding of the contributions of the fibrous architecture in guiding tissue function of fibrous tissues has motivated researchers to create scaffolds with increased structural complexity (Vasita & Katti, 2006; Wade, Bassin, Rodell, et al., 2015; Wade & Burdick, 2012) in addition to matching tissue stiffness. The fibrous nature of the ECM in these tissues optimize the mechanical force transmission essential for locomotion and are composed of several fibrous proteins such as collagen and elastin (Frantz et al., 2010; Hynes, 2009; Theocharis et al., 2016). Therefore, functional tissue engineering for fibrous tissue repair, especially in the cases where surgical reconstruction or replacement grafts are required, call for a combination of approaches to address these complex injuries (Woo et al., 2007). Together, these studies demonstrate the importance of adjusting mechanical features of the biomaterial design when fibrous tissues are the target tissue niche. Biomaterials systems for fibrous tissue repair can be synthesized from a range of natural and synthetic polymers, many of which have been reviewed extensively elsewhere (Alshomer et al., 2018; Beldjilali-Labro et al., 2018; Kuo et al., 2010; Kwee & Mooney, 2017; J. Liu et al., 2018). The work in this dissertation will focus on hyaluronic acid (HA) systems as they are highly versatile and can exhibit a wide range of physical, chemical, and biological properties such as biocompatibility, mechanical integrity, and degradability (Highley et al., 2016; Katti et al., 2008; Prestwich et al., 2000).

1.2.2 Polymeric hydrogels

Materials that can recapitulate features of the native ECM, particularly hydrogels, are attractive for their ability to mimic tissue-like properties such as high water content and soft tissue mechanics (Caliari & Burdick, 2016; Place et al., 2009; Wade & Burdick, 2012). Hydrogels are one of the most prominent and versatile classes of biomaterials due to their ability to mimic many characteristics of native tissues (Caliari & Burdick, 2016; Kyburz & Anseth, 2015; Spicer, 2020). Mechanical properties of these highly hydrated scaffolds are readily tunable via polymer backbone, degree of crosslinking, and the types of crosslinks. Many natural polymers, such as HA, collagen, or alginate, are popular for tissue engineering applications due to their inherent bioactivity and support of cell outcomes such as cell viability and proliferation (Highley et al., 2015; Rodell et al., 2013). Building on this, studies investigating the impact of hydrogels with a fibrous architecture have demonstrated an increase in local adhesion ligand density (B. M. Baker et al., 2015) and cell spreading (Matera et al., 2019) compared to non-fibrous scaffolds. Moreover, in studies where HA hydrogels matched the mechanical stiffness of native fibrous tissue, the cultured cells exhibited self-renewal *in vitro* and *de novo* tissue formation *in vivo* (Gilbert et al., 2010). In terms of creating a fibrous scaffold using these hydrogel systems, electrospinning has

become a popular technique to fabricate nanofibers mimicking tissue-scale structures (Doostmohammadi et al., 2020; B. Miller et al., 2021; Tamayol et al., 2013). Electrospinning has been widely adapted for manufacturing biomimetic nanoscale fibrous structure for tissue engineering applications(Lim et al., 2019; X. Zhang et al., 2021) with self-assembling peptide fibers an alternative to creating the fibrous topography (Eskandari et al., 2017; Rajagopal & Schneider, 2004). However, fibrous hydrogels made using peptides suffer from poor long term mechanical properties, reducing their ability to provide the ideal scaffold microenvironment. Therefore, the ability of HA hydrogels to mimic the architecture and mechanical stiffness of fibrous tissue show their great potential for tissue engineering for fibrous tissue applications.

1.2.3 Injectable materials

In addition to recreating the ECM biophysical cues, such as stiffness and fibrous architecture, there is increasing interest in developing engineered materials amenable to injectable delivery (Raucci et al., 2020). Clinically, these materials are capable of minimally invasive delivery and offer major advantages such as reduced patient discomfort and treatment cost (Loebel et al., 2017; Yu & Ding, 2008). To this end, materials are either designed to polymerize *in situ* or engineered to be shear-thinning, which is defined as the ability of a material to decrease in viscosity with increasing shear (often applied during an injection) (M. H. Chen et al., 2017) In designs where materials rely on the shear-thinning and self-healing mechanisms to achieve injectability, secondary crosslinking may be necessary to achieve the desired level of mechanical stability (Ouyang et al., 2016). Guest-host supramolecular chemistries are attractive for hydrogel design due to their ability to support the shear-thinning and self-healing behavior while also allowing careful tuning of mechanical properties through both primary and secondary cross-linking mechanisms (Rodell et al., 2013, 2015). Beyond the delivery mechanism, tunability is especially important since the final hydrogel must be tailored to each fibrous tissue for optimal outcomes. Ultimately, the ideal tissue engineered material is one that maximizes tissue-like properties while satisfying clinical needs for delivery.

1.3 Clinical significance of fibrous tissue injuries

Injuries that impact the musculoskeletal system impose a significant burden to society and the economy (Lim et al., 2019). Surgical repair via primary suture of autologous transfer techniques are considered the gold standard modality of care following injury (Alshomer et al., 2018; Corona et al., 2015; Lim et al., 2019; Pollot & Corona, 2016). However, surgical repair is not always successful and leads to further complications as is the case in pelvic organ prolapse (POP) and volumetric muscle loss (VML) repair attempts. Shortcomings in POP treatment are largely unknown as the female pelvic floor is an understudied region of the body (Ashton-Miller & DeLancey, 2007) while deficiencies in VML treatment stem from the non-uniform size and shape as well as the sheer magnitude of the soft tissue damage inflicted (Corona et al., 2015; Owens et al., 2007). Both examples highlight the need for improved treatment options for fibrous tissue types that can address the limitations of current technology.

1.3.1 Pelvic organ prolapse

The female pelvic floor, made up of levator ani muscles, uterosacral ligaments (USLs) and cardinal ligaments, supports the abdominal organs such as the uterus, bladder, and rectum (Herschorn, 2004). Failure of the pelvic floor leads to the descent of the pelvic organs beyond their normal position in the peritoneal cavity and is referred to as pelvic organ prolapse(NIH Office of Women's Health, 2016). The compromised state of the anatomical structures leads to bothersome symptoms of vaginal bulge or pressure, bowel, bladder, and sexual dysfunction, and overall reduced quality of life (B. J. Miller et al., 2022). Despite the fact that roughly 50% of parous women (Samuelsson et al., 1999) will experience some loss of pelvic floor integrity over their lifetime, treatment options with successful outcomes are lacking. One common native tissue (suture only) repair surgery is the uterosacral ligament suspension (USLS) procedure, but it suffers from a failure rate of up to 40% (Jelovsek et al., 2018; Lavelle et al., 2016). Exacerbating this issue, prior to the work in chapter 3 of this dissertation, no small animal model for uterosacral ligament suspension existed. Without animal models specific to prolapse repair, researchers have utilized hernia repair models to investigate materials for the pelvic floor (Whooley et al., 2020; Yuan et al., 2021), ultimately leading to the misconception that materials compatible with the abdominal wall are suitable for use in the pelvic floor. After the unacceptable outcomes in humans following implantation of polypropylene mesh in the pelvic floor (*FDA takes action to protect women's health, orders manufacturers of surgical mesh intended for transvaginal repair of pelvic organ prolapse to stop selling all devices*, 2019), approved from hernia mesh studies, it became clear that current models are poor predictors of pelvic outcomes. Therefore, there is a strong clinical need for materials to be investigated for prolapse treatment within the tissues of pelvic floor.

1.3.2 Volumetric muscle loss

Skeletal muscle is a highly dynamic tissue that continuously adapts and remodels in response to external stimuli in an effort to maintain homeostasis and support daily function (Frontera & Ochala, 2015). The tissue is made up of individual muscle fibers organized in such a way to achieve effective force transfer from the fibers to the surrounding ECM and ultimately to the skeletal system to enable movement (Järvinen et al., 2005). Minor injuries such as small muscle tears are within the body's capabilities of repair, but larger muscle injuries trigger scar tissue formation and ultimately a loss of function due to diminished mass (C. J. Mann et al., 2011). Large muscle defects in the case of VML injuries compromise the body's inherent regenerative capacity which results in permanent physical impairment (Corona et al., 2015). While most common among military populations, VML also affects the civilian population as VML injuries typically arise from high energy traumas such as gun shots, blast injuries, or car accidents (Corona et al., 2015). Available treatment options include autologous muscle transfer (Owens et al., 2007), but they are largely ineffective therefore demonstrating a clear need to improve therapeutic options for VML repair (Bursac et al., 2015). Using established animal models (Basurto et al., 2021; Mintz et al., 2016; Pollot & Corona, 2016), ongoing efforts investigate new materials to augment VML repair yet complete recovery of skeletal muscle function to preinjury levels remains a challenge.

Therefore, there is a clinical need for continued material investigation that continue to explore biomaterial design for the repair of VML injuries.

1.4 Research objectives

Overall, the goal of this dissertation was to create a tunable fibrous biomaterial platform capable of modifications to accommodate the augmentation of multiple fibrous tissue types. In chapter 2, we aimed to inform therapeutic design by elucidating the role that hydrogel fibers play in cell viability post injection as well as cell proliferation and elongation. For chapter 3, we designed a USLS model in multiparous female rats to address the lack of accessible animal models in the investigation of pelvic organ prolapse surgical techniques. Chapter 4 explores the efficacy of a fibrous injectable hydrogel scaffold in restoring pelvic floor mechanical integrity via augmentation of the USLS procedure. In chapter 5, we mimicked skeletal muscle fibrous organization by designing a hydrogel system encapsulating hydrogel fibers for the treatment of VML. Finally, chapter 6 provides a summary of the presented work and discusses areas of future research to expand upon our findings. Altogether, this work describes both a novel hydrogel platform and corresponding animal model in the investigation of therapeutics for USLS augmentation, and generally should inform subsequent future biomaterial design for POP and VML repair.

CHAPTER 2: GUEST-HOST SUPRAMOLECULAR ASSEMBLY OF INJECTABLE HYDROGEL NANOFIBERS FOR CELL ENCAPSULATION

This chapter has been adapted from the following publication: Miller, B., Hansrisuk, A., Highley, C.B., Caliari, S.R. *Guest-host supramolecular assembly of injectable hydrogel nanofibers for cell encapsulation*. *ACS Biomater. Sci. Eng.* **2021**.

2.1 Abstract

The fibrous architecture of the extracellular matrix (ECM) is recognized as an integral regulator of cell function. However, there is an unmet need to develop mechanically robust biomaterials mimicking nanofibrous tissue topography that are also injectable to enable minimally invasive delivery. In this study we have developed a fibrous hydrogel composed of supramolecularly-assembled hyaluronic acid (HA) nanofibers that exhibits mechanical integrity, shear-thinning, rapid self-healing, and cytocompatibility. HA was modified with methacrylates to permit fiber photocrosslinking following electrospinning, and either 'guest' adamantane or 'host' β-cyclodextrin groups to guide supramolecular fiber assembly. Analysis of fibrous hydrogel rheological properties showed that the mixed guest-host fibrous hydrogel was more mechanically robust (6.6 ± 2.0 kPa, storage modulus (G′)) than unmixed guest hydrogel fibers (1.0 ± 0.1 kPa) or host hydrogel fibers (1.1 ± 0.1 kPa) separately. The reversible nature of the guest-host interactions also allowed for shear-thinning and self-healing behavior as demonstrated by cyclic deformation testing. Human mesenchymal stromal cells (hMSCs) encapsulated in fibrous hydrogels demonstrated satisfactory viability following injection and after seven days of culture (> 85%). Encapsulated hMSCs were more spread and elongated when cultured in viscoelastic guest-host hydrogels compared to non-fibrous elastic controls, with hMSCs also showing significantly decreased circularity in fibrous guest-host hydrogels compared to non-fibrous guest-host hydrogels. Together, these data highlight the potential of this injectable fibrous hydrogel platform for cell and tissue engineering applications requiring minimally invasive delivery.

2.2 Introduction

The extracellular matrix (ECM) is a complex three-dimensional (3D) microenvironment that provides mechanical support, protection, and regulatory signals to embedded cells (Frantz et al., 2010; Rosso et al., 2004). Hydrogels are widely used to mimic native ECM due to their ability to exhibit tissue-like properties, including viscoelastic mechanics and high water content comparable to the tissues they are intended to model and replace (Caliari & Burdick, 2016; Courtney et al., 2006; K. Y. Lee & Mooney, 2001). In the context of tissue engineering, there is growing appreciation for the importance of the fibrillar architecture of ECM and its role in providing biophysical cues that regulate cell behavior (Pathak & Kumar, 2011; Pedersen & Swartz, 2005; Rose & De Laporte, 2018; Vasita & Katti, 2006). There is significant interest in robust 3D hydrogels that can mimic the fibrous networks present in many musculoskeletal tissues while allowing tuning of network biophysical and biochemical properties (Alberts et al., 2002; Fu et al., 2018; Hinderer et al., 2016; Tibbitt & Anseth, 2009). A popular method of forming mechanically robust fibrous materials is electrospinning, a simple, scalable, and cost-effective technique that produces nanofibers with tunable physicochemical properties (Christopherson et al., 2009; Greiner & Wendorff, 2007; W.-J. Li et al., 2006; Teo & Ramakrishna, 2006). Electrospinning has also garnered interest due to its ability to produce nanofibers, typically using synthetic polymers (Grewal & Highley, 2021; Lutolf & Hubbell, 2005), with topography similar to collagen and elastin fibrils within the native ECM (Burdick & Prestwich, 2011; Highley et al., 2016; Scott, 1995; X. Zhang et al., 2021).

Currently, much of our understanding of how cells interact with fibrous microenvironments stems from two-dimensional (2D) culture studies of cells seeded atop electrospun fibers. Importantly, recent work has demonstrated that human mesenchymal stromal cells (hMSCs) cultured on electrospun synthetic fibers recapitulate many of the behaviors observed when cells are cultured in natural matrices like collagen, in contrast to observations of cells grown on synthetic hydrogels (B. M. Baker et al., 2015). A separate study using a naturally-derived fibrous collagen platform showed similar results, demonstrating that hMSCs grown on more compliant collagen fibers were able to remodel their surroundings more easily, leading to increased spreading and focal adhesion organization (Xie et al., 2017). While these studies were critical in establishing the importance of including fibrous architectural cues in biomimetic cell culture models, cell behavior in 3D microenvironments can depart dramatically from 2D culture formats. While these studies were critical in establishing the importance of including fibrous architectural cues in biomimetic cell culture models, cell behavior in 3D microenvironments can depart dramatically from 2D culture formats (B. M. Baker & Chen, 2012; Tibbitt & Anseth, 2009). To that end, recent findings demonstrated that the inclusion of embedded nanofibers in 3D hydrogels drives increased cell spreading and nuclear localization of the mechanoregulatory transcriptional coactivator Yes-associated protein (YAP) (Matera et al., 2019). Further, a study utilizing multifunctional peptide-based assemblies to form mechanically robust and hierarchically-structured hydrogels found that matrices with longer fibrils promoted hMSC morphologies similar to those in native collagen

environments (Hilderbrand et al., 2020). This growing body of work underscores the importance of integrating fibrous structural signals into biomaterial design.

While recreating ECM biophysical cues, such as fibrous architecture, has been a focus of the tissue engineering community in recent years (Matellan & del Rıó Hernández, 2019), interest in developing injectable (shear-thinning and self-healing) or *in situ* gelling materials has intensified for both clinical (including drug delivery (J. Li & Mooney, 2016) and tissue engineering (Dimatteo et al., 2018) with minimally invasive delivery) and additive manufacturing (3D-printing (Jammalamadaka & Tappa, 2018)) applications. Clinically, injectable materials offer major advantages such as reduced patient discomfort and treatment cost (Loebel et al., 2017; Yu & Ding, 2008). Recent advancements in synthetic chemistry and materials science have provided researchers with a library of techniques to create injectable biomaterials (Dimatteo et al., 2018). Injectable strategies include the use of ionically crosslinked materials (Park et al., 2014), jammed particles (Highley et al., 2019; Riley et al., 2019), supramolecular polymeric materials (J. L. Mann et al., 2017), and materials that gel *in situ* via thermoresponsive (Tang et al., 2019) or pH-responsive (Hu et al., 2020) self-assembly. Guest-host supramolecular chemistries are attractive for injectable hydrogel design due to their ability to support shear-thinning and self-healing behavior while also allowing careful tuning of viscoelastic mechanical properties through both primary and secondary crosslinking mechanisms (Rodell et al., 2013, 2015). Guest-host assembled hydrogels are also suitable cell carriers for injectable delivery since their non-Newtonian properties help protect cells from excessive shear during needle extrusion (Gaffey et al., 2015). However, achieving fibrillar topographies in mechanically robust injectable hydrogels remains challenging. While self-assembling peptides can serve as injectable nanofibrous hydrogels (Rajagopal & Schneider, 2004), these materials are often limited by poor long-term mechanical properties (Caliari & Burdick, 2016; Pedersen & Swartz, 2005). Electrospun hydrogel materials, as described earlier, show robust mechanics and support biomimetic cellular behaviors. However, electrospun scaffolds typically require physical implantation and are not amenable to injectable delivery (Khorshidi et al., 2016; Wade & Burdick, 2012).

To address the need for a fibrous hydrogel system amenable to minimally invasive delivery, we have combined strategies in biomanufacturing, supramolecular chemistry, and tissue engineering to produce a mechanically robust injectable fibrous hydrogel capable of supporting cell encapsulation. The engineering design brings together hyaluronic acid (HA) electrospun hydrogel nanofibers, functionalized with either guest (adamantane, Ad) or host (β-cyclodextrin, CD) supramolecular moieties, that when joined together create a shear-thinning and self-healing hydrogel fiber network via guest-host complexation. HA was utilized for its amenability to functionalization with reactive groups enabling both photocrosslinking and guest-host assembly as well as its decades-long record of clinical use as a naturally-derived biopolymer (Burdick & Prestwich, 2011). In this work we assessed the architecture of the fabricated hydrogel nanofibers, their rheological properties, and their ability to support sustained cell viability following injection.

2.3 Materials and methods

Materials: Sodium hyaluronate (sodium HA, 64 kDa) was purchased from Lifecore Biosciences. β-cyclodextrin (CD), hexamethylenediamine (HDA), ammonium chloride, and p-Toluenesulfonyl chloride were purchased from TCI America. Tetrabutylammonium hydroxide (TBA-OH) was purchased from Acros Organics. All other materials were purchased from Sigma-Aldrich.

Synthesis of β-CD-HDA: Synthesis of 6-(6-aminohexyl)amino-6-deoxy-β-cyclodextrin (β-CD-HDA) was performed as previously described (Loebel et al., 2017; Rodell et al., 2013) first via synthesis of the intermediate 6-o-monotosyl-6-deoxy-β-cyclodextrin (CD-Tos) using β-cyclodextrin (β-CD) and p-toluenesulfonyl chloride (TosCl). Briefly, β-CD was suspended in water and cooled to 0°C. TosCl was dissolved in minimal acetonitrile and added dropwise. After stirring at room temperature for 2 h, sodium hydroxide was added dropwise. The reaction was stirred at room temperature for 30 min before the addition of solid ammonium chloride to obtain a pH of 8.5. The solution was cooled on ice and the precipitate collected. The CD-Tos product was washed first with cold deionized (DI) water and then cold acetone before being dried under vacuum. After product confirmation using ^{1}H NMR (500 MHz Varian Inova 500), a round bottom flask was charged with the CD-Tos, HDA, and dimethyl formamide (DMF). The reaction vessel was purged with nitrogen and then the reaction was allowed to proceed with constant nitrogen flow at 80°C for 18 h. The product was precipitated in cold acetone (5 × 50 mL/g CD-Tos), washed thrice with cold diethyl ether, and dried. The degree of modification was determined by ^{1}H NMR.

Synthesis of Ad-MeHA and CD-MeHA: Methacrylate modification of the HA backbone was achieved via methacrylate esterification with the primary hydroxyl group of sodium HA at basic pH (Highley et al., 2015; Smeds & Grinstaff, 2001). The degree of methacrylate modification was controlled by the amount of methacrylic anhydride introduced during synthesis and was determined to be 28% of the HA disaccharides via ^{1}H NMR (Figure S2.1). Next, the methacrylated HA (MeHA) was reacted with proton exchange resin and titrated with TBA-OH to yield methacrylated hyaluronic acid tert-butyl ammonium salt (MeHA-TBA) as previously described (Loebel et al., 2017) (Figure S2.2). Next, Ad-modified MeHA (Ad-MeHA) and β-CD-modified MeHA (CD-MeHA) were synthesized (Highley et al., 2015) by anhydrous coupling. Ad-MeHA was prepared using 1-adamantane acetic acid via di-tert-butyl bicarbonate (BOC_2O)/4-dimethylaminopyridine (DMAP) esterification while CD-MeHA was prepared using CD-HDA via (benzotriazol-1-yloxy) tris(dimethylamino) phosphonium hexafluorophosphate (BOP) amidation. Products were dialyzed against DI water and degree of modification was determined using ^{1}H NMR. Esterification of MeHA with 1-adamantane acetic acid resulted in 43% adamantane modification (by ^{1}H-NMR, Figure S2.3) while coupling β-CD-HDA to MeHA via amidation resulted in 26% of the HA disaccharides modified with β-cyclodextrin (by ^{1}H-NMR, Figure S2.4).

Electrospinning: Ad-MeHA, or CD-MeHA, was dissolved at 2% (w/v) in DI water along with 3.5% (w/v) poly(ethylene oxide) (PEO, 900 kDa) and 0.05% (w/v) Irgacure 2959 (I2959) for 24-48 h prior to electrospinning. The polymer solutions were electrospun using a Spraybase (Kildare, Ireland) collection plate set-up and using the following collection parameters: applied voltage: 9.5-

10.5 kV, distance from needle to collector: 16 cm, needle gauge: 20, flow rate: 0.4 mL h^{-1}. Hydrogel nanofibers were deposited onto foil covering the collector plate, placed into a container which was purged with nitrogen, and crosslinked with UV light (365 nm) for 15 minutes. Electrospinning parameters were chosen based on previous work with MeHA (Sundararaghavan & Burdick, 2011) and CD-MeHA (Highley et al., 2014).

Nanofiber imaging and morphological characterization: To measure the diameters of the Ad-MeHA and CD-MeHA fibers, samples were electrospun onto foil. After electrospinning, samples were photocrosslinked and analyzed in both dry and swollen states. Dry fibers were imaged using scanning electron microscopy (SEM, FEI Quanta 650) at a magnification of 10,000x. To visualize swollen fibers, a methacrylated rhodamine dye (MeRho, Polysciences, 2 mM) was incorporated prior to electrospinning. Rhodamine-labeled fibers were hydrated, and broken up via trituration through increasingly smaller needle gauges (16G-30G) before encapsulation in a 2% (w/v) MeHA hydrogel to facilitate image analysis. Fibers were encapsulated at 0.2% (w/v) for hydrated fiber diameter quantification and at 0.05% (w/v) for post-trituration fiber length quantification. The hydrated fibers were allowed to equilibrate within the MeHA hydrogels overnight in PBS before being imaged using confocal microscopy (Leica inverted confocal microscope, DMi8). Fiber diameters (n = 300 fibers per group) and fiber lengths (n = 90) were quantified from the resulting SEM (dry fibers) and confocal images (hydrated fibers) using ImageJ (NIH). The corresponding violin plots were made using R. The fiber mass swelling ratio Q_M for the Ad-MeHA and the CD-MeHA hydrogel fibers was calculated using the equation:

$$Q_M = \frac{M_w - M_d}{M_d} \qquad \text{Equation 2.1}$$

where M_W is the fiber wet mass and M_D is the fiber dry mass. Swelling ratios were measured in triplicate for each fiber type.

Hydrogel formulations: Collected guest Ad-MeHA and host CD-MeHA fibers were hydrated (0.1% w/v in DI water) overnight at 37°C to remove PEO from the electrospinning process (Ji et al., 2006), centrifuged, supernatant discarded, and then lyophilized. Once dry, the fibers were again hydrated at 0.1% w/v in DI water, allowed to swell at 37°C for at least 2 hours, and then passed through needles of progressively smaller gauge sizes via trituration. Starting with a 16G needle and progressing up to a 30G needle, the fibers were passed through the needles until the fiber solution could easily pass through the needle. This process separated any adjoined fibers and resulted in a reproducible fiber suspension. Fiber density was calculated as the weight percentage of the dry fiber mass per volume solvent (w/v). When determining the volume, the dry fibers were first hydrated in a known volume of DI water and allowed to swell overnight. Hydrated fibers were then centrifuged to remove excess liquid. Finally, water was added back to the hydrated fibers to achieve the desired w/v density (Matera et al., 2019). For mechanical testing, the complementary guest and host hydrogel fibers were gently mixed directly on the rheology plate to create the mixed fibrous guest-host network. Non-fibrous MeHA and guest-host (Ad-MeHA/CD-MeHA) hydrogel groups were prepared as 3% (w/v) solutions and underwent covalent crosslinking (for mechanical

stabilization) via photopolymerization in the presence of UV light (365 nm, 10 mW cm^{-2}) and 1 mM lithium acylphosphinate (LAP) photoinitiator for 5 min. LAP was used as the photoinitiator for cell culture studies due to its ability to facilitate increased polymerization rates under cytocompatible longer wavelength (365-405 nm) light, even at lower intensities, when compared to I2959 (Fairbanks et al., 2009). However, since dense electrospinning solutions take 1-2 days to homogenize (and since cells are not present in electrospinning), it is advantageous to use the less efficient photoinitiator I2959 to prevent solution gelation prior to electrospinning.

Rheology: All rheological measurements were performed on an Anton Paar MCR 302 rheometer with the plate temperature set at 37°C. The non-fibrous MeHA and guest-host hydrogels were characterized using a cone-plate geometry (25 mm diameter, 0.5°, 25 μm gap) immediately following photopolymerization while guest-host fibrous hydrogels were characterized using a parallel-plate geometry (25 mm diameter, 25 μm gap). Mechanical properties for the non-fibrous MeHA and guest-host hydrogel groups were tested using oscillatory frequency sweeps (0.1−10 Hz, 0.5% strain). Fibrous guest-host hydrogels mechanical properties were tested using oscillatory frequency sweeps (also 0.1−10 Hz, 0.5% strain), strain sweeps, and cyclic deformation tests alternating between 0.5% and 250% strain to assess shear-thinning and self-healing capabilities (Rodell et al., 2013).

Cell culture: Human mesenchymal stromal cells (hMSCs, Lonza) were used at passage 7 for all experiments. Culture media contained Gibco minimum essential medium (MEM-α) supplemented with 20 v/v% fetal bovine serum (Gibco) and 1 v/v% penicillin/streptomycin/amphotericin B (1000 U/mL, 1000 μg/mL, and 0.25 μg/ mL final concentrations, respectively, Gibco). Prior to cell encapsulation, all materials were modified with thiolated RGD peptide (GCGYGRGDSPG, Genscript) via Michael-type addition in 0.2 M triethanolamine at pH 8, dialyzed against DI water, and then lyophilized. The final RGD concentration was 1 mM for all hydrogel formulations used for cell culture. After materials were put into solution (non-fibrous MeHA and guest-host hydrogels) or hydrated (guest-host fibers), the materials were sterilized using germicidal UV irradiation for 3 h. Prior to the addition of cells, guest-host fibers were centrifuged briefly, with excess liquid aspirated under sterile conditions. To evaluate cell protection during injection under needle flow, hMSCs were added to the non-fibrous hydrogels or hydrogel fibers such that the final encapsulation density was 1 x 10^6 cells/mL. Prior to UV exposure, materials with cells were loaded into 1 mL tuberculin syringes and hydrogels were injected through a 16G needle at 12 mL h^{-1} using a syringe pump. The extruded material was used to make hydrogel plugs with identical volumes of 40 μL. All groups were subjected to 5 min UV polymerization post-injection to ensure that differences in cell viability were not due to UV cytotoxicity. For all cell culture experiments, media was replaced every 2-3 days.

Confocal imaging and analysis: Cell viability was assessed with a LIVE/DEAD assay kit (Invitrogen) by incubating hydrogels at 37°C for 30 min with 2 mM calcein-AM and 4 mM ethidium homodimer-1 in PBS plus glucose (G-PBS, glucose 25 mM) followed by three PBS washes. Cells were imaged using a Leica DMi8 inverted confocal microscope and live/dead cells

were quantified from 50 μm thick z-stacks (10 μm slices) using ImageJ's 3D object counter tool. Cell projected area, cell shape index (CSI), and aspect ratio were determined using ImageJ's measurement tool. CSI determines the circularity of the cell, where a line and a circle have CSI values of 0 and 1, respectively, and was calculated using the formula $CSI = \frac{4\pi A}{P^2}$ where A is the cell projected area and P is the cell perimeter. Individual measurements were made for 60 cells from at least 6 hydrogels per experimental group.

Statistical Analysis: All experimental groups included at least 6 hydrogels for analysis of cell viability and shape. Cell viability and shape data were statistically analyzed using one-way analysis of variance (ANOVA) followed by Tukey's HSD post-hoc testing. These statistical analyses were conducted using GraphPad Prism 9.0 and R. P values < 0.05 were considered statistically significant. For analysis of hydrogel rheological properties, 3 hydrogels were tested per group where the mean values are plotted. Bar graph heights correspond to the mean with standard deviation error bars and individual data points are included as scatter plots overlaying the bars. Tukey box plots of individual cell data show the second and third quartiles as boxes, the median as a line between the boxes, and error bars with the lower value of either 1.5 times the interquartile range or the maximum/minimum value. Data points outside this range are shown individually.

2.4 Results and discussion

2.4.1. Guest-host hydrogel fiber design, synthesis, and quantification of fiber properties.

In this study, we report the design, synthesis, and characterization of a self-assembling guest-host fibrous hydrogel that can serve as a cell carrier for injectable tissue engineering applications. Hydrophobic Ad (guest) groups associate strongly with the hydrophobic core of CD (host) molecules resulting in a stable, yet reversible, guest-host interaction (association constant, $K_a = 1 \times 10^5\ M^{-1}$) (G. Chen & Jiang, 2011) (**Figure 2.1**). Ad and CD moieties were separately coupled to methacrylate-modified HA (MeHA) (Burdick et al., 2005), forming Ad-MeHA and CD-MeHA (Highley et al., 2014) respectively (**Figure 2.1A**). Methacrylate modification of the HA backbone enables covalent photocrosslinking of the electrospun hydrogel nanofibers in the presence of photoinitiator via UV light-mediated radical polymerization. Following photocrosslinking, the stabilized polymeric fibers will imbibe water upon hydration rather than dissolving (Highley et al., 2014; Wade, Bassin, Gramlich, et al., 2015), creating a water-swollen hydrogel fiber structure. When the hydrated guest and host fibers are mixed, we hypothesized that the complementary nanofibers would associate via hydrophobic supramolecular interactions to form a mechanically robust 3D fibrous hydrogel (**Figure 2.1D**) capable of shear-thinning and self-healing. The supramolecularly-assembled fibers can create a hierarchical assembly that provide physical cues to cells at different length scales, mimicking the 3D cues provided by the native fibrous ECM. Additionally, the hydrogel design enables the facile addition of ligands, such as cell adhesion peptides, creating the potential to capture and modulate multiple features of native ECM in addition to biophysical cues.

To create the electrospun hydrogel nanofibers capable of supramolecular assembly, Ad-MeHA and CD-MeHA (2% w/v) aqueous polymer solutions were mixed separately with poly(ethylene oxide) (PEO) and the photoinitiator Irgacure 2959 (I2959), and then electrospun to produce guest and host fiber populations (**Figure 2.1C**). Addition of the photoinitiator allowed for subsequent stabilization of the fibers by UV light-mediated radical crosslinking of methacrylates while PEO was included as a bioinert carrier polymer. As a carrier polymer, PEO aids in the electrospinning process by making the solution more viscous, thereby disrupting the relatively high surface tension and inducing chain entanglements of the low molecular weight HA solution (Ji et al., 2006). Crosslinked hydrogel nanofibers were examined in their dry state via scanning electron microscopy (SEM, **Figure 2.2A**) and in their hydrated form via confocal microscopy (**Figure 2.2B**). Dry Ad-MeHA nanofibers had an average diameter of 234 ± 64 nm while the average dry CD-MeHA fiber diameter was 171 ± 64 nm. Upon hydration, the hydrophilic nanofibers imbibe water, resulting in significant fiber swelling and increased diameter. The hydrated Ad-MeHA nanofibers swelled to an average diameter of 2.16 ± 0.92 μm and hydrated CD-MeHA nanofibers swelled to an average diameter of 1.65 ± 0.54 μm. SEM analysis of native fibrous ECMs has reported fibril diameters in the range of 75-400 nm (Abrams et al., 2000; Bancelin et al., 2014) with small type I collagen fibers in the 1-5 μm range (Ushiki, 2002). Therefore, these CD-MeHA and Ad-MeHA hydrogel nanofibers are within the physiologically relevant range for fibrous ECM components (Greiner & Wendorff, 2007).

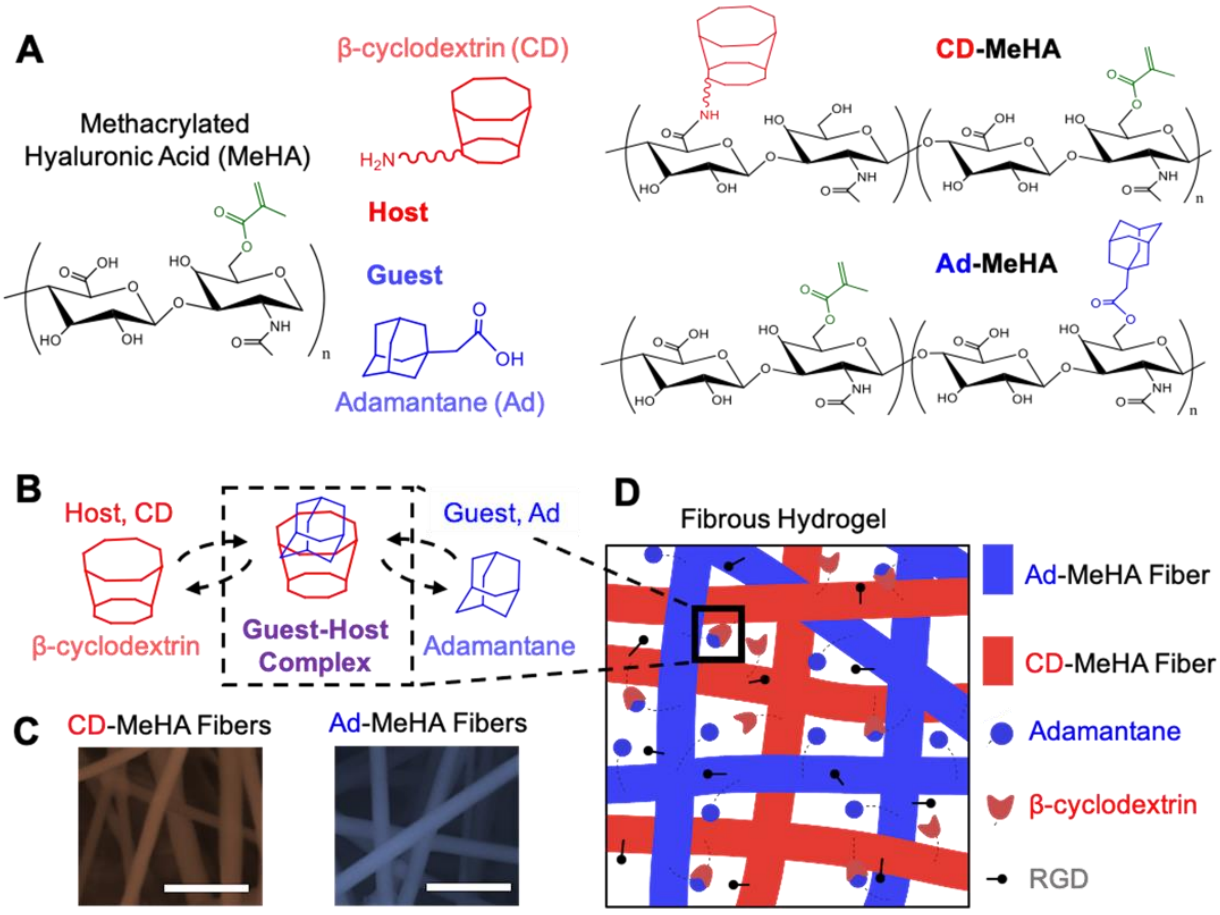

Figure 2.1. Guest-host supramolecular design to make injectable fibrous hydrogels. A) Structures of guest (Ad-MeHA) and host (CD-MeHA) macromers. The methacrylates enable photocrosslinking to stabilize the fiber structure following electrospinning while B) interaction of β-cyclodextrin (CD, host) and adamantane (Ad, guest) groups forms a reversible guest-host inclusion complex to enable shear-thinning and self-healing. C) SEM of host (CD-MeHA) and guest (Ad-MeHA) electrospun fibers prior to hydration and hydrogel formation. Scale bars = 1 μm. D) Schematic of the fibrous hydrogel composed of mixed guest and host fibers decorated with RGD to permit integrin-mediated cell adhesion. The interactions between Ad and CD on complementary fibers result in assembly of a macroscale fibrous hydrogel scaffold.

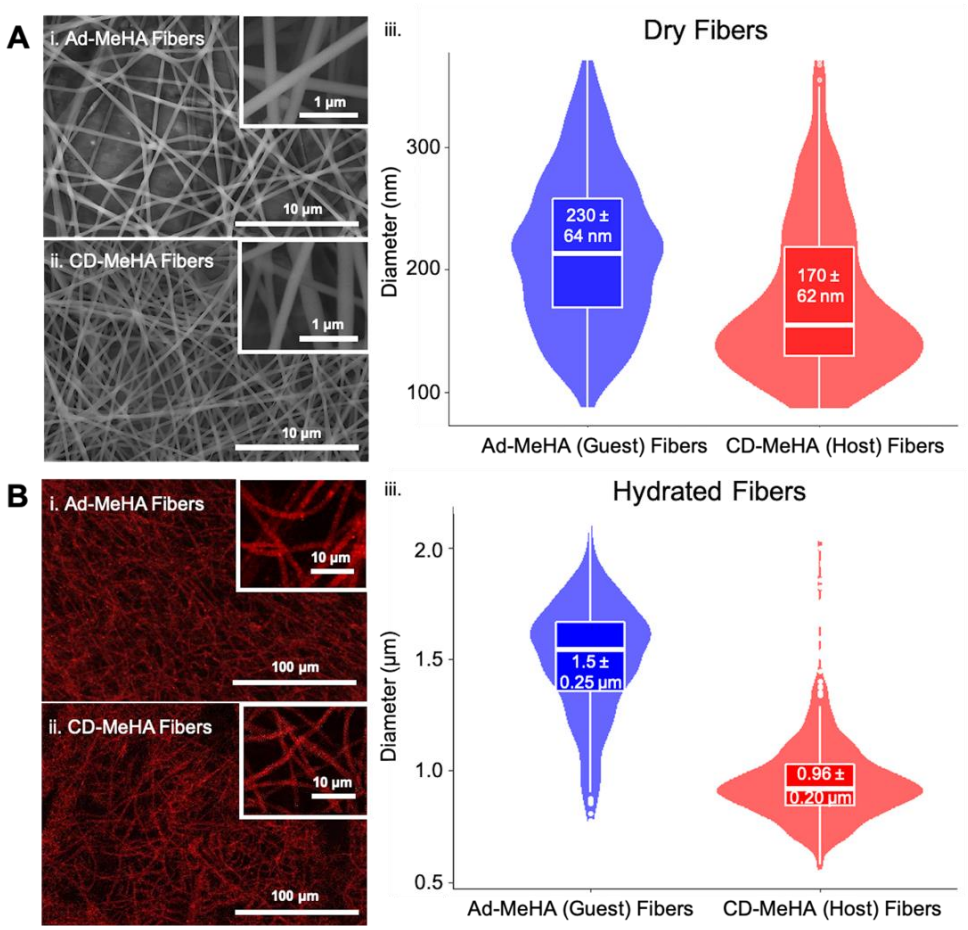

Figure 2.2. Guest and host fiber morphology and diameter distribution. A) SEM images of photocrosslinked guest (A.i.) and host (A.ii.) fibers prior to hydration with quantification (A.iii.) of dry fiber diameter (n = 300 fibers). B) Confocal images of hydrated guest (B.i.) and host (B.ii.) fibers and quantification (B.iii) of the swollen hydrogel fiber diameter (n = 300 fibers).

In addition, both the distribution of hydrogel nanofiber diameters (Ik et al., 2004; Ji et al., 2006) and the morphological change of the nanofibers following hydration (and the resulting PEO extraction) (Ji et al., 2006; A. R. Tan et al., 2008) have been previously observed in electrospun materials. Likewise, the swelling of the HA-based fibers was anticipated as this same phenomenon was previously reported in electrospun HA matrices (Davidson et al., 2019; Wade, Bassin, Rodell, et al., 2015). Calculated swelling ratios for the guest Ad-MeHA fibers and host CD-MeHA fibers were 93 ± 15 and 49 ± 4.8 respectively. These results correlate with the greater degree of swelling in the Ad-MeHA fibers seen in **Figure 2.2** as quantified by the wet/dry fold change in fiber diameter (~ 5.5 for Ad-MeHA versus ~ 4.6 for CD-MeHA). The extent of swelling for HA fibers has been shown to depend on the crosslinking density with denser crosslinking leading to reduced fiber swelling (Davidson et al., 2019; Kim et al., 2013). However, this does not account for the observed differences in fiber swelling between the Ad-MeHA and CD-MeHA fibers since both formulations have the same degree of methacrylate modification. One possible explanation for the CD-MeHA fibers being smaller is a packing phenomenon previous reported where cyclodextrin can form nanoscale aggregates (Loftsson et al., 2019; Messner et al., 2010). Additionally, the hydrophobic nature of the bulky CD group (1.53 nm outer diameter and tapered cavity 0.79 nm in height (J. Zhang & Ma, 2013)) coupled with the hydrophobic hexamethylenediamine linker used to conjugate the CD to HA could also influence the reduced swelling in these fibers. Even though the degree of modification with Ad was high (43%), the guest Ad-MeHA fibers were still ~ 80% hydrophilic HA by mass. In contrast, the CD-MeHA host fibers were only ~ 55% HA by mass.

2.4.2 Guest-host-assembled fibers show mechanical integrity as well as shear-thinning and self-healing character.

With the stable structure of the hydrated electrospun hydrogel nanofibers confirmed via confocal microscopy, mechanical properties of the fibrous hydrogels were then characterized via oscillatory shear rheology (**Figure 2.3**). To form fibrous hydrogels amenable to injection and cell encapsulation, hydrated hydrogel fibers were triturated repeatedly via needle extrusion to produce short fiber segments of length 12.7 ± 5.0 μm (Figure S2.5). A 2:1 molar ratio of guest Ad to host CD groups within the fiber mixture was chosen based on previous work with non-fibrous guest-host hydrogels showing that excess Ad groups promoted longer-term mechanical stability (Rodell et al., 2013). The fiber density of each group in Figure 3 was 1% w/v such that any change in material properties could be directly attributed to guest-host interactions. Guest and host fiber populations, measured separately, showed a higher storage modulus than loss modulus as these bulk measurements reflect the properties of the photocrosslinked fibers and their ability to entangle. The guest-host fibrous network also demonstrated a higher storage modulus (G′, 6.6 ± 2.0 kPa) than loss modulus (G″, 1.2 ± 0.5 kPa), but the increase in storage modulus of the mixed guest-host fibers compared to the individual fiber populations highlights the combined mechanical contributions of the individual covalently-crosslinked fibers and the supramolecular interactions between complementary fiber types (**Figure 2.3A**). Importantly, the guest-host interactions between complementary fibers were necessary for mechanical stability as shown by a qualitative vial inversion test (**Figure 2.3B**).

Biopolymer density can also be adjusted to tune mechanical properties. Fibrous hydrogel matrices formed with 5% fiber density (also 2:1 Ad:CD molar ratio) showed improved storage moduli over the 1% fiber density formulation (Figure S2.6). These results are consistent with previous work demonstrating that the mechanical properties of guest-host materials are dependent on the quantity of guest species compared to host moieties present in the network (Rodell et al., 2013; Sisso et al., 2020) and biopolymer density (Rodell et al., 2013). Other work with electrospun CD-MeHA fibers assessed the guest-host Ad-CD association strength by "gluing" together two CD-MeHA fiber layers with Ad-functionalized HA (AdHA) (Highley et al., 2014). This study similarly found that the guest-host pair outperformed groups without supramolecular assembly in terms of adhesion strength between the fiber layers. While not explored in this work, other factors such as surface flexibility and the supramolecular group density have been reported to impact mechanics. Likewise, we would anticipate that smaller fiber diameters would lead to increased mechanical properties because the increased surface area to volume ratio would result in higher surface availability of Ad and CD groups to associate with each other. The ability to tune the mechanical properties of the fibrous hydrogel scaffold, by controlling the density of fibers and the ratio of host to guest moieties, is an important feature that may allow access to a range of mechanical properties suitable for fibrous tissue repair.

Having demonstrated the guest-host assembly of the functionalized HA hydrogel fibers, we sought to assess their shear-thinning and self-healing capabilities. Strain sweep testing of the fibrous guest-host hydrogel showed loss moduli crossover at strains > 100%, highlighting the potential for injectability (**Figure 2.3C**). The guest-host fibrous scaffold was then subjected to cyclic deformations to investigate the responsiveness to shear force and the ability of the fibers to undergo self-healing, i.e., testing the injectable capabilities of the material. Shear-thinning hydrogels will demonstrate sharp decreases in storage and loss moduli when subjected to shear forces with loss moduli crossover (exceeding storage moduli), which is predictive of liquid-like behavior during needle flow upon injection. Conversely, upon cessation of shear, the storage and loss moduli recover for self-healing hydrogels. Multiple cycles of high strain (250%) followed by short recovery periods at low strain (0.5% strain) demonstrated the guest-host fibrous hydrogel's ability to both shear-thin and self-heal following mechanical deformation (**Figure 2.3D**). Based on these experimental findings, we anticipated that the shear forces associated with syringe-based extrusion would induce the same reversible liquid-like to solid-like transitions.

Seminal work using non-fibrous Ad-CD guest-host assembled hydrogels demonstrated the utility of this supramolecular pair, showing tunable mechanics and flow characteristics of the guest-host assembly by altering the guest-host pair ratio and density as well as network structure (Kakuta et al., 2013; Osman et al., 2011; Rodell et al., 2013). The fibrous hydrogel developed here displays analogous rheological behavior to non-fibrous guest-host hydrogels. As a result of the dynamic bonding interactions between fibers, the guest-host fibrous hydrogel is capable of shear-induced flow (injectability) and rapid recovery.

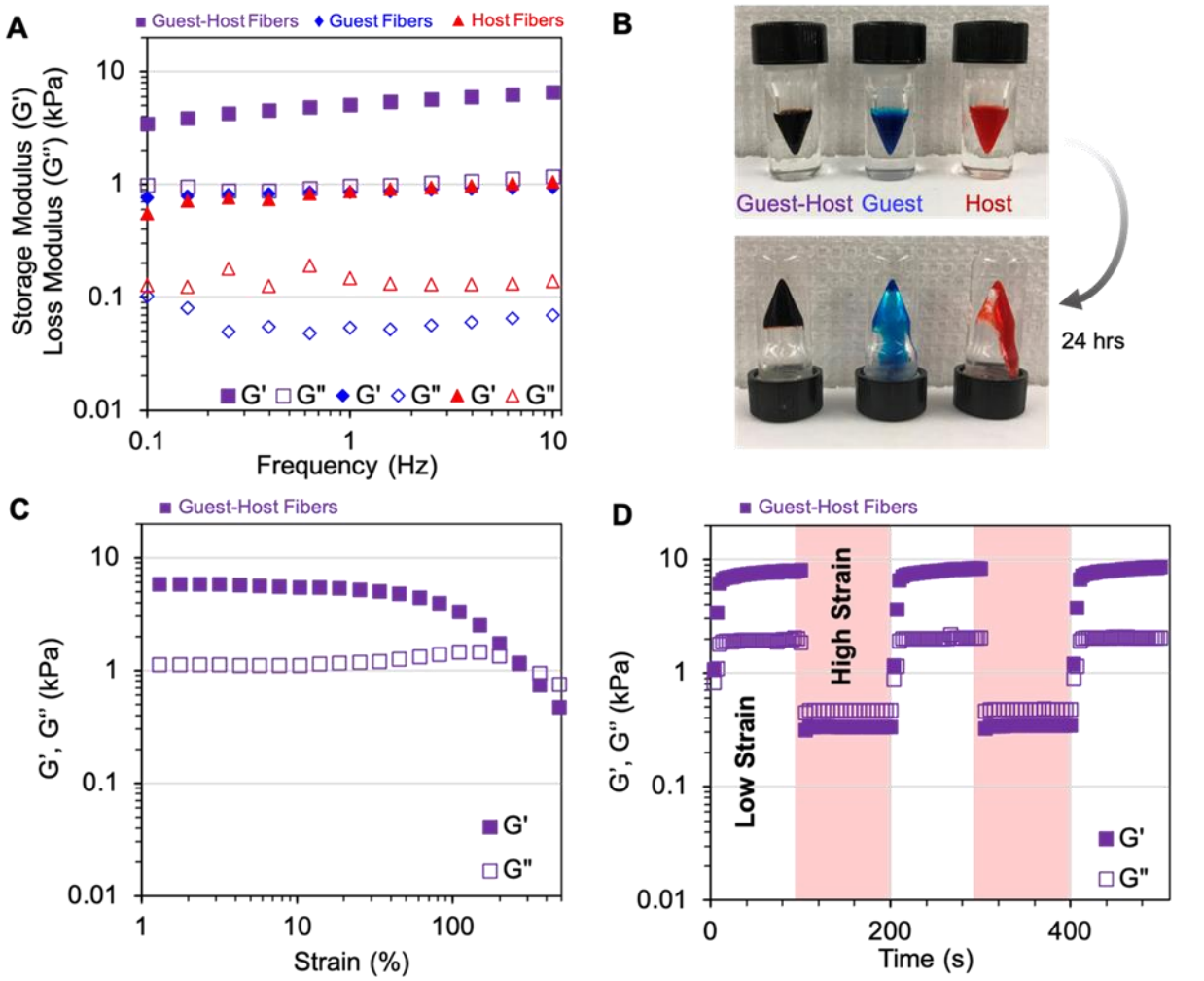

Figure 2.3. Guest-host-assembled fibers show mechanical integrity as well as shear-thinning and self-healing character. A) Frequency sweep of individual, Ad-MeHA (guest) and CD-MeHA (host), hydrogel fibers and mixed guest-host fibers at constant strain of 0.5%. The storage moduli (G′) of all fiber populations are greater than the loss modulus (G″), reflecting the properties of the photocrosslinked fibers and their ability to entangle. However, the higher moduli of the guest-host hydrogel fiber mixture demonstrates the combined contributions of fiber photocrosslinking and supramolecular interactions between the complementary fiber populations. Additionally, G″ is within an order of magnitude of G', indicative of the viscoelastic nature of the fibrous hydrogel. B) Qualitative inversion test of mixed guest-host (dark purple, left), guest (blue, middle), and host (red, right) fibers following injection into vials using a 16G needle. When fibers were left inverted for 24 hr, the mixed guest-host fibers demonstrated long-term mechanical stability and maintenance of their original shape while the guest fibers and host fibers did not. C) Strain sweep of the mixed guest-host fibers showed loss moduli crossover at strains > 100%, highlighting the potential injectability of the fibers. D) Five-step strain sweeps of low strain (0.5%,100 s) and high strain (250%, 100 s). Guest-host fibrous hydrogels show higher loss moduli than storage moduli at high strains and quickly recover viscoelastic properties at low strains, highlighting shear-thinning and self-healing properties.

Overall, rheological analysis of the guest-host fibrous hydrogel demonstrated properties of robust mechanical integrity, shear-thinning, and rapid recovery for stability post-injection. Indeed, the fibrous hydrogel scaffold was readily injectable, flowing easily through a needle (12 mL h^{-1}, 16G) and recovered as a stable hydrogel plug.

2.4.3 Injected hMSCs encapsulated in fibrous hydrogels are viable and show increased spreading compared to non-fibrous hydrogels.

Finally, we tested the ability of the fibrous guest-host hydrogel to support viability and spreading of encapsulated hMSCs following injection. We chose hMSCs for these experiments due to their multipotential for differentiation toward cell types relevant for a broad range of fibrous tissues (Gonzalez-Fernandez et al., 2019) such as muscle, tendon, and ligament (Eder et al., 2020). Protecting cells during injection and preserving high viability is one of the fundamental requirements for subsequent therapeutic application, but many injectable delivery vehicles suffer from poor cell survival (Aguado et al., 2012; Ning et al., 2020). Previous studies have addressed this using materials that leverage physical crosslinking since their compliant mechanical properties support non-uniform network deformation (Madl et al., 2020; Sisso et al., 2020; Tang et al., 2019). In these non-uniform matrices, mechanical stresses imposed on the material create non-uniform strain fields allowing network deformations to dissipate stress (Pedersen & Swartz, 2005). Therefore, we anticipated that the guest-host fibers could mitigate cell-damaging forces during injection due to the force dissipation capabilities of guest-host materials.

We investigated the post-injection viability and spreading of hMSCs when cultured in three hydrogel groups: non-fibrous MeHA, non-fibrous guest-host, and fibrous guest-host (**Figure 2.4**). Groups were chosen such that the influence of fibrous architecture on cell behavior could be assessed independently from the role of guest-host complexation. All groups contained 1 mM RGD peptide to support cell adhesion and had similar storage moduli (rheology of non-fibrous hydrogels is shown in Figure S2.7). Cell viability was quantified at three time points: immediately following injection, day 3 of culture, and day 7 of culture. Following injection, hMSCs in the fibrous guest-host hydrogel were 85 ± 5% viable, a value that was statistically indistinguishable from the hMSCs encapsulated in either of the non-fibrous hydrogels: MeHA (88 ± 4%) or guest-host (89 ± 3%). Previous studies have reported the highest cell survival in injectable hydrogels (~ 90%) utilizing formulations with modest mechanical properties ($G' \sim 30$ Pa) (Aguado et al., 2012; Chopin-Doroteo et al., 2021). More recently, a self-assembled fibrous peptide hydrogel reported 86.8% cell viability post-injection despite a substantially higher storage modulus (3.1 kPa) (Tang et al., 2019). One possible explanation for the fibrous materials' ability to protect cells during injection, despite the more robust bulk mechanical stiffnesses compared to other successful cell carrier materials, is the stochastic nature of self-assembling fiber hierarchical structures allowing microstructural deformation mechanisms such as shear attenuation via fiber sliding (Disney et al., 2018; Knapp et al., 1997; Kurniawan & Bouten, 2018). Local shear attenuation is important for native tissue mechanical function and may be mimicked by the supramolecular interactions between complementary guest and host hydrogel fibers, leading to increased force dissipation and thereby protecting encapsulated cells from extensional flow at the entrance of the syringe needle

and the subsequent disruption of the cellular membrane (Aguado et al., 2012; Ning et al., 2020; Pedersen & Swartz, 2005).

Similar to the initial cell viability, the live cell fractions observed on days 3 and 7 were largely the same (day 3: non-fibrous MeHA: 83 ± 3% and guest-host: 83 ± 3% versus the fibrous guest-host hydrogel: 82 ± 6%), although on day 7 there was a small but statistically significant difference in viability between the non-fibrous MeHA hydrogel group compared to both guest-host hydrogel groups (non-fibrous: 86 ± 2%, fibrous: 87 ± 3%). Although hMSC viability was similar across all experimental groups, qualitative differences in cell shape/spreading observed at day 7 motivated us to quantify hMSC shape metrics such as projected cell area, cell shape index (CSI, a measure of cell circularity), and aspect ratio (**Figure 2.4D**). The ability of encapsulated hMSCs to spread is particularly important for supporting the active mechanical signaling (Caliari et al., 2016) necessary for cells to differentiate and deposit tissue-specific ECM (Chaudhuri et al., 2016; H. Lee et al., 2017) during fibrous musculoskeletal tissue repair.

Confocal imaging of hMSCs in fibrous networks showed direct hMSC interactions with fiber segments (Figure S2.8) as well as the highest levels of spreading and elongation (as measured by both CSI and aspect ratio) compared to the non-fibrous hydrogel groups. In particular, the differences in cell shape were the greatest between cells encapsulated in the guest-host hydrogels, both fibrous (spread area: 1130 ± 146 μm^2, CSI: 0.28 ± 0.04, aspect ratio: 1.54 ± 0.33) and non-fibrous (spread area: 850 ± 333 μm^2, CSI: 0.34 ± 0.02, aspect ratio: 1.33 ± 0.09) compared to the MeHA hydrogels which showed more rounded hMSC morphologies (spread area: 400 ± 93 μm^2, CSI: 0.76 ± 0.02, aspect ratio: 1.17 ± 0.05). The reduction in hMSC spreading and elongation found in MeHA hydrogels compared to the guest-host hydrogels is likely due to differences in viscoelasticity. The guest-host hydrogel networks contain both covalent crosslinking and guest-host supramolecular interactions, leading to viscoelastic properties as shown in our rheological analysis while MeHA hydrogels are covalently crosslinked and behave like elastic solids. Numerous recent studies, including one using the Ad-CD guest-host pair (Loebel et al., 2019), highlighted the role of hydrogel viscoelasticity in supporting increased cell spreading and elongation in 3D cultures (Chaudhuri et al., 2016; Lou et al., 2018). Our findings, in particular the significant reduction in CSI observed for hMSCs in fibrous guest-host hydrogels compared to non-fibrous guest host hydrogels, are also supported by recent work demonstrating that human fibroblasts show increased outgrowth and spreading within fiber-containing hydrogel composites compared to non-fibrous hydrogels (Matera et al., 2019). Other possible explanations for our observed results include CD interactions with aromatic amino acids to provide additional cell anchoring points (Aachmann et al., 2012) and local strain stiffening via fiber recruitment as observed in native ECM and in hydrogel fiber networks (B. M. Baker et al., 2015; Davidson et al., 2019). Together, the data from these experiments underscore the suitability of our fibrous hydrogel design for injectable encapsulation of hMSCs in a microenvironment supportive of cell spreading and elongation.

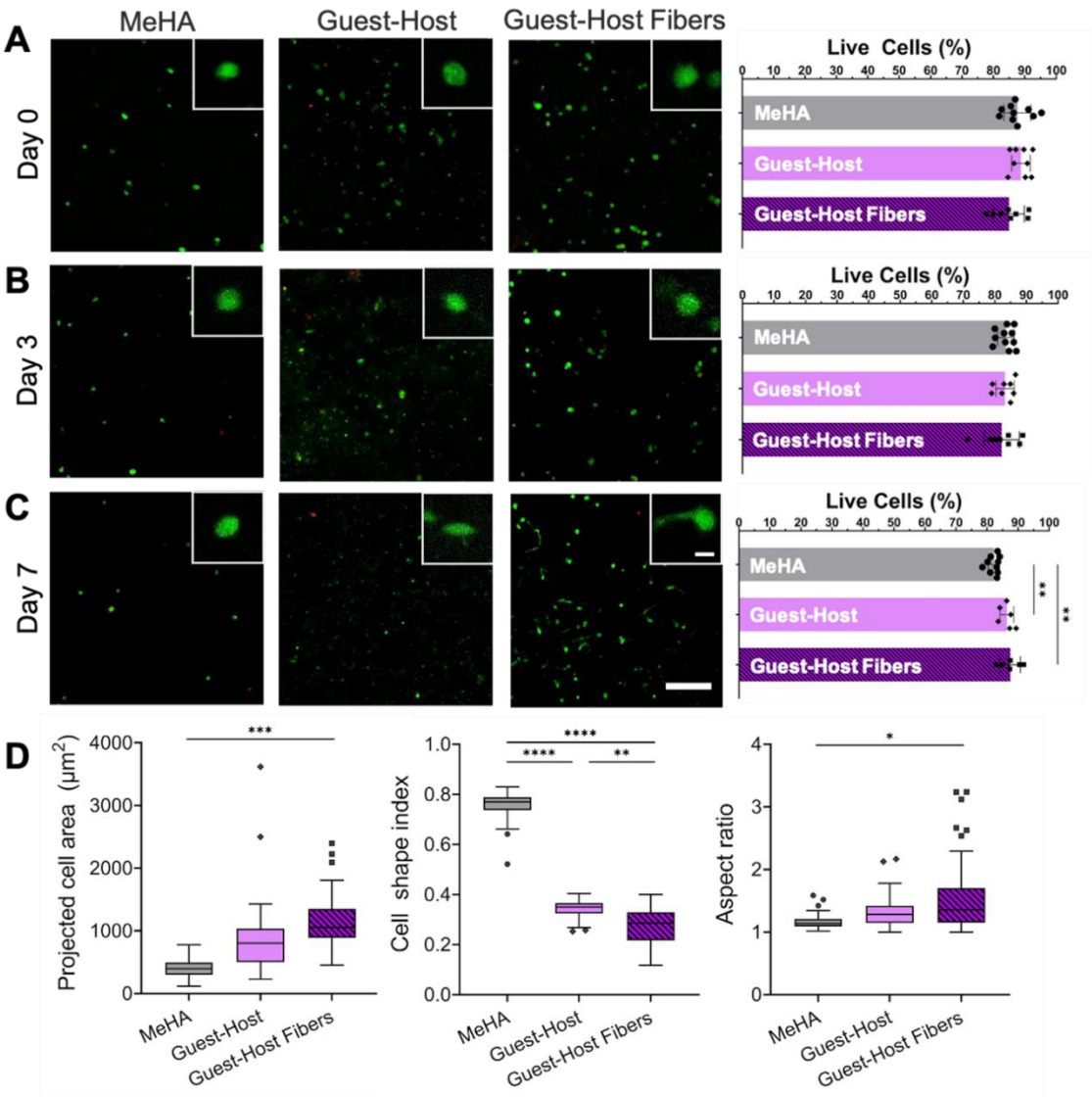

Figure 2.4. Injected hMSCs encapsulated in fibrous hydrogels are viable and show increased spreading compared to non-fibrous hydrogels. Human mesenchymal stromal cells (hMSCs) were encapsulated in non-fibrous MeHA, non-fibrous guest-host, and fibrous guest-host hydrogels. Live/Dead images of viable (*green*) and membrane damaged (*red*) cells as well as cell viability quantification for all groups is shown A) immediately following injection (Day 0), B) after 3 days of culture, and C) after 7 days of culture. Inset image scale bar = 10 μm. Full image scale bar = 100 μm. Cell viability was comparable across the different hydrogel formulations. D) Quantification of day 7 cell shape metrics. Cells in fibrous guest-host hydrogels showed significantly increased projected cell area and elongation compared to cells in MeHA hydrogels. Additionally, hMSCs in fibrous guest-host hydrogels showed significantly reduced cell shape index (circularity) compared to hMSCs in non-fibrous guest-host hydrogels. Viability data are presented as mean +/- SD. Tukey box plots of individual cell data (60 cells per group) show the second and third quartiles as boxes, the median as a line between the boxes, and error bars with the lower value of either 1.5 times the interquartile range or the maximum/minimum value. Data points outside this range are shown individually. * $P < 0.05$, ** $P < 0.01$, *** $P < 0.001$, **** $P < 0.0001$. n = at least 6 hydrogels per experimental group.

2.5 Conclusions

In summary, we designed and fabricated an injectable fibrous hydrogel capable of shear-thinning and self-healing under physiologic conditions. Using HA as a naturally-derived polymer already applied in clinical settings for decades, these materials offer unique advantages with respect to biocompatibility and mechanical integrity ($G' = 6.6 \pm 2.0$ kPa) while also recapitulating the fibrous architecture of tissue. In addition to exhibiting shear-thinning and self-healing behavior, the guest-host fibrous hydrogel demonstrated injectability wherein encapsulated hMSCs were protected from membrane-disrupting shear forces during injection, resulting in sustained 3D hMSC viability (> 85%). Cells were also more spread and elongated in viscoelastic guest-host hydrogels compared to non-fibrous elastic hydrogel controls, with hMSCs showing significantly reduced CSI (circularity) in fibrous guest-host hydrogels compared to both non-fibrous MeHA and non-fibrous guest-host hydrogels. In summary, the injectable fibrous hydrogel platform introduced here offers the potential to broaden minimally invasive delivery to musculoskeletal tissue engineering applications requiring robust structural properties while also laying the foundation for future opportunities in 3D bioprinting and fundamental studies of cell-microenvironment interactions.

2.6 Acknowledgments

The authors thank Prof. Rachel Letteri and Dr. Matthew D. Davidson for helpful discussions as well as Erica Hui for providing initial hydrogel synthesis training. Utilization of the FEI Quanta 650 SEM within UVA's Nanoscale Materials Characterization Facility (NMCF) was fundamental to this work and we thank the staff for equipment training. This work was supported by the University of Virginia, the DoD (W81XWH-19-1-0157), and the NIH (R21AR075181). The content is solely the responsibility of the authors and does not necessarily represent the official views of the National Institutes of Health.

2.7. Supplemental information

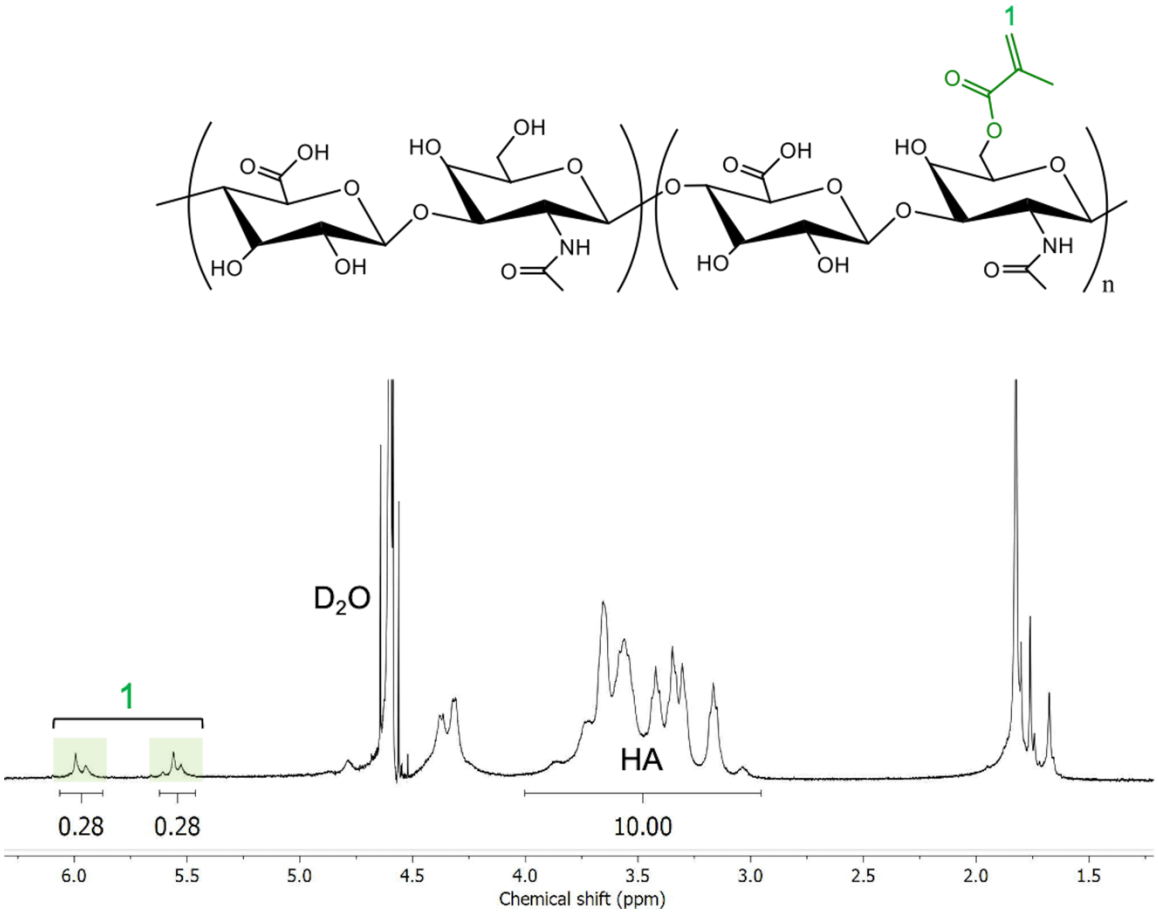

Figure S2.1. ^{1}H NMR spectrum of methacrylate-modified hyaluronic acid (MeHA). The degree of HA modification with methacrylates was determined to be 28%. Degree of functionalization was determined from integration of the methylene (δ = 5.82, 1H and δ = 6.25, 1H) highlighted green and labeled '1' relative to the HA backbone, (δ = 3.10-4.10, 10H).

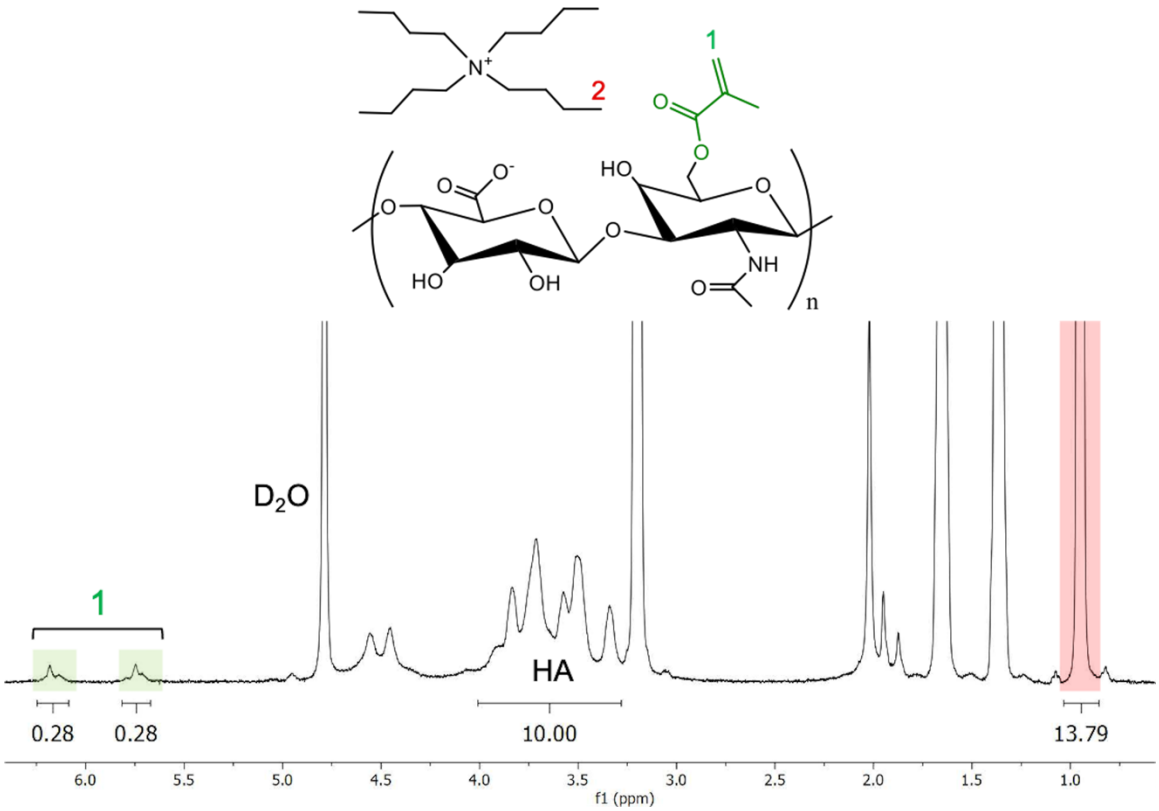

Figure S2.2. ^{1}H NMR spectrum of methacrylated hyaluronic acid tert-butyl ammonium salt (MeHA-TBA). The MeHA used for the synthesis of Ad (guest) and CD (host) derivatives underwent addition of the TBA salt (highlighted red) to enable further HA modification.

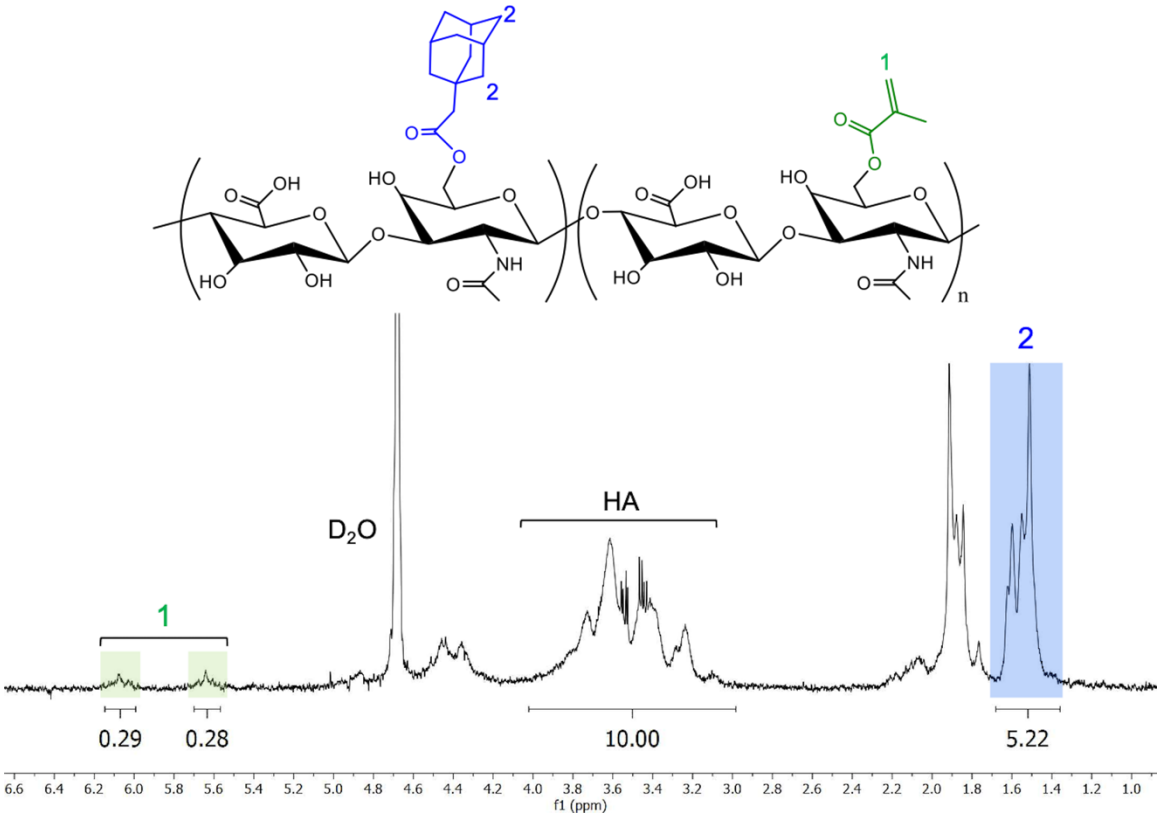

Figure S2.3. ^{1}H NMR spectrum of adamantane and methacrylate-modified hyaluronic acid (Ad-MeHA). The degree of MeHA modification with adamantane was determined to be 43%. The integration of the ethyl multiplet of adamantane (δ = 1.40-1.70, 12H) highlighted in blue gives the degree of modification relative to the HA backbone (δ = 3.10-4.10, 10H).

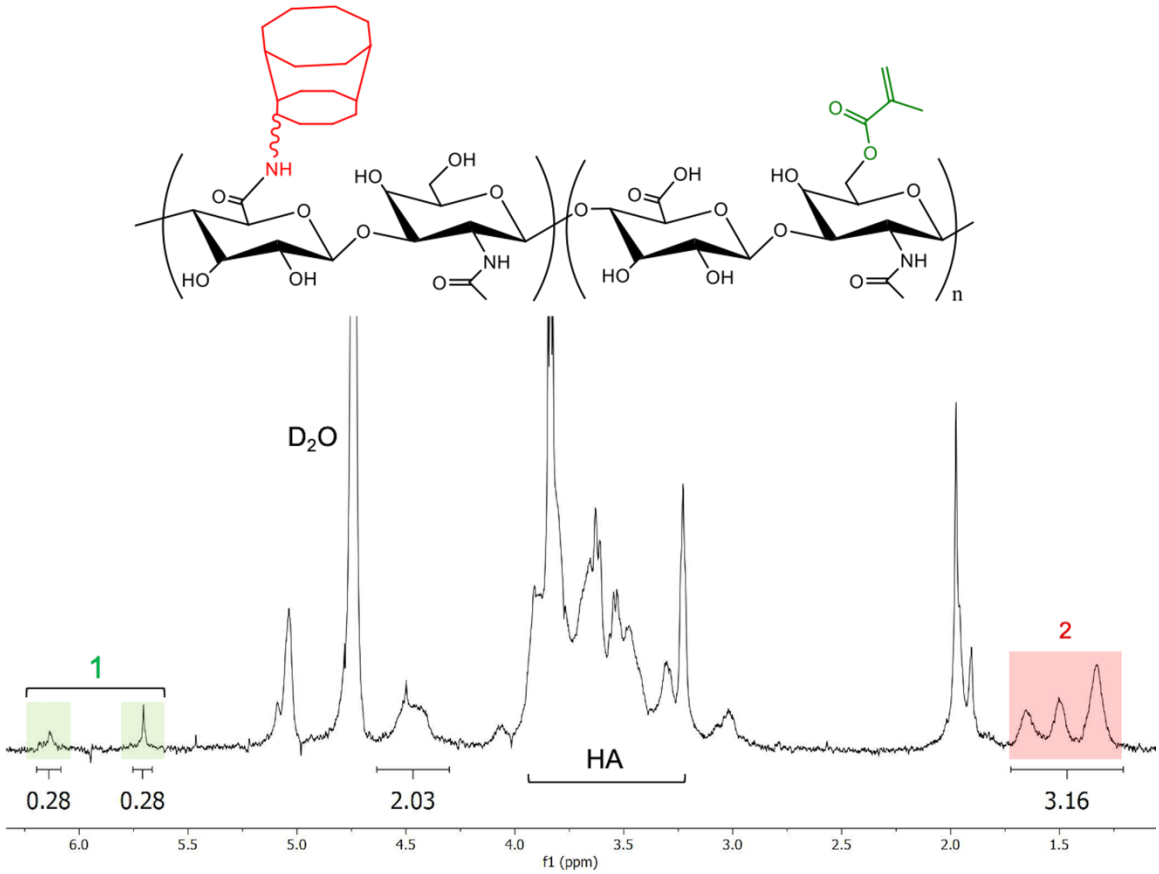

Figure S2.4. ^{1}H NMR spectrum of β-cyclodextrin and methacrylate-modified hyaluronic acid (CD-MeHA). The degree of MeHA modification with β-cyclodextrin was determined to be 26%. This was calculated from the integration of the hexane linker (δ = 1.20-1.75, 12H) highlighted in red relative to the methacrylate modification, which is assumed to stay constant.

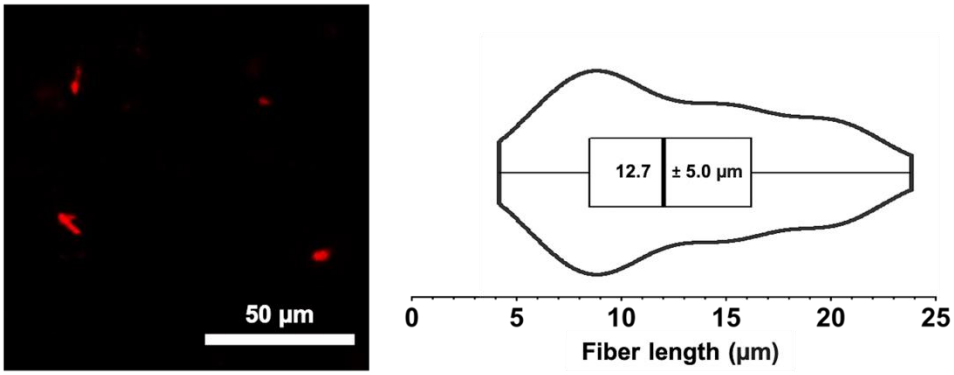

Figure S2.5. Fiber length distribution following trituration. The lengths of rhodamine-labeled Ad-MeHA 'guest' and CD-MeHA 'host' fibers were separately evaluated following sequential needle trituration. Fiber lengths (n = 90) were measured using confocal images and processed in ImageJ. A representative image of Ad-MeHA guest fibers is shown here.

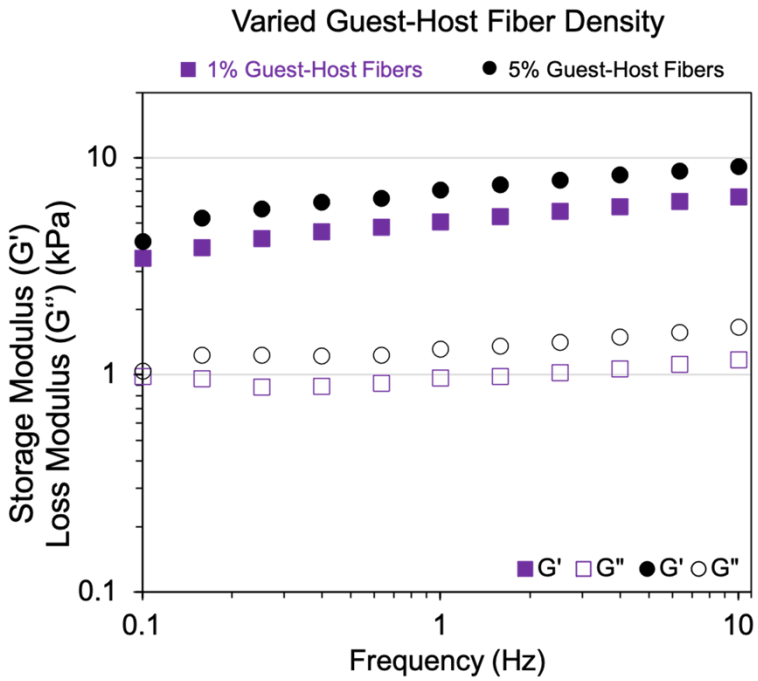

Figure S2.6. Rheological properties of the guest-host fiber network with varying fiber density. The frequency-dependent behavior was measured using a constant strain of 0.5%. The 1% fibrous hydrogel reached a final storage modulus (G′) of 6.6 kPa and the 5% fibrous hydrogel a G′ of 9.2 kPa at 10 Hz.

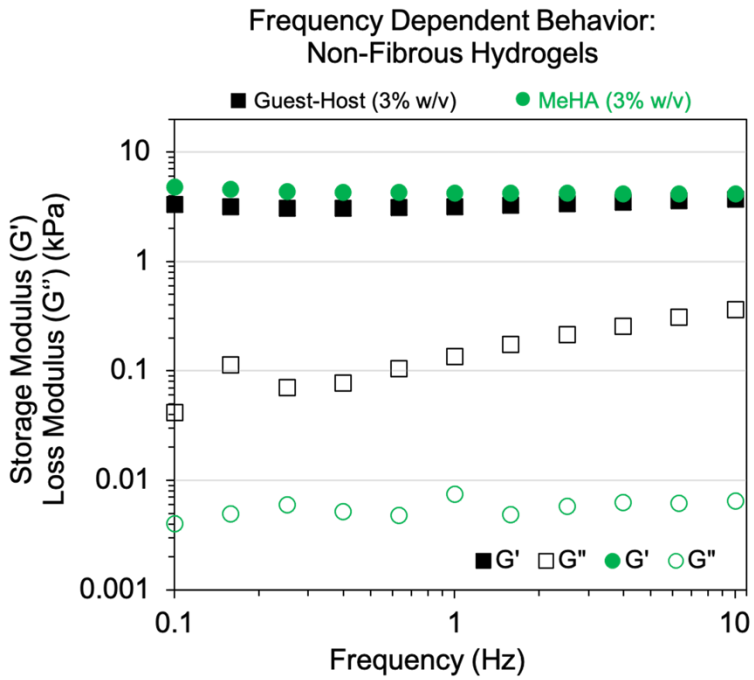

Figure S2.7. Rheological properties of the non-fibrous MeHA and guest-host hydrogels used for cell encapsulation. The frequency-dependent behavior was measured using a constant strain of 0.5%. The non-fibrous 3% MeHA hydrogel formulation reached a final storage modulus (G′) of 4.2 kPa and the non-fibrous 3% guest-host hydrogel formulation reached a final G′ of 3.7 kPa at 10 Hz.

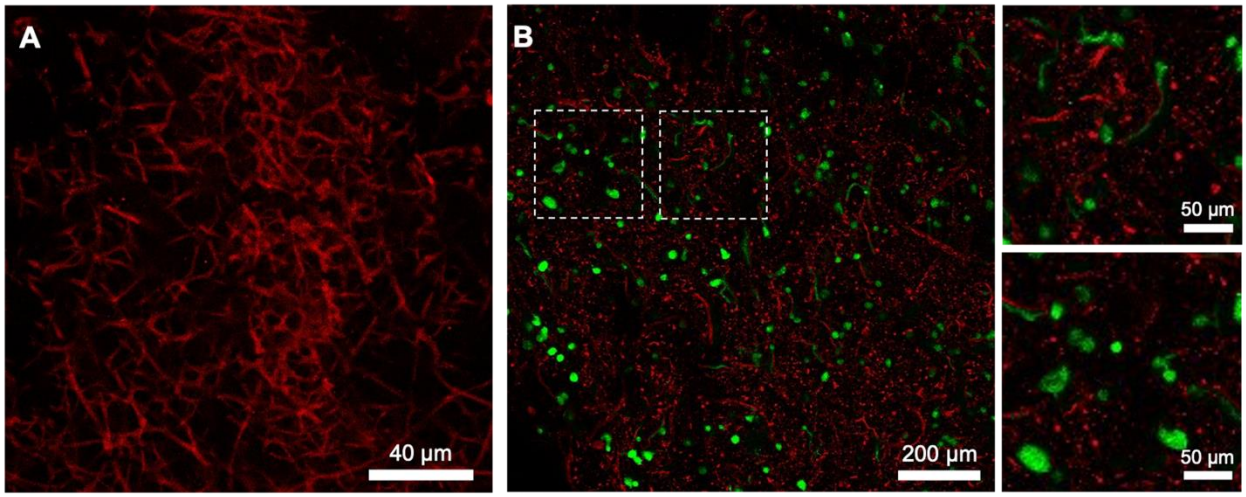

Figure S2.8. Visualization of the fibrous guest-host hydrogel structure. Rhodamine-labeled HA fibers show A) the morphology of the fibrous guest-host hydrogel (*red*) without encapsulated cells and B) hMSCs (*green*) encapsulated within the fibrous guest-host hydrogel (*red*) after 7 days of culture.

CHAPTER 3: DEVELOPMENT OF A UTEROSACRAL LIGAMENT SUSPENSION RAT MODEL

This chapter has been adapted from the following publication: Miller, B. J., Jones, B. K., Turner, J. S., Caliari, S. R. & Vaughan, M. H. *Development of a Uterosacral Ligament Suspension Rat Model*. *J. Vis. Exp.* 186. **2022**.

3.1. Abstract

Pelvic organ prolapse (POP) is a common pelvic floor disorder (PFD) with the potential to significantly impact a woman's quality of life. Approximately 10%–20% of women undergo pelvic floor repair surgery to treat prolapse in the United States. PFD cases result in an overall $26.3 billion annual cost in the United States alone. This multifactorial condition has a negative impact on the quality of life and yet the treatment options have only dwindled in the recent past. One common surgical option is uterosacral ligament suspension (USLS), which is typically performed by affixing the vaginal vault to the uterosacral ligament in the pelvis. This repair has a lower incidence of complications compared to those with mesh augmentation, but is notable for a relatively high failure rate of up to 40%. Considering the lack of standard animal models to study pelvic floor dysfunction, there is an urgent clinical need for innovation in this field with a focus on developing cost-effective and accessible animal models. In this manuscript, we describe a rat model of USLS involving a complete hysterectomy followed by fixation of the remaining vaginal vault to the uterosacral ligament. The goal of this model is to mimic the procedure performed on women to be able to use the model to then investigate reparative strategies that improve the mechanical integrity of the ligament attachment. Importantly, we also describe the development of an *in situ* tensile testing procedure to characterize interface integrity at chosen time points following surgical intervention. Overall, this model will be a useful tool for future studies that investigate treatment options for POP repair *via* USLS.

3.2. Introduction

Pelvic organ prolapse (POP) is a common pelvic floor disorder affecting millions of women worldwide with the potential to significantly impact many aspects of a woman's life, particularly with age (Olsen et al., 1997). Notably, approximately 13% of women in the United States will undergo surgery for prolapse or urinary incontinence (J. M. Wu et al., 2014). A condition most common after pregnancy and childbirth, prolapse is characterized by the descent of pelvic organs, predominantly the various compartments of the vagina and/or uterus, beyond their normal position in the peritoneal cavity. This leads to bothersome symptoms of vaginal bulge or pressure, bowel, bladder, and sexual dysfunction, and overall reduced quality of life. Other risk factors for POP include obesity, tobacco use, chronic cough, and constipation (Kenton, Kimberyly; Mueller, 2006).

In healthy women, the pelvic floor organs are supported by the levator ani muscles, uterosacral ligaments (USLs), cardinal ligaments, connective tissue attachments to the pelvic sidewall and the distal structures of the perineal body (Herschorn, 2004; Jelovsek et al., 2007). The USLs are among the most important apical supportive structures for both the uterus and apical vagina, and thus, are often used in surgical correction of POP (**Figure 3.1**). Structural support from the USL stems from the dense collagenous connective tissue in the sacral region that transitions into closely packed smooth muscle. Due to this compositional gradient, the USL becomes interwoven with the uterine and vaginal musculature to provide sturdy support for the pelvic organs (Campbell, 1950; Reisenauer et al., 2008). In the uterosacral ligament suspension (USLS), the USLs are secured to the vaginal vault following a hysterectomy, restoring the vagina and the surrounding structures to their anatomical position in the abdominal compartment. However, regardless of a transvaginal or laparoscopic route, the USLS procedure is plagued by a relatively high failure rate of up to 40% in some studies (Jelovsek et al., 2018; Lavelle et al., 2016). The recurrence rate of bothersome vaginal bulge symptoms at 5 years post-repair for apical compartment prolapse, such as USLs, was approximately 40% in a large multicenter randomized controlled trial (Jelovsek et al., 2018). In the same trial, retreatment for recurrent prolapse at 5 years was approximately 10%. The mechanism of this high failure rate has not been studied, but restoring the vagina and the surrounding structures to their anatomical position requires suture placement in the dense collagenous region of the USL (Bradley et al., 2020; Cola et al., 2022) rather than the smooth muscle region. Therefore, the high failure rate could be due to the mechanical and compositional mismatch of the surgically formed vagina-USL interface compared to the complete integration seen in the native cervical-USL attachment.

The economic impact of treating these disorders is also notable, with approximately $300 million spent annually in the US on ambulatory care (Sung et al., 2010), and more than $1 billion spent annually in direct costs for surgical procedures (Subak et al., 2001). Despite the vast economic resources dedicated to treating these conditions, the complications arising from many prolapse surgeries remain discouraging. For example, polypropylene mesh-based apical prolapse repairs, such as sacrocolpopexy, offer higher success rates compared to native tissue repairs (Siddiqui et al., 2015), but at the cost of potential complications such as mesh exposure or erosion.

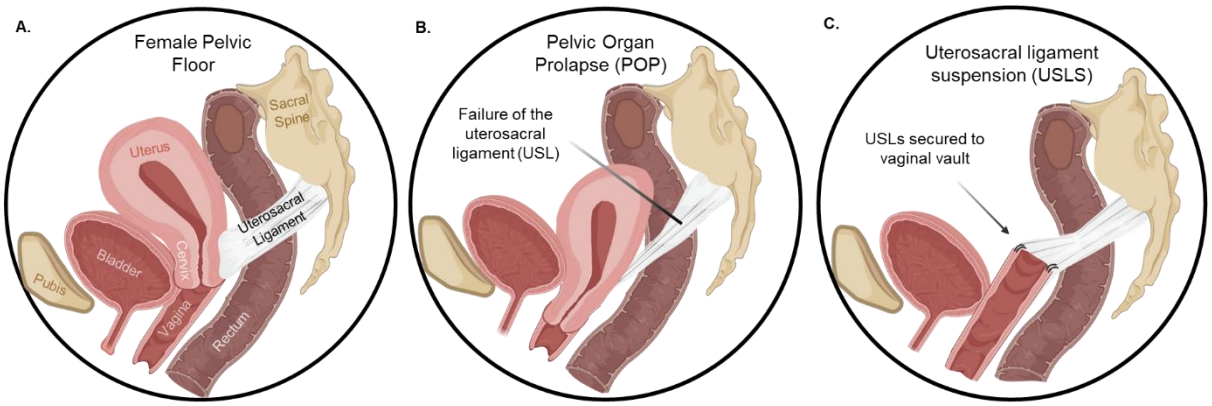

Figure 3.1: Pelvic organ prolapse. (**A**) The normal orientation of organs in the peritoneal cavity and (**B**) the dramatic organ descension when prolapse occurs. Following hysterectomy, (**C**) uterosacral ligament suspension restores the vagina and surrounding structures to their proper anatomical position.

The FDA received nearly 3,000 complaints related to mesh complications between 2008 and 2010 alone. This culminated in an order by the FDA to halt the manufacture and sale of all transvaginally-placed mesh products for POP in April 2019 (*FDA takes action to protect women's health, orders manufacturers of surgical mesh intended for transvaginal repair of pelvic organ prolapse to stop selling all devices*, 2019). Therefore, there is a strong clinical need for materials other than polypropylene, and models with which to test them, that may augment native tissue prolapse repairs and increase success rates compared to traditional techniques with suture alone.

Since the FDA announcement in 2019, most pelvic surgeons have stopped using transvaginally-placed mesh for prolapse repairs, prompting investigators to seek new tissue engineering approaches to augment native tissue repairs (Brincat, 2019; Cundiff, Geoffrey W. MD, FACOG, FACS, 2020; Luchristt et al., 2022) such as with mesenchymal stromal cells (MSCs)[9,20]. With this shift in focus, there is an urgent need for the refinement of animal models that can assist with development of new materials; the challenge in this process is balancing clinical relevance with cost. To this end, basic science and clinical investigators studying pelvic organ prolapse have taken advantage of several animal models thus far, including rats, mice, rabbits, sheep, swine, and non-human primates (Couri et al., 2012). The process of identifying an optimal animal model is challenging, as humans are bipedal, have no tail, and have a traumatic birth process compared to other mammalian species(Mori da Cunha et al., 2021). Swine (Kasabwala et al., 2019) have been utilized to simulate robotic sacrocolpopexy, while sheep have been used to simulate vaginal prolapse repairs (Mansoor et al., 2017). These animal models, while clinically relevant, are limited in feasibility by cost and maintenance. Non-human primates have been used to study the pathogenesis of prolapse; squirrel monkeys in particular are one of the only species other than humans that can develop spontaneous prolapse, making them one of the most relevant animal models (Mori da Cunha et al., 2021). Non-human primates have also been used to study gynecologic surgical procedures such as sacrocolpopexy (Liang et al., 2015) and uterine transplantation (Johannesson et al., 2013). Similar to their sheep and swine counterparts, the

primary limitation of non-human primates as an animal model of prolapse is the cost of maintenance, care, and boarding (Couri et al., 2012).

Although the rodent pelvis is oriented horizontally with a much smaller head-to-birth canal size ratio compared to humans (Couri et al., 2012), rats are suitable for small animal studies of USLS surgery since they have similar USL anatomy, cellularity, histological architecture, and matrix composition compared to the human USL (Iwanaga et al., 2016). Moreover, they are beneficial in terms of maintenance and boarding. Despite these beneficial attributes, there are no published reports of a rat model of USLS repair. Therefore, the aim is to describe a protocol for hysterectomy and USLS in the multiparous Lewis rat. This protocol will be beneficial for investigators who aim to study the pathophysiology and surgical components of POP using this accessible animal model.

3.3. Protocol

Follow all Institutional Animal Care and Use Committee (IACUC) guidelines, obtaining approval for all animal procedures before beginning. Requirements for aseptic surgery technique can be found from The Guide(National Research Council, 2011) and the Animal Welfare Regulations(National Archives, 2022). The study was approved by the University of Virginia Institutional Animal Care and Use Committee protocol number 4332-11-20. Obtain multiparous (two litter) female breeders. Rats should be pair housed in a vivarium accredited by the American Association for the Accreditation of Laboratory Animal Care and provided with food and water *ad libitum*. Animals in this study were Lewis rats obtained from Charles River and were between 4 and 6 months of age to accommodate the two-litter requirement. Animals were maintained on a 12 h light-dark cycle.

3.3.1. Pelvic organ prolapse repair using uterosacral ligament suspension

1. Equipment and surgical area preparation for live animal surgery

1.1. Prepare the surgical area such that the surgical board is heated to 37 °C using recirculating hot water heating pads along with a sterile waterproof pad. Ensure sterility of the surgical board and surgical area using a bleach free surface disinfectant followed by 70% ethanol wipe.

1.2. Use autoclave heat sterilization to sterilize all autoclave safe supplies, including surgical instruments, surgical sponges (gauze), cotton swabs, and a disposable drape. Obtain sterile packaged surgical gloves.

1.3. Obtain electric clippers, ophthalmic ointment, ethanol wipes, cotton swabs, and iodine solution, along with sterile packaged scalpel blade and sutures, and place at the work bench.

2. Animal preparation for live animal surgery

2.1. Carefully place the animal into an anesthesia chamber supplied with 2% isoflurane and weigh the animal after the proper plane of anesthesia is reached. Proper anesthetization is confirmed when the animal is non-responsive to a toe pinch.

2.2. Place the animal onto the surgery board in the prone position with the nose securely in the anesthesia cone with 2% isoflurane. Apply ophthalmic ointment to each of the animals' eyes.

2.3. Administer opioid analgesic and NSAID analgesic subcutaneously.

2.4. Place the animal in the supine position, as shown in **Figure 3.2**, and shave off the abdominal fur from the xiphoid process down to the urethral orifice (8 cm x 4 cm). Sterilize the abdomen with three charges of iodine and alcohol to prepare the incision site.

NOTE: If shaving results in bleeding, achieve hemostasis with pressure prior to preparing the skin with iodine and alcohol prep pad. Maintain iodine on the skin for 30 s.

2.5. If there is no surgical assistant available, deposit sterile supplies and instruments onto a sterile instrument tray, including sterile cotton swabs, drape(s), sponges (gauze), surgical blade, sutures, and surgical marker (optional). If a surgical assistant is available, then this step can be omitted, and the assistant can provide the sterile instruments following step 3.1.

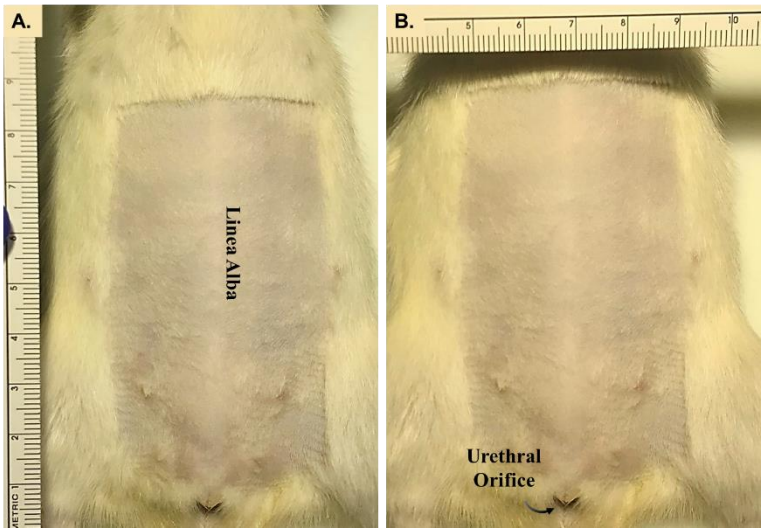

Figure 3.2. Animal preparation for live surgery. Removing fur from the area surrounding the incision site is necessary for proper aseptic technique. The area shown in panels (A) and (B) are guidelines. Researchers should remove enough hair such that sterile instruments make no contact with hair during surgery.

3. Hysterectomy and uterosacral ligament suspension (USLS)

3.1. Don a surgical gown, head cover, mask, and sterile gloves. Drape the animal with a sterile field, leaving only the abdomen exposed.

3.2. Make a 7 cm incision down the linea alba from just below the xiphoid process to the lower nipple line using a scalpel blade. The incision should end ~0.5–1.0 cm rostral from the urethral orifice. Then, make an incision through the muscle layer underneath. Avoid the abdominal wall blood vessel to prevent bleeding.

3.3. Assemble the abdominal retractor and inspect the abdominal cavity (**Figure 3.3A**). Using iris forceps, gently locate the left uterine horn. The uterus is deep inside the bowel, which is often the structure first encountered upon entering the peritoneal cavity. It is beneficial to first identify the ovary (**Figure 3.3B**) and the associated ovarian fat pad.

3.4. Gently elevate the left uterine horn with a grasper or mosquito clamp and begin hysterectomy by ligating the horn below the ovary and oviduct using a mosquito clamp. The ovaries are delicate structures and are easily damaged or devascularized with manipulation. Take care when elevating the uterine horns; grasp the horn a safe distance from the ovary.

3.5. Continue the hysterectomy by clamping and trimming adjacent vasculature, connective tissue, and fat from the uterine horn using micro scissors. Clamp the connective tissue prior to removal to reduce bleeding. Place the clamps as close to the uterine interface as possible, all the way down to the uterocervical junction (also termed as horn bifurcation).

3.6. Clamp across the uterine horn near the point of bifurcation using mosquito forceps (**Figure 3.4A–C**). Excise the ipsilateral horn just cephalad to the clamp to avoid bleeding. This is located between the utero-cervical junction (just rostral to the cervix) and the utero-tubal ligation point. The vaginal vault will remain post the hysterectomy (**Figure 3.4D**).

3.7. Repeat steps 3.3–3.6 on the right uterine horn to perform a total hysterectomy.

3.8. Adjust the abdominal retractor to expose the lower pelvis. Inspect the exposed vaginal vault and the pelvic floor support ligamental and connective tissues, which can be seen attached to the vagina and cervix. If possible, identify the ureter bilaterally, which is just medial to the ovaries.

3.9. Identify the uterosacral ligaments (Ma et al., 2012; Moalli et al., 2005), shown in **Figure 3.5A**, which can be found attached to the cervix just below the remaining stumps of the uterine horns (vaginal vault). The ligament is traced in a cephalad-medial orientation toward the sacrum.

3.10. Using a 3-0 polydiaxanone suture on a small, tapered needle, place a stitch through the left uterosacral ligament. Place the stitch high on the ligament, close to the sacrum.

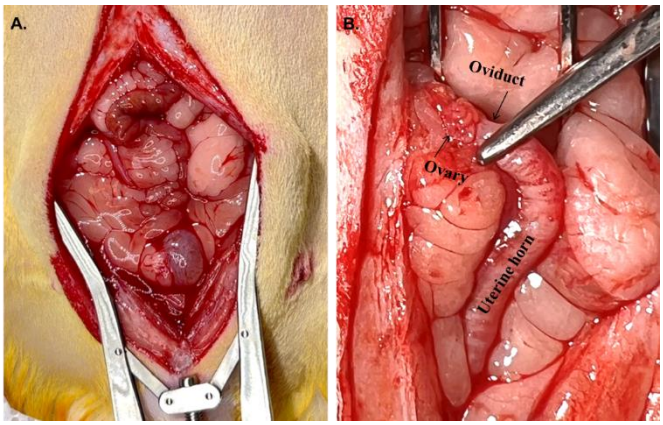

Figure 3.3. Preserving the ovaries. The uterine horns are typically not visible when the abdomen is first opened, as shown in (A). Once a horn is located and followed to find (B) the ovary and oviduct where they connect to the horn, the top of the horn can be clamped, and the horn separated to begin hysterectomy.

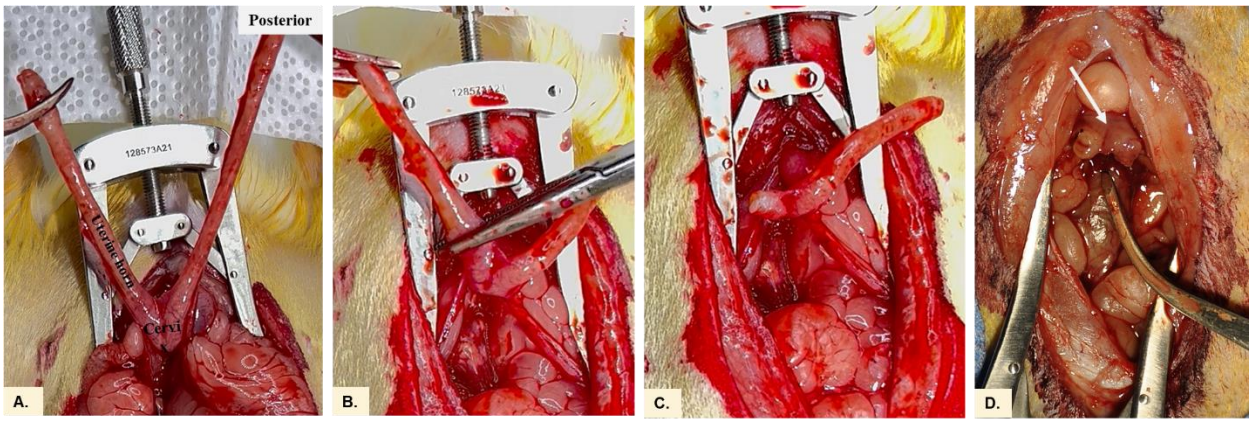

Figure 3.4. Removing the uterine horns. Hysterectomy in the rat involves (A) both uterine horns (B) clamped at the uterocervical junction and (C) excised. The vaginal vault from each horn remains with the (D) cervical/uterine stump (arrow) connecting them.

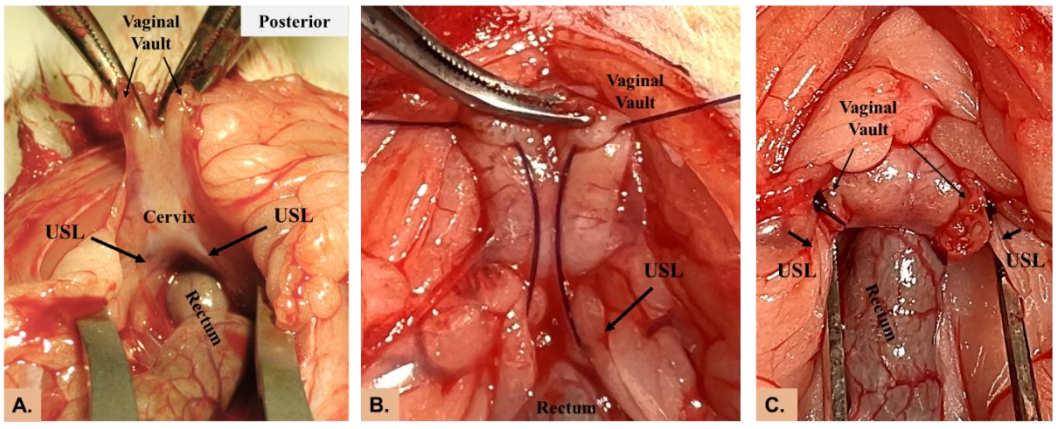

Figure 3.5. Uterosacral ligament suspension. (A) Orientation of the uterosacral ligaments in relation to the created vaginal vault structures. When placing sutures for the uterosacral ligament suspension (USLS) repair, (B) sutures capture the uterosacral ligament and then pass through both the anterior and posterior aspects of the vaginal cuff. (C) Secured to the uterosacral ligament, the vaginal vault is now elevated cephalad toward the sacrum.

3.11. Tug on the stitch to ensure it has captured the uterosacral ligament—the USL structure inserts into the cervix with the origin diving behind the rectum where it attaches to the sacrum. Again, identify the ureter to ensure it has not been incorporated into or kinked with the uterosacral stitch.

3.12. Then, pass the left polydiaxanone stitch through the left aspect of the vaginal vault (**Figure 3.5B**), with care to incorporate both the anterior and posterior aspects of the vaginal cuff. Repeat the steps to complete the USLS procedure on the right side. Multiple stitches can be placed bilaterally, if desired.

3.13. Once the uterosacral stitches are placed bilaterally, securely tie the suture using a square knot, as shown in **Figure 3.5C**, such that the vaginal vault is elevated cephalad toward the sacrum; this completes the uterosacral ligament suspension.

4. Closing the surgical wound

4.1. Replace the abdominal contents back into their anatomical position within the peritoneal cavity. Close the deep layers of the abdominal wall (peritoneum, fascia, muscle) with a running stitch of 4-0 to 6-0 polyglactin 910 or polydiaxanone suture.

4.2. Close the skin with a running subcuticular (or interrupted) stitch of 4-0 to 6-0 polydiaxanone or polyglactin 910. Administer antibiotic subcutaneously as needed for surgical site infection prophylaxis.

4.3. Perform post-surgical monitoring until the animal has regained sufficient consciousness to maintain sternal recumbency. Do not return the animal to social housing until fully recovered.

3.3.2. Uniaxial tensile testing

NOTE: The testing system and software used was operated following the manufacturer's guidelines for calibration and testing. All testing occurred at 22 °C.

1. Specimen preparation

1.1. Expose the vaginal vault in preparation for tensile mechanical testing. In the current study, perform tensile testing on native uterosacral ligaments (control), as well as on animals who had undergone uterosacral ligament suspension as described above (POP).

1.2. Test ligaments *in situ* 24 weeks following surgery. A terminal timepoint of minimum 8 weeks is suggested to allow for the complete reabsorption of the sutures.

1.2.1. Euthanize the rat using an IACUC-approved pharmacological procedure. Ensure death *via* secondary physical method. Here, CO_2 inhalation was used followed by cardiac puncture. Make an incision down the linea alba to expose the abdomen.

1.2.2. Begin dissecting off the adipose tissue until the vaginal vault is visible. Continue to dissect off the abdominal fat pads until the intact USLs is clearly visible (control animals, **Figure 3.6A**) or the junction between the uterosacral ligament and the vaginal vault is visible (POP animals, **Figure 3.6C**). Use caution to not pull on the junction to remove adipose tissue, but rather using careful cuts with micro-scissors to maintain consistency between samples.

1.2.3. Using a flexible ruler, measure the distance between the uterosacral insertion (posterior to the rectum) and the vaginal vault. This value is the original length of the tissue.

NOTE: The original length of the tissue, the gauge length, for control USLs measured 13.4 ± 0.5 mm while the gauge length for USLs repair measured 12.8 ± 0.4 mm.

1.2.4. Thread umbilical tape behind the intact USL (control, **Figure 3.6B**) or the USLS junction (POP, **Figure 3.6D**) such that the tissue is centered on the umbilical tape. Measure the height and width of the tissue where it intersects with the umbilical tape using digital calipers. These values will be used to calculate cross-sectional area.

1.2.5. Attach a large compression plate *via* the base adapter and position the animal atop such that the specimen is centered beneath the grip holder.

2. Tensile testing

2.1. Program the tensile testing regime into the software: pre-load, pre-condition, pull to failure. This follows previous pelvic floor (Moalli et al., 2005) and reproductive tissue (Yoshida et al., 2019) mechanical testing protocols.

2.2. Set up the instrument in preparation of tensile testing. Used here, a 10 N load cell, a 3D printed grip, and a base adapter to attach a compression platen (**Figure 3.7)**.

NOTE: Any base set-up that can support the full size of the animal is acceptable. Use any grip that can securely hold the umbilical tape. A custom 3D printed holder and grip from previous studies (Christ et al., 2021; Smith & Christ, 2019) was used in this testing.

2.2.1. Position the animal such that the specimen is centered beneath the grip (**Figure 3.8A**). Immobilize the pelvic region surrounding the specimen by securing the animal to the platen (**Figure 3.8B**).

2.2.2. Lower the load cell such that the tails of the umbilical tape easily reach the grip. Secure the umbilical tape in the grip, leaving the tape slack to avoid specimen manipulation.

2.3. Open the pre-conditioning test in the software interface and label the test with the sample name. Ensure that the pre-conditioning method includes the pre-load step.

2.4. Click to start the pre-conditioning test, which will pre-load the sample at 0.015 N. Once the pre-load force is stable, the test will precondition the sample at an elongation rate of 0.1 mm/s for 30 s. Allow the tissue to rest for 1 min. While waiting, load the pull-to-failure testing regime.

NOTE: The pre-load force may vary depending on the instrument and the testing conditions. Refer to previous studies where the reported pre-load ranges from 0.015 N to 0.1 N (Baah-Dwomoh et al., 2016; Becker & De Vita, 2015; Donaldson et al., 2021; Moalli et al., 2005; T. Tan et al., 2016).

2.5 Open the testing regime that is programmed to pull to failure. Label the test with the sample name and click on **Okay** to get to the next window. Input the gauge length of the sample and then click on **Next** to transition to the test page.

2.4. Balance all and click on **Start**. Allow the test to run at an elongation rate of 0.1 mm/s until the tissue has been pulled to failure. The test will produce load-displacement data.

3. Calculation of stress, strain, and modulus for tensile testing

3.1. Using the load-displacement data, the cross-sectional area, and the gauge length from the sample, calculate the stress (MPa) and strain (%) as previously reported (S. D. Abramowitch et al., 2009; Andrew Feola et al., 2010; Griffin et al., 2016; Kurtaliaj et al., 2019; T. Tan et al., 2015). Use Equation 3.1 and Equation 3.2 shown below. Note that stretching of the tape during testing should also be accounted for in these calculations.

3.1.1. From the load-displacement curve (**Figure 3.9A,D**), calculate the stiffness (linear slope, N/mm) and ultimate load. From the stress strain curve, calculate the tangent modulus (linear slope, MPa) and the ultimate stress. The linear region of the stress strain curve is

noted in **Figure 3.9B,E** with the calculated tangent modulus from this region shown in **Figure 3.9C,F** for both groups.

NOTE: For both the stiffness and tangent modulus, identify the linear portion by choosing a window of points that maximizes the R^2 value for a linear regression (S. D. Abramowitch et al., 2009; Kurtaliaj et al., 2019).

$$Stress\ (MPa) = \frac{Load(N)}{cross - sectional\ area\ of\ sample\ (mm^2)} \qquad \text{Equation 3.1}$$

$$Strain\ (\%) = \left(\frac{length\ (mm)_{displacement} - length\ (mm)_{original}}{length\ (mm)_{original}}\right) x\ 100 \qquad \text{Equation 3.2}$$

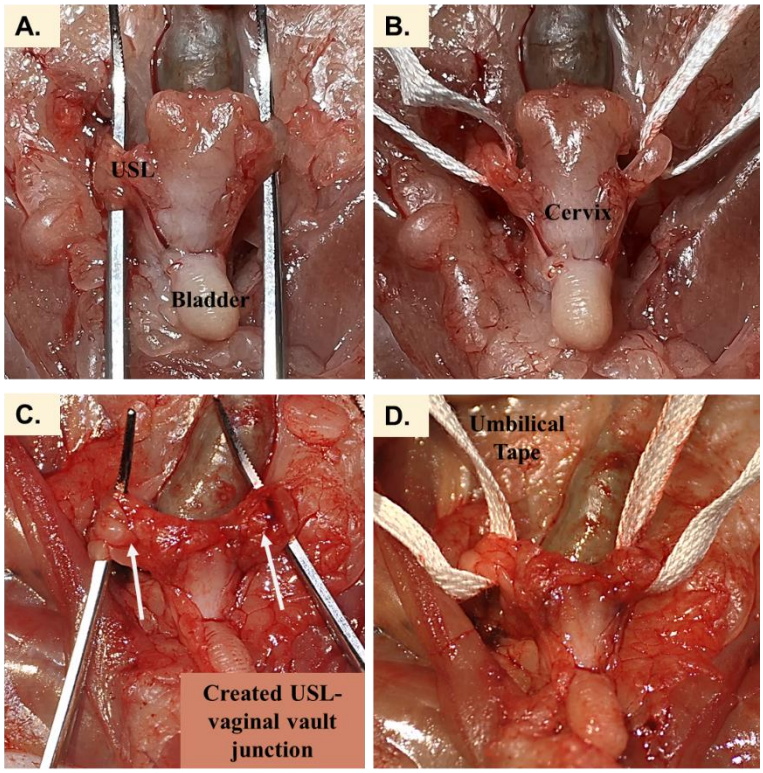

Figure 3.6. Specimen preparation for uniaxial tensile testing. (A) The exposed control USLs before (B) the umbilical tape is threaded behind the tissue. (C) USL-vaginal vault junction after the complete dissolution of the sutures with (B) the umbilical tape threaded behind the tissue in preparation of tensile testing.

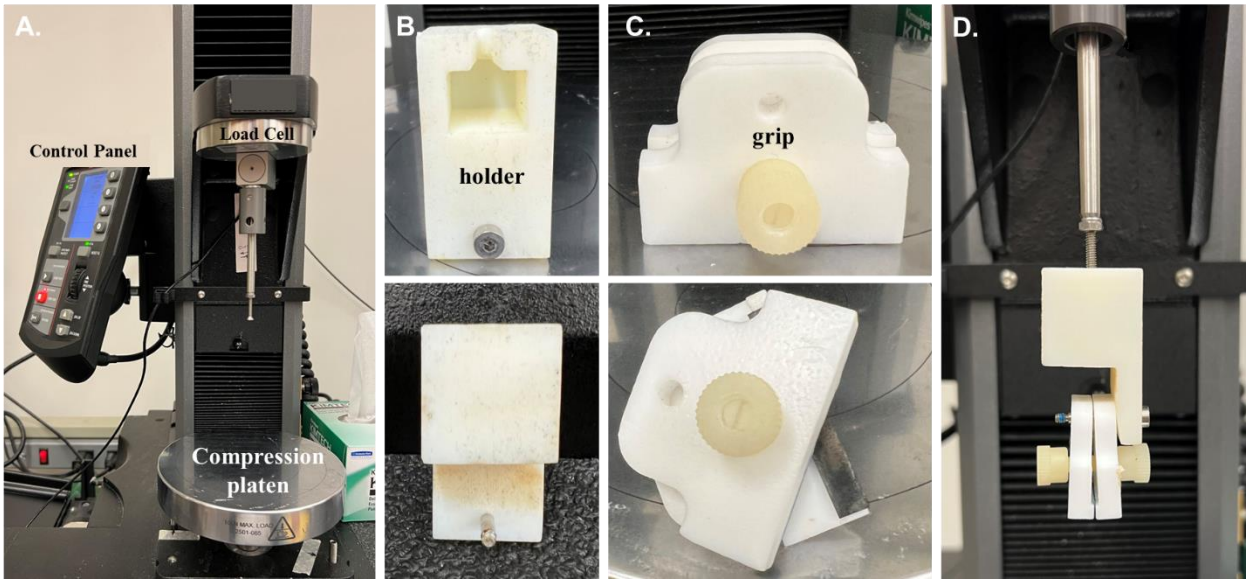

Figure 3.7. The mechanical testing system. (A) The testing system in tensile testing mode used with (B) 3D printed holder and (C) 3D printed sample grip complete with a textured strip to improve grip. Configuration of the pieces shown in panel (D).

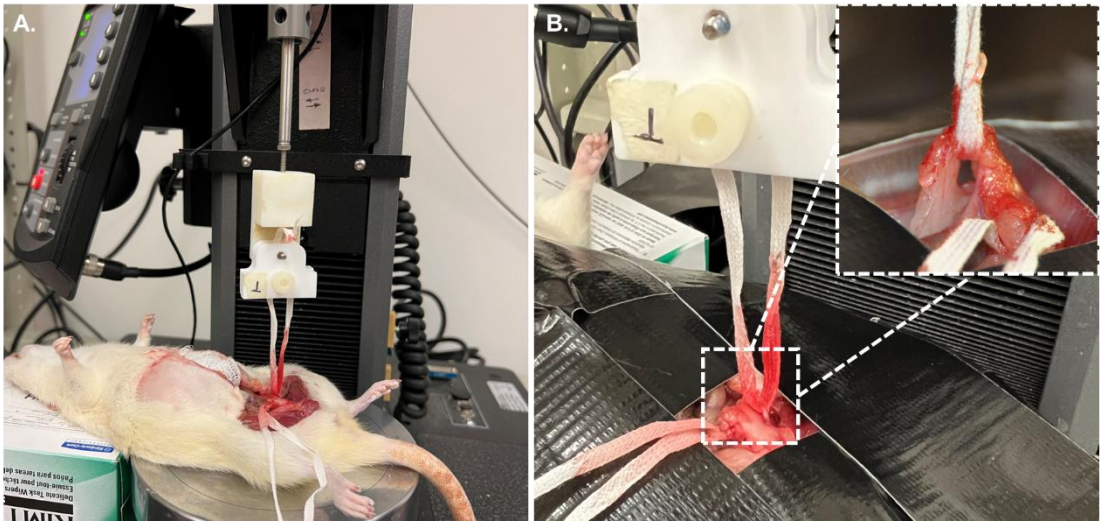

Figure 3.8. Set-up of the tensile testing. (A) The specimen is centered beneath the grip and holder. (B) The animal and tissue surrounding the specimen are held stationary prior to the start of the tensile test. As shown by the inset image, securing the surrounding tissue is essential to isolate the tissue of interest.

3.4. Representative results

3.4.1. Surgical feasibility and uterosacral suture placement

There were no intraoperative complications related to hysterectomy or uterosacral ligament suspension in any of the animals. There was minimal bleeding during removal of the uterine horns, provided the adjacent vasculature was clamped prior to removal. Limited bleeding allowed for good visualization of the uterosacral ligaments for suture placement and prevented intra-operative bowel, rectum, ureteral, or bladder injury. Following placement of the sutures, the newly formed USL-vaginal vault junction prevented movement of the cervical/uterine stump as shown in **Figure 3.5C**. Based on our experience with 16 animal surgeries (n = 8 for both control and USLS groups), a drop in weight should be expected in the first week following surgery with an average loss of 5.7 ± 1.4% from surgery day weight. As expected, the rats slowly gained weight over the subsequent 23 weeks, with an average weight gain of 15.1 ± 4.5% over the course of the experiment.

3.4.2. Mechanical testing of the USLS repair

To demonstrate the functionality of the USLS repair, uniaxial tensile testing was performed. After euthanasia of the animal at the chosen post-operative timepoint, 24 weeks in this study, the surgical area should be carefully dissected to visualize the USL-vaginal vault junction as shown in **Figure 3.6A**. Compared to other methodologies for testing the rat USLs together with other supportive structures and pelvic organs (Lowder et al., 2007; Moalli et al., 2005), the method described here is the first to test the rat USL in an isolated manner. The umbilical tape used in this study was strategically chosen for its flexibility as the tape compliance allowed for minimal disruption of the tissue during tensile testing preparation. Load displacement data, therefore, must be adjusted to account for the small amount of stretch contributed by the umbilical tape. **Figure 3.9** provides an example of data obtained *via* tensile testing with **Figure 3.9A** providing an example of a typical stress-strain plot. Reporting of stress-strain data is recommended as this information is normalized and independent of the size of the specimens (Donaldson et al., 2021) and can be better compared across studies. For the intact uterosacral ligament, we report structural properties such as ultimate load (2.9 ± 0.5 N) and stiffness (0.4 ± 0.1 N/mm) as well as normalized material properties such as ultimate stress (2.1 ± 0.4 MPa), ultimate strain (1.6 ± 0.5) and tangent modulus (4.0 ± 1.1 MPa). In the uniaxial tests performed on the rat reproductive organs and all their supportive tissue connections by Moalli et al., they reported an ultimate load at failure (13.2 ± 1.1 N) and stiffness (2.9 ± 0.9 N/mm) higher than the isolated USL (Moalli et al., 2005). The work done by Moalli and other studies (Baah-Dwomoh et al., 2016; Donaldson et al., 2021) mention the high variability between tested specimens as shown in the data presented here. For the uterosacral ligament suspension repair, we found all structural material properties (stiffness, 0.33 ± 0.13 N/mm; ultimate load, 2.6 ± 1.3 N) and normalized material properties (ultimate stress, 1.8 ± 0.7 MPa; ultimate strain 1.3 ± 0.3; tangent modulus, 3.0 ± 0.9 MPa) to be lower than that of the native USL.

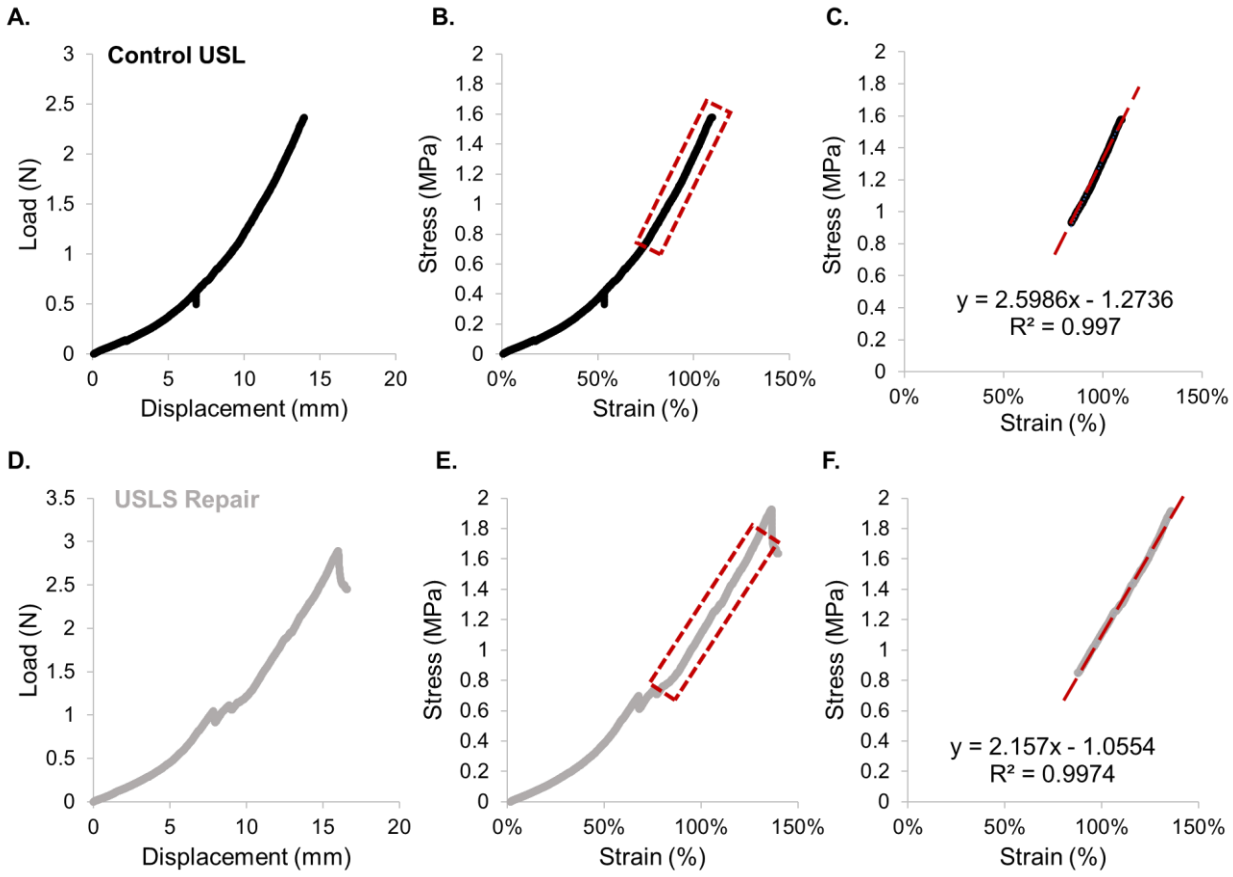

Figure 3.9. Example of tensile test data output and analysis. (A) The load-displacement curve for a control sample followed by (B) the stress strain analysis and (C) the slope of the line curve fit equation showing the tangent modulus in MPa. (D–F) shows the same process for a USLS sample.

3.5. Discussion

The protocol is notable for several reasons. To our knowledge, it is the first published description of USLS in the rat model and will provide future investigators with reproducible steps for performing this procedure in the research setting. Second, we include a novel protocol for tensile testing of the native and surgical interface of the USL. The tensile testing protocol could be utilized in similar studies that investigate new tissue engineering approaches to augment native tissue repairs such as USLS. Moreover, the rat model itself is useful for the study of pelvic floor disorders due to ease of handling/boarding, short lifespan, and cost efficiency compared to larger animal models. Limitations of the protocol include an inability to assess one of the main complications of USLS, ureteral kinking. Despite this, we had no cases of presumed ureteral injury in this study. Another consideration is that the horizontal orientation of the pelvis, small fetal head-to-birth canal ratio, and lack of spontaneous prolapse in the rat model does limit some applicability of results to humans. However, the use of multiparous rats is a strength of this study since this accounts for the leading risk factor in the development of POP (Kenton, Kimberyly; Mueller, 2006).

The establishment of a successful protocol for hysterectomy and USLS in the Lewis rat will be a useful tool for future researchers investigating surgical components of POP, while minimizing variability in testing the mechanical behavior of the USL. Surgical animal models are beneficial in that they allow researchers to design clinically relevant experiments that control for parity, body mass, disease, and nutrition (Donaldson et al., 2021) while mitigating the ethical risk of initial study in humans. Further, standardized models for POP allow researchers to bypass the limitations of human tissue collection. In particular, the tensile testing methods described in this protocol will enable consistency between studies. Previous rodent models tested the mechanical properties of the entire pelvic region, which includes the cervix, vagina, and the multiple pelvic support ligaments (Lowder et al., 2007; Moalli et al., 2005).

The methods described here allow for measurement of the USL in a way that maintains the native spinal and cervical attachments. It should be noted that the tensile testing methods do not assess the USL alone, but rather the USL in combination with its insertion at the sacrum and cervix. This is a strength of the study as it reflects the usual *in situ* forces to which the ligament is subjected. We acknowledge that the mechanical behavior of the isolated ligament would be different if it were tested *ex vivo* without its native attachments. This is especially true since the rat structures are small and limit the feasibility of collecting a sample suitable for *ex vivo* testing. The USLs do experience loading in multiple directions *in situ*, so the uniaxial nature of the test is a limitation, but using this method allows for meaningful comparisons between previous studies of rat USL mechanics (Lowder et al., 2007; Moalli et al., 2005). While there is currently no widely accepted standard mechanical testing protocol, this model will be a useful tool for future tissue engineering studies in the field.

Several steps described in this protocol are critical to the health and well-being of the animals as well as the reproducibility of the USLS surgery and subsequent tensile testing. First, it is essential to obtain both the analgesic and the anti-inflammatory drugs described as the analgesic alone was found to be inadequate for pain management. The prophylactic antibiotic decreases the risk of surgical site infection and is the standard of care in human surgery. Regarding the USLS surgical procedure, avoiding damage to the ovaries and minimizing blood loss are essential for a successful surgery. Steps 3.3 and 3.4 describe separating the top of the uterine horn from the adjacent ovary; care should be taken to maintain this dissection on the side of the uterine horn to prevent disruption of delicate vessels around the ovary, which can result in excessive bleeding. Of note, other investigators have shown that ovarian function is preserved after removal of the uterine horns (Koebele et al., 2019). Moreover, if the ovaries are disrupted or removed, the overall collagen fibril architecture will be disturbed, altering the mechanical properties of its tissues (Daghma et al., 2018; Kafantari et al., 2000). Once the uterine horn is safely separated from the ovary, there is a clear plane of dissection allowing isolation of the uterine horn from the surrounding fat pads and vasculature. Despite the clear plane of dissection, the pedicles along the uterine horn should be secured with a clamp prior to transection with micro scissors. Contrary to surgical practice in humans, we have found that suture ligation of the hysterectomy pedicles is unnecessary, as clamping the pedicle prior to transection ensures adequate hemostasis. Step 1.3.6 of the protocol describes this careful process to minimize blood loss. As the hysterectomy is being performed, great care should be taken to identify the ureters as mentioned in steps 1.3.6 and 1.3.8. Understanding the anatomical proximity of the ureter is critical, as one of the most common complications associated with the USLs in humans is ureteral injury (Manodoro et al., 2018).

In conclusion, we present a novel protocol for performing hysterectomy, uterosacral ligament suspension, and tensile testing of the USL in a rat model. We anticipate that our findings will assist future basic science investigators by providing a clear, reproducible description of these procedures and thereby allow for advancement of pelvic organ prolapse research.

3.6. Acknowledgments

The authors Prof. Silvia Blemker for use of her Instron and Prof. George Christ for use of his surgical space as well as the 3D printed holder and grip. This work was supported by the UVA-Coulter Translational Research Partnership and the DoD (W81XWH-19-1-0157).

CHAPTER 4: SUPRAMOLECULAR FIBROUS HYDROGEL AUGMENTATION OF UTEROSACRAL LIGAMENT SUSPENSION FOR TREATMENT OF PELVIC ORGAN PROLAPSE

This chapter has been adapted from the following publication: Miller, B., Wolfe, W.H., Gentry, J., Grewal, G., Highley, C.B., De Vita, R., Vaughan, M.H., Caliari, S.R. *Supramolecular fibrous hydrogel augmentation of rodent uterosacral ligament suspension for treatment of pelvic organ prolapse*. (*in preparation)*. **2022**.

4.1. Abstract

Uterosacral ligament suspension (USLS) is a common surgical treatment for pelvic organ prolapse (POP). However, the relatively high failure rate of up to 40% demonstrates a strong clinical need for complementary treatment strategies, such as biomaterial augmentation. Herein, we describe the first hydrogel biomaterial augmentation of USLS in a recently established rat model using an injectable fibrous hydrogel composite. Supramolecularly-assembled hyaluronic acid (HA) hydrogel nanofibers encapsulated in a matrix metalloproteinase (MMP)-degradable HA hydrogel create an injectable scaffold showing excellent biocompatibility and hemocompatibility. The hydrogel can be successfully delivered and localized to the suture sites of the USLS procedure, where it gradually degrades over 6 weeks. *In situ* mechanical testing 24 weeks post-operative in the multiparous USLS rat model shows the ultimate load (load at failure) to be 1.70 ± 0.36 N for the intact uterosacral ligament (USL), 0.89 ± 0.28 N for the USLS repair, and 1.37 ± 0.31 N for the USLS + hydrogel (USLS+H) repair (n = 8). These results indicate that the hydrogel composite significantly improved load required for tissue failure compared to the standard USLS, even after the hydrogel degrades, and that this hydrogel-based approach could potentially reduce the high failure rate associated with USLS.

4.2. Introduction

Women's health is an important, but chronically underfunded (Mirin, 2021) and therefore understudied, area of research. Increasing recognition of the unique aspects specific to women's health (Grimm, 2019) has likely been influenced by the National Institutes of Health revised guidelines (*History of women's participation in clinical research*, n.d.) that required "women be included in all clinical studies" and "sex as a biological variable" to be considered beginning in 1994 and 2016, respectively. To address the substantial gaps in medical knowledge, researchers have leveraged tissue engineering approaches to transform our understanding of ovarian follicle development (Shikanov et al., 2009), endometriosis (Gnecco et al., 2020), gynecological cancers (Cook et al., 2022), and other disorders of the endometrium(Murphy et al., 2022). In addition, special journal issues focusing on engineering for women's health (De Vita & Munson, 2021; K. S. Miller et al., 2019; Robinson et al., 2020) and in-depth review articles (Cadena et al., 2020; Fogg et al., 2022) have increased visibility for this body of work. However, there is still much to be done to address the urgent clinical need to develop and investigate translational therapies(Liang et al., 2017). This is especially true for pelvic organ prolapse (POP) as surgical demand is predicted to increase by 50% (J. M. Wu et al., 2011) and outcomes from some treatment options, such as the uterosacral ligament suspension (USLS) procedure, remain discouraging (Aubé & Tu, 2018).

POP is a common condition affecting roughly 50% of parous women (Samuelsson et al., 1999) resulting in the descent of pelvic organs (vagina, bladder, uterus, small bowel, and rectum) due to compromised anatomical support structures (Haylen et al., 2016). In healthy women, the levator ani muscles, the uterosacral ligaments (USLs), and cardinal ligaments support the pelvic floor organs via connective tissue attachments to the pelvis, while distal structures of the perineal body reinforce this supportive framework (Herschorn, 2004; Jelovsek et al., 2007). Due to the relatively high failure rate of some native tissue repairs, an estimated one third of POP surgeries in 2010 relied on non-absorbable lightweight polypropylene (PP) mesh. However, unacceptable post-surgical complications, such as tissue erosion, led the FDA to remove transvaginal mesh kits from the market by 2019 (*FDA takes action to protect women's health, orders manufacturers of surgical mesh intended for transvaginal repair of pelvic organ prolapse to stop selling all devices*, 2019). While PP mesh is still used by many pelvic surgeons to perform sacrocolpopexies, the current international climate and associated litigation surrounding the use of mesh leads many patients and their surgeons to seek mesh-free treatment options. The USLS procedure is a native tissue (suture only) alternative (Aubé & Tu, 2018) to mesh augmentation, but it is plagued by a failure rate of up to 40% (Jelovsek et al., 2018; Lavelle et al., 2016). This procedure utilizes the dense collagenous sacral region of the USL to restore the vagina and surrounding structures to their anatomical position in the abdominal compartment via absorbable or non-absorbable sutures. According to recent studies (J. M. Wu et al., 2014), a woman's lifetime risk of undergoing prolapse surgery is approximately 20% (J. M. Wu et al., 2014), and that number is expected to rise in the coming years. Therefore, there is an urgent clinical need to develop regenerative medicine strategies to provide safe and effective alternatives to mesh-based augmentation or suture only surgical procedures for POP.

There is growing interest in synthetic or biological materials to augment native tissue repairs (Gigliobianco et al., 2015; X. Wu et al., 2020). Namely, biodegradable polymers engineered to interact with the host tissue to promote constructive remodeling and integration (Christman et al., 2022; Mukherjee et al., 2019) could be a promising therapeutic platform for prolapse repair. Hydrogel biomaterials specifically provide an attractive alternative to mesh-based treatments due to the variety of material systems and chemistries available. The ideal biomaterial for use in pelvic floor reconstructive surgeries is yet to be determined (Krause & Goh, 2009), but refinement of animal models can assist in the development of new materials. Several animal models including rats, mice, rabbits, sheep, swine, and non-human primates have been utilized (Couri et al., 2012) in the study of POP, with rodent models being optimal due to low cost and general accessibility. Despite this, the first POP surgical treatment rodent model was only recently established by our team (B. J. Miller et al., 2022). Previous studies investigating materials for POP repair in rats have used an abdominal hernia repair model (Chapple et al., 2015; Hansen et al., 2019; Hympanova et al., 2017; Paul et al., 2019, 2020; Y. Wang et al., 2019) due to the convenience of the established animal model (Ayubi et al., 2008; Klinge et al., 1998) and perceived conservation of outcomes between the abdominal wall and the pelvic floor (Whooley et al., 2020; Yuan et al., 2021). Conversely, while hernia repair studies have demonstrated beneficial outcomes using increasingly stiff constructs (Vashaghian et al., 2018; X. Wu et al., 2020), pelvic floor studies have found that stiffness is directly linked to the deterioration of vaginal smooth muscle and the surrounding pelvic floor (A. Feola et al., 2013; Paul et al., 2020). This "stress-shielding" phenomena has also been seen in studies of bone (De Witte et al., 2018) as well as tendons and ligaments (C. H. Lee et al., 2005), where the stiffer material shields the adjacent tissue from experiencing physiological loads (Tomasek et al., 2002), causing the less stiff tissue to degenerate (Krause & Goh, 2009). Given this information, the abdominal wall hernia repair procedure is not the proven "proof of concept" model (Chang et al., 2017; Yuan et al., 2021) that it was once thought to be.

To address the need for alternative materials and a suitable animal model to investigate prolapse repair, our lab developed a hyaluronic acid (HA) based fibrous hydrogel (B. Miller et al., 2021) as well as a rodent USLS model (B. J. Miller et al., 2022) to investigate the augmentation of native tissue repair procedures. In this work, we present what we believe is the first study to use a rodent prolapse model to investigate a hydrogel biomaterial for the treatment of POP. The central aim of this study was to determine the impact of augmenting the USLS with a degradable hydrogel to restore mechanical integrity of the pelvic floor. A multiparous rat model was used due to its cost effective nature and literature demonstrating the similar USL anatomy, cellularity, and matrix composition between rodents and humans (Iwanaga et al., 2016). Since failure of the native tissue repair is not well understood, the strength of the USL structures with their anatomical connections was assessed *in situ*. Our hypothesis was that the hydrogel augmentation of USLS would improve tissue integration at the USL-vaginal vault junction, therefore improving stability of the repair compared to sutures alone. Using a mechanical pull-off test (Gent & Kaang, 1986), surgeries with the hydrogel augmentation demonstrated a significant increase in force required for failure compared to the USLS repair alone.

4.3. Materials and Methods

Ad-MeHA and CD-MeHA hydrogel synthesis: Hyaluronic acid (HA) was functionalized with photoreactive methacrylates (Me) (Sundararaghavan & Burdick, 2011) and then either adamantane (Ad) or β-cyclodextrin (CD) (B. Miller et al., 2021) as previously described. Briefly, the HA backbone was methacrylated to produce methacrylate-modified HA (MeHA) via esterification with the primary hydroxyl group of sodium HA at basic pH, between 8 and 9. Next, the MeHA was reacted with proton exchange resin and titrated with tert-butyl ammonium salt (TBA)-OH to yield methacrylated HA-TBA (MeHA-TBA). Ad-modified MeHA (Ad-MeHA) and CD-modified MeHA (CD-MeHA) were then synthesized by anhydrous coupling. In Ad-MeHA synthesis, MeHA was modified with 1-adamantane acetic acid via di-tert-butyl bicarbonate (BOC_2O)/4-dimethylaminopyridine (DMAP) esterification. Separately, CD-MeHA was prepared by coupling 6-(6-aminohexyl)amino-6-deoxy-β-cyclodextrin (CD-HDA) to HA via (benzotriazol-1-yloxy) tris(dimethylamino) phosphonium hexafluorophosphate (BOP) amidation. Synthesis products were dialyzed against deionized water, frozen, and lyophilized. The degree of Me modification was controlled by the amount of methacrylic anhydride introduced during synthesis, determined to be 16%. Modification of the HA backbone with Ad and CD was determined to be 16.5% (Figure S4.1) and 16% (Figure S4.2) respectively, with all percentages calculated by ^{1}H NMR.

Solid-phase peptide synthesis: Using a Liberty Blue automated microwave-assisted peptide synthesizer, peptides were synthesized via solid-phase synthesis as described previously (Patterson & Hubbell, 2010; Wade, Bassin, Rodell, et al., 2015). Briefly, rink Amide MBHA high-loaded (0.78 mmol/g) resin was used along with solid-supported Fmoc-protected amino acid residues. The resin was swelled with 20% (v/v) piperidine in DMF and the amino acids were sequentially added from C to N-terminus. The resulting peptides were collected and cleaved in 92.5% trifluoroacetic acid, 2.5% triisopropylsilane, 2.5% (2,2- (ethylenedioxy)diethanethiol), and 2.5% water for 2 hr and filtered to separate the resin. Two methacrylate-modified peptides were synthesized for use in the hydrogel system: an MMP-degradable peptide (MeP, Methacrylate-GGNS-VPMS↓MRGG-GNCG, Figure S4.3) and carrier peptide (Methacrylate-GKKCG) for later fluorophore conjugation. A Cy-7.5 fluorophore (Cyanine7.5-maleimide, Lumiprobe) was conjugated to the carrier peptide via thiol-maleimide click chemistry, mixing equal molar amounts in 1x PBS for 2 hrs. The final product was a Cy7.5 labeled methacrylated peptide (Cy7.5-Me). Peptides were precipitated in cold ether, dried overnight, resuspended in water, frozen, and lyophilized. Synthesis was confirmed via matrix-assisted laser desorption/ionization (MALDI).

MePHA hydrogel synthesis: Methacrylated degradable peptide (MeP) modified HA (MePHA) was synthesized as previously described (Wade, Bassin, Rodell, et al., 2015). Briefly, the HA backbone was modified with maleimide groups to facilitate the aqueous addition of the methacrylated degradable peptide (MeP) via thiol-maleimide "click" chemistry. In the first step, maleimide HA (MaHA) was synthesized by reacting aminated maleimide salt with tetrabutylammonium-HA (HA-TBA) via a BOP coupling agent to form an amide linkage between the carboxyl group of HA and the amine group of the maleimide salt. The thiolated peptide (containing a cysteine amino

acid) was synthesized with a terminal methacrylate group allowing later UV-initiated crosslinking capabilities. ^{1}H NMR confirmed 22% maleimide modification of the HA backbone (Figure S4.4) followed by successful conjugation with the MeP to produce MePHA (Figure S4.5).

Electrospinning: Ad-MeHA and CD-MeHA were dissolved at 2% (w/v) in DI water along with 3.5% (w/v) poly(ethylene oxide) (PEO, 900 kDa) and 0.05% (w/v) Irgacure 2959 (I2959) for 24-48 hr prior to electrospinning. The polymer solutions were electrospun using an Elmarco NanoSpider (NS Lab) with the following collection parameters: applied voltage: ~ 45 kV, electrode distance: 22 cm, orifice diameter: 0.7, substrate: Teflon paper, substrate speed: 20 mm/min, carriage speed: 100 mm/sec. Hydrogel nanofibers were deposited onto Teflon paper, placed into a container which was purged with nitrogen, and crosslinked with UV light (254 nm) for 10 min (VWR Crosslinker Box, 115V).

Hydrogel formulations: Our lab has previously described the process of collecting and preparing the guest and host electrospun fibers (B. Miller et al., 2021). Briefly, guest Ad-MeHA and host CD-MeHA fibers were hydrated (0.1% w/v in DI water) overnight at 37°C to remove PEO from the electrospinning process, centrifuged, supernatant discarded, and then lyophilized. Once dry, the fibers were again hydrated at 0.1% w/v in DI water, allowed to swell at 37°C for at least 2 hr, and then passed through needles of progressively smaller gauge sizes (16G-30G) via trituration. This process separated any adjoined fibers and resulted in a reproducible fiber suspension. MePHA (6 w/v%) was added to envelope the Ad-MeHA/CD-MeHA mixed fibers along with 1 mM lithium acylphosphinate (LAP) to allow for UV light initiated (365 nm, 10 mW cm^{-2}) polymerization. Final formulation resulted in 70 v/v% of fibers and 30 v/v% of the MePHA with LAP solution.

Rheology: All rheological measurements were performed on an Anton Paar MCR 302 rheometer with the plate temperature set at 37°C as described previously.(B. Miller et al., 2021) The hydrogel formulation was tested using a parallel plate (PP08-S; 8 mm diameter, sand blasted) geometry and 25 μm gap distance. Injectability of the hydrogel formulation was tested via a cyclic deformation test alternating between 0.5% and 250% strain to verify shear-thinning and self-healing capabilities. Next, a time sweep (1 Hz, 0.5% strain) with UV crosslinking (365 nm, 10 mW cm^{-2}, 2 min) was performed.

Hemocompatibility and cytocompatibility evaluations: Evaluation of hemocompatibility and cytocompatibility was conducted using the red blood cells (RBCs) rats and via an Alamar blue assay (Invitrogen) using human mesenchymal stromal cells (hMSCs), respectively. *In vitro* testing of the hydrogel cytotoxicity followed ISO 10993 standards where the hydrogel components were added to cell culture media (1% w/v) and then applied to a monolayer culture of hMSCs. Cells were seeded at 5000 hMSCs per well in a 48-well plate with the Alamar blue applied at predetermined time intervals of 1 and 3 days. Samples were read by a plate reader at 565/595 nm after incubation for 5 h in the dark. Hemolysis testing followed ISO 10993 and ASTM F756 standards where blood was harvested immediately prior to assay preparation. Hydrogel components were prepared as solid hydrogels as the fresh blood was suspended in 0.01% heparin

(Sigma Aldrich) in PBS. The mixture was immediately centrifuged at 1000 rpm for 15 min and then washed with PBS until the supernatant above the pellet of RBCs was clear. The RBCs were then diluted using PBS and incubated for 1 h at 37°C with the hydrogel components. After incubation, the RBCs were collected and centrifuged again at 1000 rpm for 15 min before the absorbance of the supernatants were read at 540 nm using a plate reader. The results were calculated as hemolysis (%)

$$\text{Hemolysis (\%)} = \frac{\text{OD}_t - \text{OD}_n}{\text{OD}_p - \text{OD}_n} \times 100\% \qquad \text{Equation 4.1}$$

where OD_t, OD_n, and OD_p were the absorbance values of the samples, negative control (PBS), and positive control (0.1% Triton-X-100), respectively.

Animal Care: This study was conducted in compliance with the Animal Welfare Act, the Implementing Animal Welfare Regulations, and in accordance with the principles of the Guide for the Care and Use of Laboratory Animals. The University of Virginia Animal Care and Use Committee approved all animal procedures. A total of 24 multiparous female Lewis rat breeders (Charles River Laboratories) weighing 274.8 ± 19.3 g were pair housed in a vivarium accredited by the American Association for the Accreditation of Laboratory Animal Care and provided with food and water *ad libitum*. Animals were between 4 and 6 months of age to accommodate the 2 litter requirement. Animals were maintained on a 12-hour light-dark cycle.

Anesthesia, pain management, and antibiotics: All animal-related details were described in detail previously (B. J. Miller et al., 2022). Briefly, animals were anesthetized via isoflurane and the surgical site was aseptically prepared by repeated washes with alcohol and iodine. The depth of anesthesia was monitored by the response of the animal to a slight toe pinch, where the lack of response was considered the surgical plane of anesthesia. Core temperature was maintained using a heated water perfusion system. Rats were administered slow-release buprenorphine (Bup XR – 72 hr; 1.3 mg/kg, subcutaneously), slow-release meloxicam (72 hr; 1.0 mg/kg, subcutaneously), and baytril (10 mg/kg, subcutaneously) prior to surgery. Since meloxicam is known to cause dehydration, rats were also administered 0.9% sterile saline (10 mL/kg, subcutaneously). Animal pain and distress were monitored daily by qualified members of the veterinary staff to determine the need for additional analgesia.

Surgical procedures: Using aseptic technique, a vertical midline skin incision was made along the abdomen and the fascia was separated to expose the underlying abdominal cavity. Hysterectomy was performed, where the uterine horns were trimmed after separation from the ovaries and fat pads, leaving the cervix, vagina, and its support tissues intact. One delayed absorbable suture (3.0 polydiaxanone, PDS II, Ethicon) was placed through the vaginal vault and the exposed uterosacral ligament (USL) bilaterally. Tying the sutures down simultaneously closed the vaginal vault and elevated it towards the USLs. A single uterosacral stitch was used due to limited space along the USL in the rat model and our goal to have spatial ability to perform mechanical testing of the ligament. For hydrogel augmentation, material components were sterilized separately and then

prepared aseptically. A total of 40 µL (20 µL each side) was delivered over the sutures and then UV crosslinked (365 nm, 10 mW cm^{-2}, 2 min). Animals in the sham experimental group were used for healthy animal controls to assess normal tissue properties. Animals were randomly assigned to one of the following experimental groups: sham surgery with no prolapse repair (USL; $n = 8$), prolapse repair (USLS; $n = 8$), prolapse hydrogel repair (USLS+H; $n = 8$).

In vivo *hydrogel degradation analysis:* To evaluate *in vivo* hydrogel degradation, hydrogel nanofibers were labeled with the Cy7.5-Me peptide via UV light-initiated conjugation in the presence of LAP photoinitiator. The fluorophore was covalently bound via the methacrylates present on the surface of the hydrogel fibers during photocuring. Serial images were taken during a 6 week period postoperative using a LagoX live imaging system (ex: 770 nm, em: 810 nm) with signal intensity measured by integrating equivalent areas over the region-of-interest. Quantified signal was normalized to peak intensity for individual scaffolds immediately following surgery and then averaged to obtain degradation profiles for each scaffold ($n = 4$).

Mechanical testing of the USLS and prolapse repair junction: At 24 weeks post-surgery, the uterosacral ligament (USL) or USLS prolapse repair junction (USLS, USLS+H) were prepared for mechanical testing using a single column Instron (5943 S3873) universal testing system. A 10 N load cell was used for testing. Methods were described, including a video demonstration, in previous work (B. J. Miller et al., 2022). Briefly, umbilical tape (Ethicon U10T) was threaded beneath the suture/new tissue formation between the vaginal vault and the uterosacral ligament. The tissue was pre-loaded at 0.015 N and then preconditioned at an elongation rate of 0.1 mm/s for 1 min. The tissue was then pulled to failure at the same elongation rate.

Statistical Analysis. All data are presented as means and their standard deviations (SDs). The data were statistically analyzed by one-way ANOVA tests with multiple comparisons using GraphPad Prism 9.0. P values < 0.05 were considered statistically significant where $*P < 0.05$, $**P < 0.01$, $***P < 0.001$ and $****P < 0.0001$.

4.4. Results and Discussion

This study presents the experimental outcomes following the first investigation of a hydrogel biomaterial for augmentation of the uterosacral ligament suspension (USLS) procedure in rats. We utilized our lab's recently developed rodent USLS model (B. J. Miller et al., 2022) and supramolecularly-assembled injectable and photocurable fibrous hydrogel (B. Miller et al., 2021) as a potential therapeutic for the treatment of POP. This is significant since there is an urgent clinical need for materials intended for the treatment of prolapse to be tested in pelvic floor models. While the mechanisms of mesh adverse events are not fully understood (A. Feola et al., 2013), it has become clear that the planes of fat, muscle, and fascia of the abdominal hernia repair rat model (Whooley et al., 2020) do not properly represent the smooth muscle and mucosa of the vagina and surrounding pelvic floor structures. Moreover, in addition to the USLS augmentation being more relevant for the investigation of potential prolapse therapeutics, previous work has demonstrated several similarities between rat and human USLs(Iwanaga et al., 2016), further demonstrating the benefits of the rodent model. The rodent model also allows researchers to control several variables, such as parity, which we controlled for in this study. To the authors' knowledge, this is the first study to investigate a potential non-mesh therapeutic for prolapse within the pelvic cavity.

4.4.1. Preparation of the injectable and fibrous hydrogel

Of the many classes of materials that have been used in tissue engineering, hydrogels have emerged as one of the most prominent and versatile as they can provide cells with a hydrated 3D environment that mimics native soft tissues (Spicer, 2020). Polymeric hydrogels are especially attractive biomaterial platforms due to their tunable mechanical properties and ease of processing (Caliari & Burdick, 2016; Drury & Mooney, 2003). With the stiffness of mesh-based augmentation implicated in vaginal tissue degeneration following implantation, there is an urgent clinical need for materials that can mimic mechanical properties of the pelvic floor tissues. We chose HA as our therapeutic biomaterial platform due to its hydrophilicity, degradability *in vivo*, and its role in supporting tissue repair (Highley et al., 2016). Here, the guest-host assembled HA hydrogel nanofibers were encapsulated in a matrix metalloproteinase (MMP)-degradable HA hydrogel that was delivered to the suture sites of the USLS procedure (**Figure 4.1**). The guest and host modified fiber system leverages supramolecular chemistry that both enables facile injection for minimally invasive delivery and stabilizes the hydrogel post-injection. Both guest and host hydrogel fibers also included photocrosslinkable methacrylate groups for stabilizing the fibers following electrospinning. When the hydrogel fibers are mixed, the guest and host groups interact via hydrophobic non-covalent associations, creating a solid hydrogel until shear forces during injection disrupt the non-covalent interactions creating a "liquid-like" state. In **Figure 4.1C**, delivery of the hydrogel following hysterectomy is schematically shown where the hydrogel is applied over the suture sites of the USL-vaginal vault created during the USLS procedure. For added stabilization of the self-assembling fibers within the abdominal cavity, the guest and host fibers were encapsulated in methacrylated peptide-modified HA (MePHA) engineered to be MMP-degradable, which allowed for secondary crosslinking via UV light.

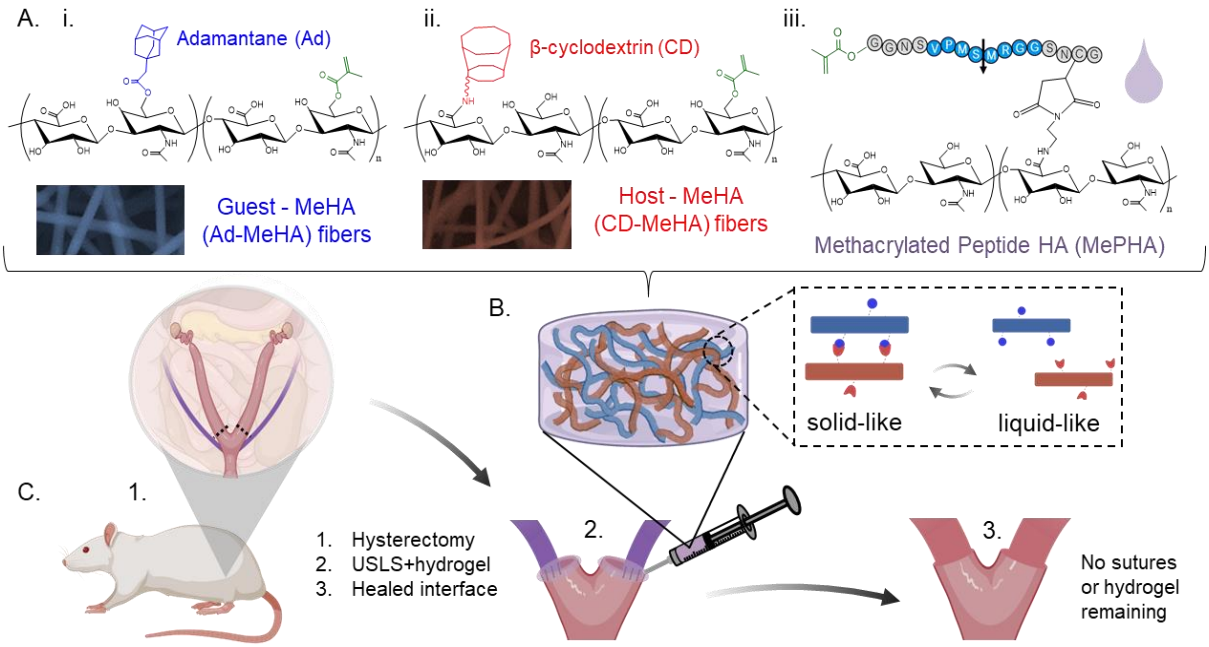

Figure 4.1. Schematic presentation of the composition of the fibrous injectable hydrogel system and uterosacral ligament suspension (USLS) augmentation process. A) Hyaluronic acid (HA) was modified with either i) the guest (adamantane, Ad) or ii) host (β-cyclodextrin, CD) molecules to create guest and host hydrogel fibers. Both guest- and host-modified HA also contained methacrylate groups to enable fiber stabilization via photocrosslinking after electrospinning. Separately, HA was functionalized with iii) a matrix metalloproteinase (MMP)-degradable photocrosslinkable peptide for encapsulating the fibers to produce B) a "solid-like" composite hydrogel capable of shear-thinning for injectable delivery to C) the sutures of the USLS procedure following hysterectomy. In situ photocrosslinking produced a mechanically stabilized biomaterial (shear modulus ~ 4 kPa) that was fully degraded, as were the sutures, by the end of the study (24 weeks post-operative).

HA is an advantageous polymer choice in hydrogel design because it can be modified with reactive crosslinking groups to enable control of material biophysical properties (i.e., stiffness) and electrospun to create extracellular matrix (ECM)-like nanofibers mimicking native tissue (B. M. Baker et al., 2015; Ji et al., 2006; Jun et al., 2018). However, replicating host tissue properties following prolapse surgery is difficult without literature to define biomechanical properties. Studies done on the human prolapsed vagina report viscoelastic mechanical properties (Peña et al., 2010) and an elastic modulus range of 2 – 13 MPa (Martins et al., 2013). The few studies that have investigated rodent pelvic support fixed the entire pelvic region and reported a linear stiffness of ~ 3 N mm^{-1} for parous rats (Lowder et al., 2007; Moalli et al., 2005). To our knowledge, there have been no experimental studies conducted on the mechanics of the pelvic floor tissues following surgical treatment of POP, likely due to lack of available tissue samples and lack of prolapse repair animal models. Ideally, the hydrogel augmentation should enhance the properties of the structurally impaired vaginal tissue. Therefore, this study utilized our lab's recently developed fibrous hydrogel platform (B. Miller et al., 2021) as a first step in understanding ideal biomaterial design for the augmentation of prolapse repair. Oscillatory shear rheology (**Figure 4.2**) robust hydrogel mechanical properties under low strain conditions and underwent reverse gelation at

higher strains mimicking injection prior to UV crosslinking. This is shown via a storage modulus (G') that is higher than the loss modulus (G") of 3.85 ± 0.61 kPa vs 0.65 ± 0.11 kPa respectively in conditions of low strain and a G' that is lower than the G" of 0.17 ± 0.01 kPa vs 0.53 ± 0.03 kPa respectively (n = 3). Importantly, the hydrogels showed full recovery of their viscoelastic properties after cyclic straining (**Figure 4.2A**). Once UV light was applied to the material, the storage modulus rapidly increased to 4.91 ± 0.51 kPa, demonstrating the stabilization of the hydrogel that would form over the suture tissue interface for the USLS augmentation (**Figure 4.2B**). Crosslinking was carried out with 365 nm light at an intensity of 10 mW cm^{-2} for 2 min.

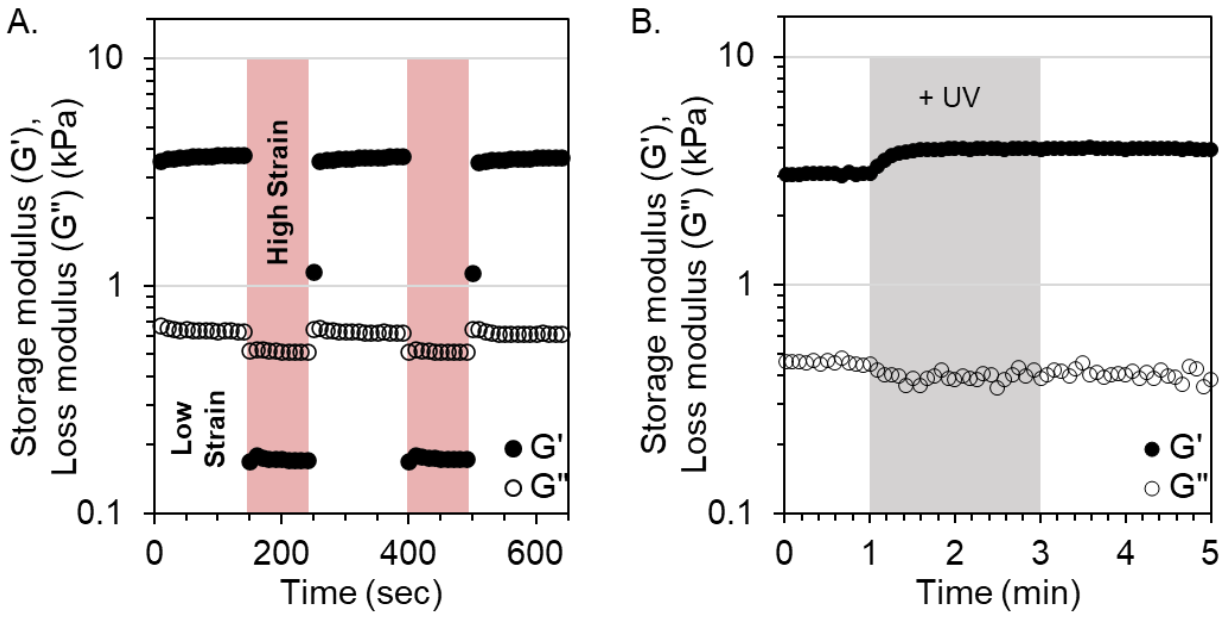

Figure 4.2. The mechanical properties of the fibrous hydrogel were measured using oscillatory shear rheology, showing A) a five-step strain sweep of low strain (0.5%, 100 s) and high strain (250%, 100 s) to illustrate the shear-thinning and self-healing properties of the hydrogel. Guest-host interactions between the fibers produced a solid-like material shown by the higher storage moduli than storage moduli at low strain. With the liquid-like behavior at high strain, shown by the storage moduli being lower than loss moduli, the material demonstrated shear-thinning and self-healing properties. B) In the presence of LAP photoinitiator, 2 min of UV light exposure increased the storage modulus of the material, indicating the crosslinking of the free methacrylates of the encapsulating MePHA hydrogel. n = 3.

4.4.2. Biocompatibility of the material in vitro

Many hydrogels formed from natural materials such as HA offer inherent biocompatibility (Highley et al., 2016; Hui et al., 2019). However, it is still important to demonstrate *in vitro* biocompatibility of any developed material system prior to use *in vivo*. Therefore, hemocompatibility and cytotoxicity assays were performed to evaluate the biocompatibility of the fibrous hydrogel composite. **Figure 4.3** shows the cytotoxicity of each hydrogel component (Ad-MeHA, CD-MeHA, and MePHA) when exposed to human mesenchymal stromal cells (hMSCs) in culture. There were no statistically significant differences for cell metabolic activity in the polymer groups compared with the PBS control group cultured for 1 and 3 days. Metabolic activity, normalized to PBS control levels after one day, were shown to be 132.3 ± 25.1 % for Ad-MeHA, 190.8 ± 33.5 % for CD-MeHA, and 158.4 ± 23.1 % for MePHA after one day of culture.

Metabolic activity after three days increased to 179.9 ± 34.1 % for Ad-MeHA, 193.6 ± 16.1 % for CD-MeHA, and 185.8 ± 37.7 % for MePHA (n = 9). These results are in alignment with the previously reported hMSC cell viability using the supramolecular fiber system which demonstrated ≥ 85% viability following injection and after 7 days of culture (B. Miller et al., 2021).

Unlike the *in vitro* studies, materials implanted *in vivo* will encounter the surrounding tissue as well as bodily fluids such as blood. While the fibrous hydrogel is designed to mimic the native ECM and support tissue function, interactions between the biomaterial and blood should also indicate compatibility prior to implantation. Therefore, assays that investigate the reaction of red blood cells (RBCs) with the scaffold provide useful information regarding possible consequences of biomaterial-blood interactions (Bélanger & Marois, 2001). **Figure 4.3B** shows the hemocompatibility for each component using freshly collected rodent RBCs. After incubation with the material components, the RBCs showed no obvious hemolysis compared to the Triton-X100 group (positive control). RBC survival rates were shown to be 99.6 ± 0.2 % for Ad-MeHA, 99.5 ± 0.4 % for CD-MeHA, and 99.3 ± 0.7 % for MePHA, with the overall material showing a survival rate of 99.4 ± 0.4 % (n = 9). The low hemolysis ratio indicates that the fibrous hydrogel scaffold possesses satisfactory blood compatibility. Together, these *in vitro* experiments demonstrated biocompatibility of the fibrous hydrogel.

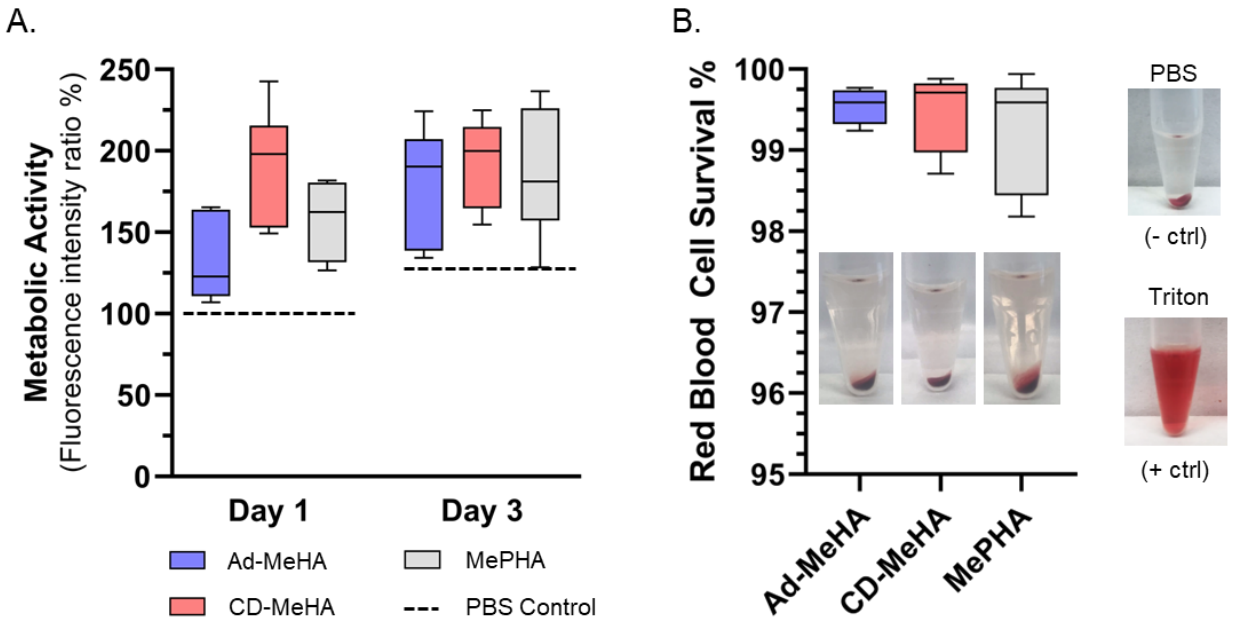

Figure 4.3. In vitro cytocompatibility and hemocompatibility tests. A) Metabolic activity, measured via an Alamar blue assay, of human mesenchymal stromal cells cultured in the presence of hydrogel components for 1 and 3 days compared to cells cultured with PBS (dashed lines). B) Percentage of rat red blood cell (RBC) survival following incubation with hydrogel components. Pictures of the RBCs after centrifugation include PBS (negative control) and Triton-X100 (positive control).

4.4.3. Augmentation of rodent USLS

The overall body of tissue engineering literature for POP repair is dominated by mesh-based augmentation, with the implication that native tissue and mesh-based repairs are the only suitable treatment options for POP. With this narrow focus on mesh-based therapeutics, it is unsurprising that the search for ideal tissue remodeling materials for urogynecological repair is ongoing. A lack of accessible, and surgically accurate, animal models is at least partially to blame for the lack of non-mesh biomaterial investigation. In fact, just last year Bickhaus and colleagues were the first to use a rodent model to investigate a new polycarbonate urethane mesh for pelvic reconstruction via implantation in the vagina (Bickhaus et al., 2021). However, this study still focused on a mesh construct and used a surgical method not used in humans when repairing prolapse. By contrast, our rodent USLS procedure mimics the surgery in humans, establishing this work as the first study to investigate biomaterial augmentation for prolapse repair in a surgically accurate rodent model.

In this study, we aimed to investigate our fibrous hydrogel composite using our established Lewis rat USLS surgery model (B. J. Miller et al., 2022). All animals were maintained and treated according to approved UVA IACUC protocol. All rats were multiparous meaning that they had delivered prior litters (two in our study). Twenty-four Lewis rats (Charles River Laboratories) between 4 and 6 months of age were used to accommodate the two-litter requirement. Detailed surgical instructions with reproducible steps are published elsewhere (B. J. Miller et al., 2022). Briefly, following anesthetization using isoflurane and aseptic preparation of the surgical site, a vertical midline skin incision was made down the linea alba and the muscle layer underneath. Removal of the uterine horns (hysterectomy) created the vaginal vault structure with the intact USLs directly below (**Figure 4.4A**). The USL-vaginal vault interface was created by suturing the remaining vaginal vault tissue to the USLs (**Figure 4.4B**). Animals were randomly assigned to one of the following experimental groups: sham surgery with no prolapse repair (USL; $n = 8$), prolapse repair (USLS; $n = 8$), or prolapse repair with hydrogel augmentation (USLS+H; $n = 8$).

For the animals randomly assigned to the USLS+H experimental group, the injectable fibrous hydrogel was administered and then UV crosslinked to stabilize the material over the suture sites (**Figure 4.4C**). Prior to delivery, the fibrous hydrogel composite was sterilized. Each component (Ad-MeHA fibers, CD-MeHA fibers, MePHA) were sterilized by overnight lyophilization followed by germicidal UV irradiation for 2-3 hr. Additionally, the LAP photoinitiator stock solution was sterile filtered before use. The supramolecular nature of the guest-host fibers kept the 20 µL of hydrogel delivered to each suture site, total of 40 µL per animal, localized while the UV crosslinking further stabilized the material. We chose UV photopolymerization for *in situ* stabilization as it is a commonly used technique for covalent crosslinking of hydrogels (Basurto et al., 2022; Kyburz & Anseth, 2015; Tibbitt & Anseth, 2009). However, to utilize the minimally invasive capabilities of the fibrous hydrogel in another animal model or in human treatment, alternative *in situ* stabilization mechanisms such as redox-initiated polymerization would potentially need to be explored. Delivery of the hydrogel was not minimally invasive in this study, but the benefit of the self-healing property of the material cannot be overstated.

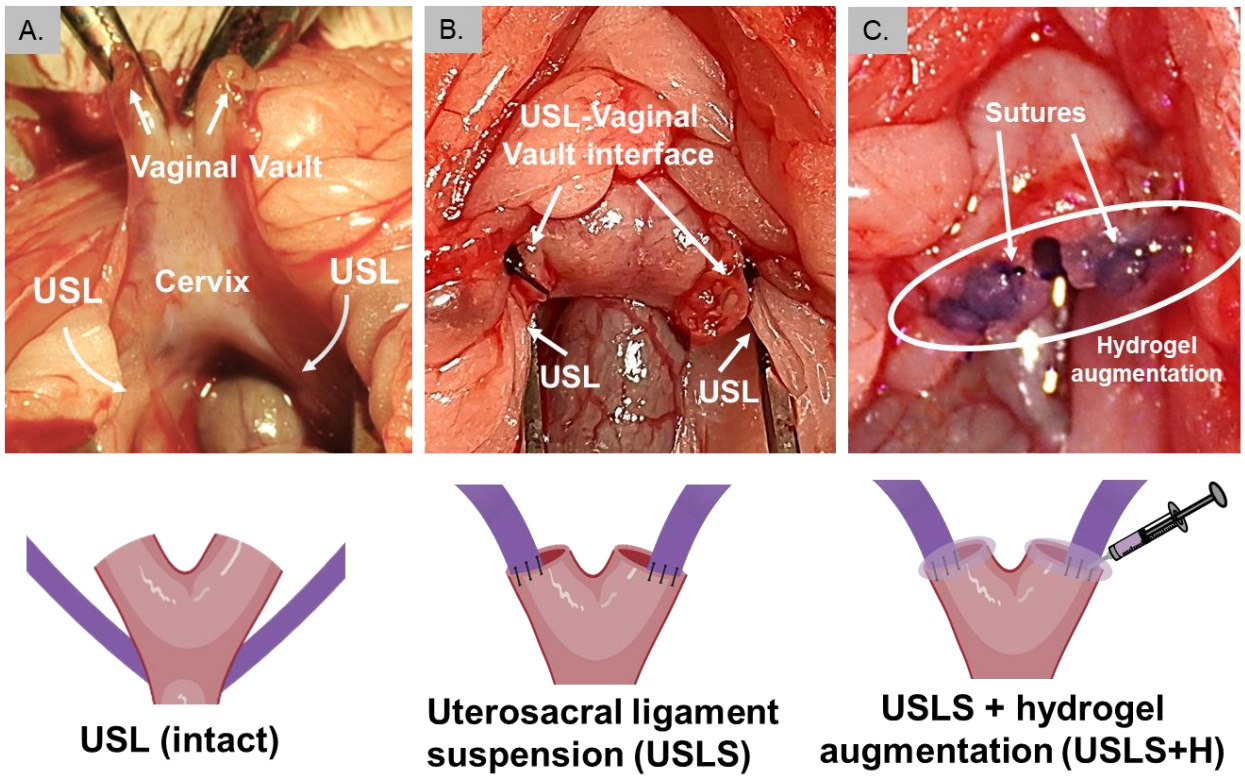

Figure 4.4. Schematic presentation of the uterosacral ligament suspension (USLS) surgical process and hydrogel augmentation (USLS+H). A) Removal of the uterine horns creates the vaginal vault structures with the USLs seen directly adjacent to the cervix. B) The USLS procedure secures the vaginal vault high on the USLs via a single suture such that the vaginal vault is elevated toward the sacrum. C) For hydrogel augmentation, 20 µL of hydrogel per side was administered such that the suture at the USL-vaginal vault interface was completely covered prior to 2 min of UV crosslinking to further stabilize the hydrogel.

The syringe and needle delivery allowed for precise placement and minimized migration of the material prior to UV stabilization. Material migration is a known issue when implanting biomaterials *in vivo* (Spicer, 2020). Given the exposure of the implanted material to the abdominal cavity, the USLS model is no different. With these things in mind, other self-healing biomaterials may be good candidates to investigate for prolapse repair due to the benefit of localized delivery.

4.4.4. In vivo assessment of hydrogel degradation

In developing materials for pelvic floor applications, biodegradability has been identified as a key consideration (Gigliobianco et al., 2015; Paul et al., 2020). *In vivo* erosion of the fibrous hydrogel scaffold was investigated by covalently attaching a near-infrared (NIR) dye to the fibers and monitoring the corresponding loss in signal intensity over a 6 week period (**Figure 4.5**). In addition, the results from the fluorescent imaging confirmed sustained placement of the hydrogel at the suture sites. A maleimide Cyanine 7.5 fluorophore (Cy7.5, Lumiprobe Corporation, Figure S4.6) was conjugated to a methacrylated peptide (Figure S4.7) to enable UV light-mediated methacrylate crosslinks to covalently attach the Cy7.5 labeled methacrylated peptide (Cy7.5-Me, Figure S4.8) to the hydrogel material. In **Figure 4.5B** the labeled hydrogel covers the sutures of the USLS procedure with Figure 5C showing serial *in vivo* optical images. The fibrous injectable

hydrogel scaffold demonstrated faster erosion over the first week (losing more than 50% of the NIR signal), showing an exponential erosion trend. The rapid degradation is hypothesized to be due to the small amount of material, the exposure to the abdominal movements (physical) and fluid erosion (convective fluid movement), and cell-mediated enzymatic degradation. It is unclear if this degradation rate is ideal as there is a limited understanding of the remodeling rate at the USL-vaginal vault junction. General tendon and ligamental remodeling has a known time-scale of a few weeks (Molloy et al., 2003), but that does not necessarily represent the supportive ligaments of the pelvic floor. Meanwhile, there is no set time-scale reported for vaginal and pelvic smooth muscle remodeling, but there are clear examples of hormone (Shynlova et al., 2013; Vodegel et al., 2022) and strain dependence (Andrew Feola et al., 2011). While only a semi-quantitative assessment of degradation, these results demonstrate the degradability of the fibrous HA composite scaffold and provide context for future studies looking at biomaterial degradation in POP models.

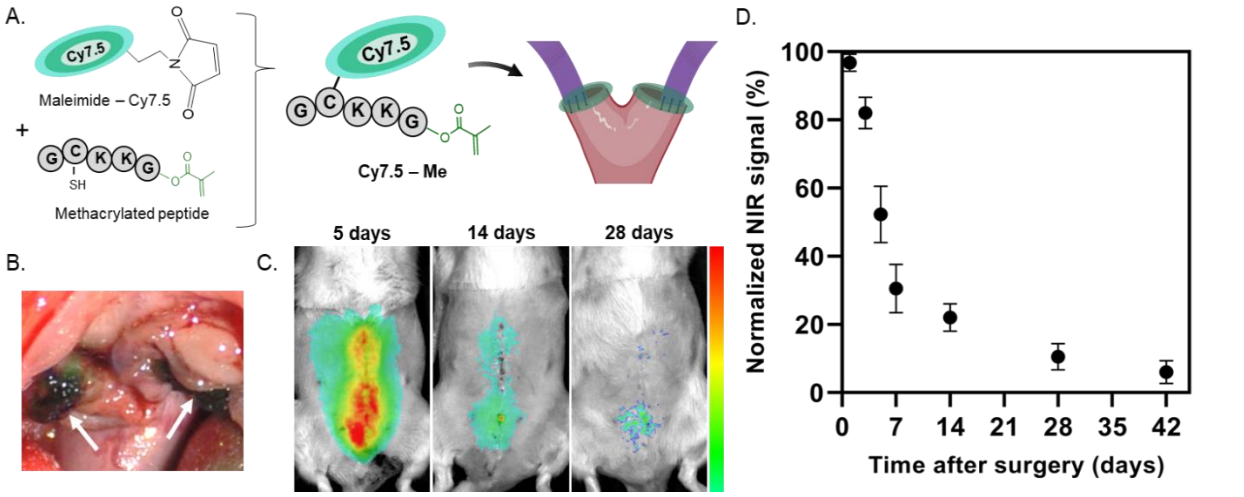

Figure 4.5. In vivo fibrous hydrogel degradation. A) Methacrylated peptide conjugated with sulfo-maleimide cyanine 7.5 (Cy7.5-Me). The methacrylated peptide was first synthesized via solid-phase synthesis and then the Cy7.5 was tethered via maleimide-thiol click chemistry. The methacrylate on the peptide allowed for covalent conjugation of the Cy7.5 dye with the fibrous hydrogel during photocuring for use in hydrogel augmentation. B) Arrows point toward the Cy7.5-labeled hydrogel following delivery. Erosion of the fibrous hydrogel, as represented by the C) serial in vivo optical images, was D) quantified by Cy7.5 signal decay (n = 4).

4.4.5. In situ assessment of specimen mechanical integrity 24 weeks post-operative

While urogynecological research is still in its infancy compared to other fields, this work builds on the previous work (S. Abramowitch & Easley, 2016; Martins et al., 2013) attempting to provide biomechanical context for the pelvic floor tissues. At 24 weeks post-operative, the mechanical properties of the USL-vaginal vault interface after suture only (USLS) and hydrogel augmentation (USLS+H) procedures were assessed and compared with mechanical properties of the intact the USL (**Figure 4.6**). Mechanical "pull-off" tests were performed *in situ* (Instron, 10 N load cell). Specimens were preloaded at 0.15 N and then preconditioned at an elongation rate of 0.1mm sec^{-1} as described in our previous work (B. J. Miller et al., 2022). Data points were collected every 0.1 sec and analyzed via MatLab. The sutures or the sutures + hydrogel were completely resorbed at

the time of testing. Briefly, the USL-vaginal vault interface of the USLS and the USLS with hydrogel (USLS+H) groups were exposed such that umbilical tape could be placed beneath the structure and then clamped in the tensile tester grip. For the intact tissue comparison, the umbilical tape was placed beneath the intact USL structure. A total of 8 specimens (n = 8) are reported per group. After specimen preparation, samples were tested until failure where **Figure 4.6B** shows a sample mid-test and **Figure 4.6C** is an overview of defined parameters of the testing.

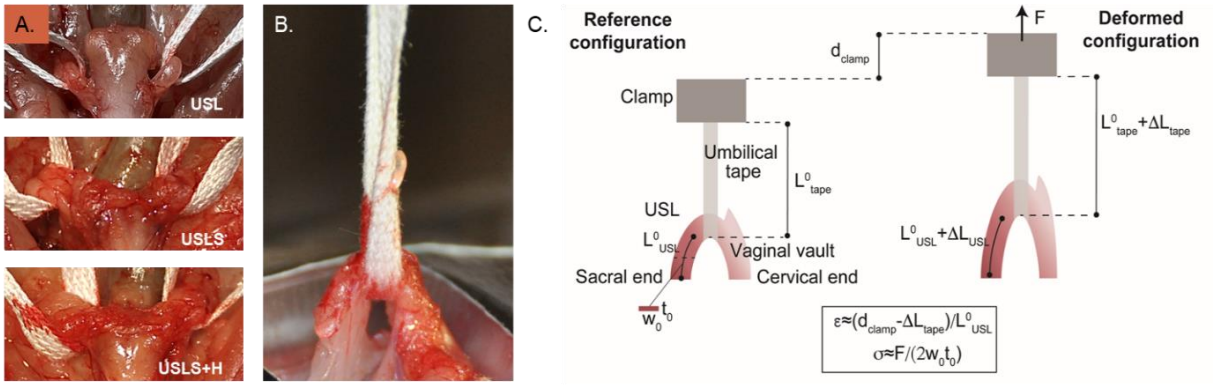

Figure 4.6. In situ tensile tests pulled to failure. A) Tissue preparation for tensile testing where the umbilical tape was placed underneath the cervical end of the structure. B) Sample undergoing the tensile "pull-out" test to failure with a schematic detailing the testing measurements during C) the reference configuration and the deformed configuration.

Load-displacement curves are reported in Figure S4.9 where displacement is defined as $d^{clamp} - \Delta L^{tape}$, where d^{clamp} is the displacement of the clamp (or cross-head displacement) and ΔL^{tape} is the change in length of the umbilical tape. The presence of several peaks in the load as the displacement increased demonstrated that the failure of the USLs, or the surgically repaired tissue, occurred gradually. As is expected for soft tissues, data were characterized by an initial toe region, a more linear region, and then a nonlinear failure region where the gradual breaking is likely due to bundles of tissue fibers breaking at various load levels.

Results showed an ultimate load of 1.70 ± 0.36 N for the intact uterosacral ligament (USL), 0.89 ± 0.28 N for the USLS repair, and 1.37 ± 0.31 N for the USLS+H group (**Figure 4.7**). The stiffness, defined as the steepest positive slope measured over a 1 mm elongation interval, resulted in 0.48 ± 0.10 N/mm for the intact USL, 0.28 ± 0.07 N/mm for the USLS procedure, and 0.42 ± 0.10 N/mm for the USLS+H group. Stress data were computed under the assumption that the USL was loaded along one axis as shown in **Figure 4.6C**. Since the strain of the USL could not be computed *in situ*, we selected to use the normalized displacement (ND) reported in **Figure 4.6C**. as a measure of the USL deformation *in situ*. Next, the stress versus the ND curves were calculated using the load-displacement data and the tissue measurements including the thickness (t_0), width (w_0), and gauge length (L_0^{USL}), where the gauge length is defined as the length of the USL from the sacral attachment to the vaginal vault/cervical insertion (**Figure 4.6C**). Average cross-sectional thickness and width were 1.9 ± 0.3 mm and 2.8 ± 0.2 mm while average gauge length was 12.3 ± 0.7 mm respectively. The highest stress in the tissue before complete failure was shown to be 0.30 ± 0.06 MPa for the intact USL, 0.17 ± 0.04 MPa for the USLS, and 0.27 ± 0.02 MPa for the USLS+H

groups. Notably, for all mechanical testing data shown in **Figure 4.7**, hydrogel augmentation (USLS+H) resulted in statistically significant increases in mechanical properties compared to the USLS-only group. Additionally, there were no statistically significant differences in mechanical properties between the USLS+H and intact USL groups. These exciting results, obtained after the complete dissolution of the hydrogel and sutures, highlight the potential of this hydrogel therapeutic to promote long-term improvement in the mechanical stability of the USL-vaginal vault interface created in USLS procedures.

The mechanical testing protocol described here represents a new method to assess the entire USL and the additional support structures *in situ* rather than *ex vivo*, providing crucial mechanical data about the role the USL plays in USLS suspension. This testing methodology allowed us to test the weakest region of the USL, the cervical region, since the force was applied directly on this region through umbilical tape. During testing, the USL experienced not only tension, but inevitably also compression and shear given the geometry of the ligament and its position relative to the applied load. Moreover, to ensure that the USL was the primary anatomical structure being pulled, we secured the surrounding pelvic tissues to the base plate of the testing machine using a strong adhesive tape. Only the vaginal vault and USL structures were left exposed for testing. Although this prevented significant loading of other anatomical structures, other pelvic tissues were likely loaded and stretched together with the USL. The loads reported here may thus overestimate the loads that are experienced by the USL alone, without their connections to the pelvis. Despite the limitations, the load values we reported fall within the values reported in the literature when loading the rat vagina and USL attachments together *in vivo* (Moalli et al., 2005) and uniaxially testing the isolated rat USL *ex vivo* (Donaldson & De Vita, 2022). The load-displacement curves are very similar to those reported by Donaldson and De Vita, both qualitatively and quantitatively.

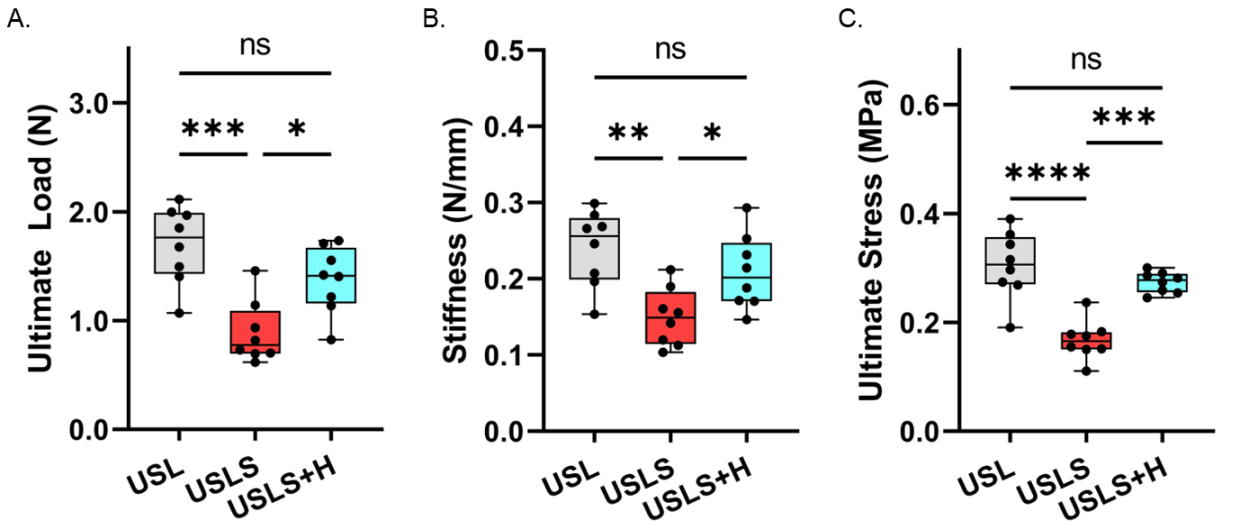

Figure 4.7. Analysis of sample mechanical properties based on the load-displacement data and calculated stress. Data presented are A) force at failure, or ultimate load, B) slopes of the load-displacement curves (stiffness), C) and the stress at failure, or ultimate stress. n = 8, * P < 0.05, ** P < 0.01, *** P < 0.001, **** P < 0.0001.

4.4.6. Study advantages and limitations

The principal strength of this study was the use of a prolapse surgical model to investigate a potential therapeutic for prolapse repair. In the last year, the first study to describe implantation of a mesh biomaterial in the rodent vagina was published (Bickhaus et al., 2021), but moving away from mesh-based repairs is advantageous to explore a wide array of possible therapeutics. Other studies investigating materials for prolapse repair utilized abdominal wall hernia models which are poorly predictive of material compatibility with the pelvic organs (A. Feola et al., 2013; Whooley et al., 2020). Next, the *in situ* mechanical testing of the USL-vaginal interface following suture only repair and repair with augmentation provides measurable outcomes to assess the therapeutic potential of the implanted material for POP. The mechanical testing protocol described here can also be adjusted for use in other pelvic floor models, expanding the range of tools available to researchers to measure outcomes of new biomaterial interventions. Last, the surgical procedures were performed by one surgeon rather than multiple surgeons.

However, this study was subject to several limitations. Controlling for parity of the vendor available animals had the major drawback of receiving animals without exact age information. Without information regarding how recently the rats had delivered their second litters, animal weight was also not possible to control. Additionally, the rodent pelvis has a horizontal orientation that does not replicate the gravitational effects seen in humans or non-human primates. This and the lack of spontaneous prolapse in the rat models does limit some applicability of results to humans, but the use of multiparous rats is a strength of this work since this accounts for the leading risk factor in the development of POP (Kenton, Kimberyly; Mueller, 2006). Last, although it is ideal to have a study with a single surgeon, the homogeneity in surgical technique does not capture the variability of a diverse population of surgeons (Palmerola & Rosenblum, 2019).

4.5. Conclusion

With this study we describe the first hydrogel augmentation of USLS in rodents, demonstrating the usefulness of the USLS rat model in the investigation of therapeutics for prolapse treatment. With a reoperation rate following prolapse surgery of up to 30% (Olsen et al., 1997; Siddiqui et al., 2015; J. M. Wu et al., 2011) and major drawbacks to the use of mesh-based biomaterials, there is an urgent need explore alternative biomaterials with properties that are more compatible with the vagina and pelvic floor. The USLS model provides the means for these materials investigations. We were able to assess the *in vivo* efficacy of our supramolecular fibrous hydrogel composite to augment USLS repair in our newly developed animal model. With a carrier hydrogel to encapsulate the guest-host fibers, the material was used to augment the USL-vaginal vault interface created during the USLS procedure. Applying an *in situ* tensile testing method, the repair with hydrogel augmentation significantly increased the pull-out load (~ 1.4 N) compared to the USLS procedure with sutures alone (~ 0.9 N). This demonstrated that the hydrogel assisted in recovery of mechanical properties to be closer to the intact USL tissue (pull-out force ~ 1.7 N). *In vivo* hydrogel degradation tracking demonstrated exponential decay of Cy7.5 fluorescent signal resulting in near dissolution of the hydrogel at 6 weeks post-surgery (~ 94% degraded), further supporting the premise that superior tissue healing and integration accounts for the recovery of tensile resistance. Together, these results are encouraging as to the potential of this hydrogel platform to augment USLS procedures.

4.6. Acknowledgements

The authors thank Luna Innovations for the use of their NanoSpider for hydrogel nanofiber production, Prof. Rachel Letteri for the use of her peptide synthesizer, and Prof. George Christ for use of his surgical space. This work was supported by the UVA-Coulter Translational Research Partnership and the DoD (W81XWH-19-1-0157).

4.7. Supplemental information

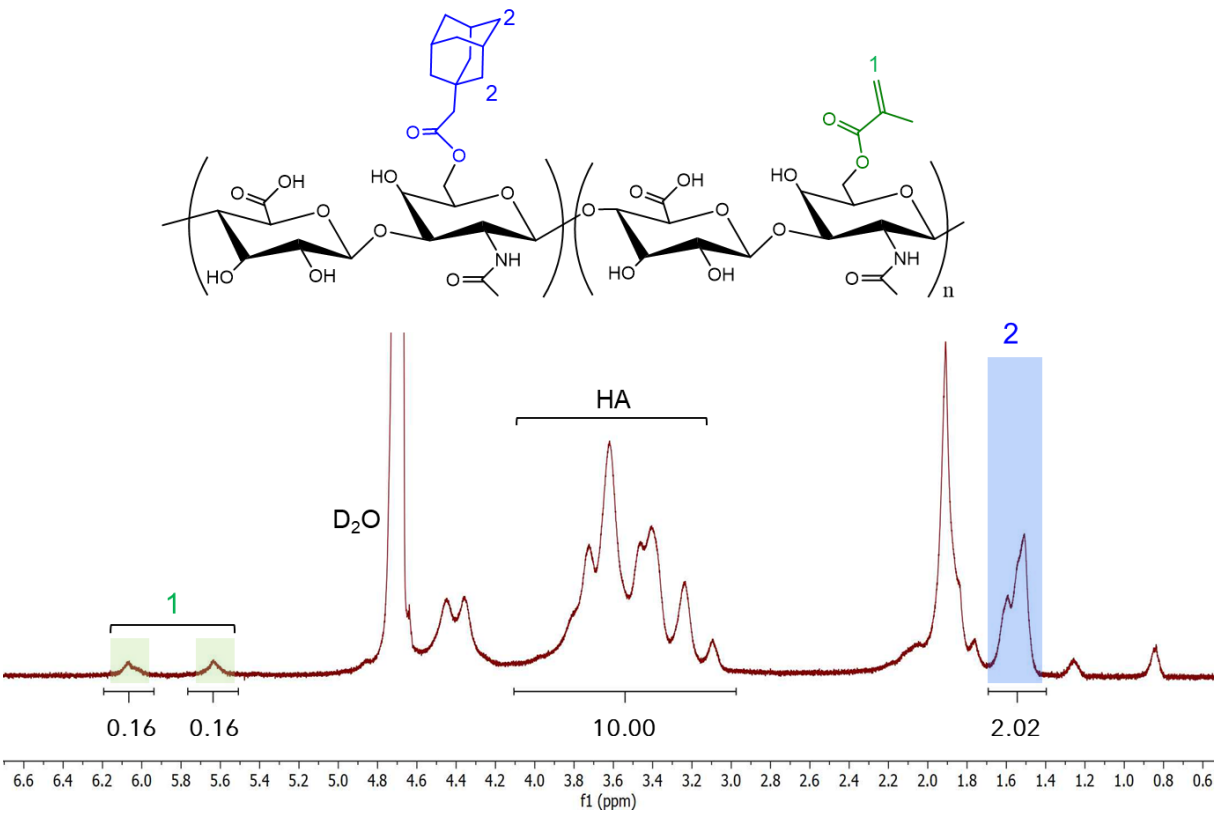

Figure S4.1. **^{1}H NMR spectrum of methacrylate and adamantane modified hyaluronic acid (Ad-MeHA).** The degree of modification was determined to be 16.5% for the adamantane and 16% for the methacrylate. Methacrylate functionalization was determined via integration of the vinyl group in the methacrylate, δ=5.82, 1 H and δ=6.25, 1 H (highlighted green), while integration of the ethyl multiplet of adamantane, δ=1.40 – 1.70, 12 H (highlighted blue), gives the degree of modification relative to the HA backbone, δ=3.10- 4.10, 10 H.

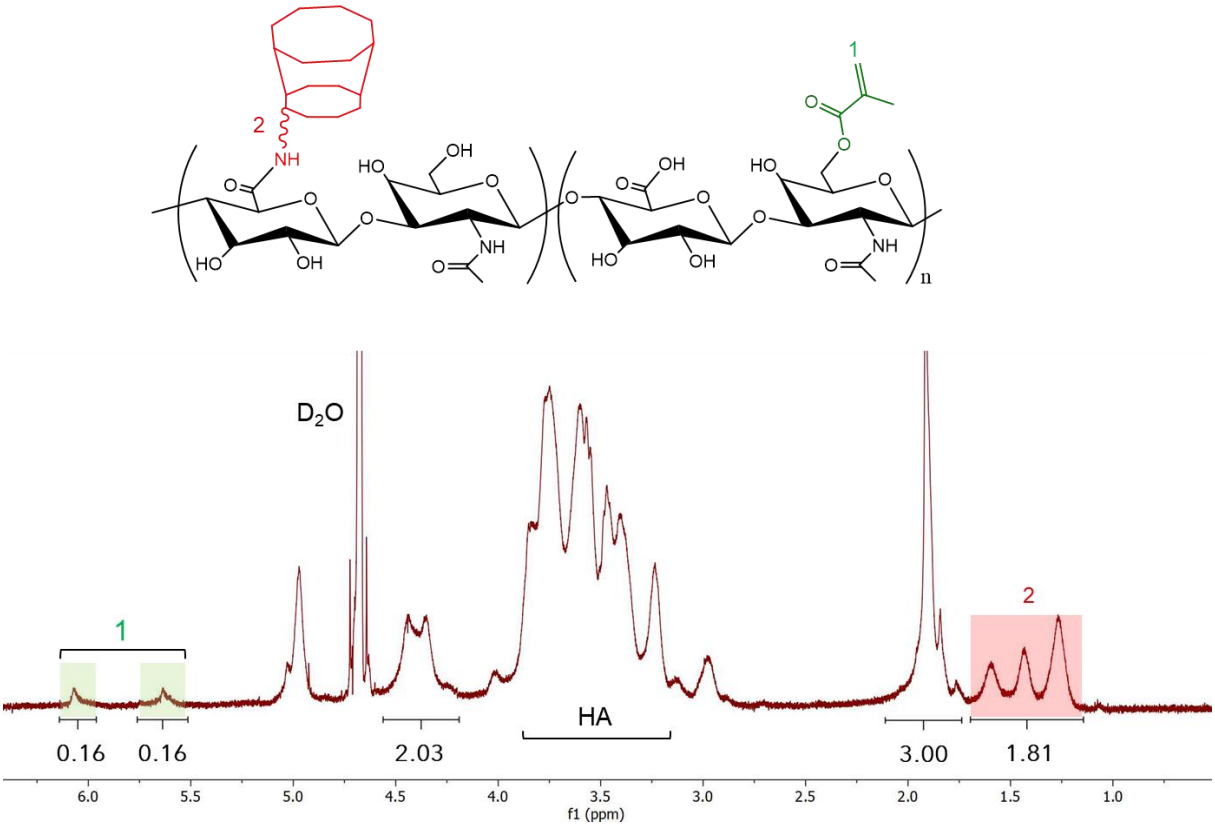

Figure S4.2. ^{1}H NMR spectrum of methacrylate and β-cyclodextrin modified hyaluronic acid (CD-MeHA). The degree of modification was determined to be 16% for the β-cyclodextrin (CD) and 16% for the methacrylate. Methacrylate functionalization was determined via integration of the vinyl group in the methacrylate, δ=5.82, 1 H and δ=6.25, 1 H (highlighted green), and integration of the hexane linker, δ=1.20-1.75, 12 H (highlighted red), gives the degree of modification of CD relative to the methyl singlet of HA (δ=2.1, 3 H).

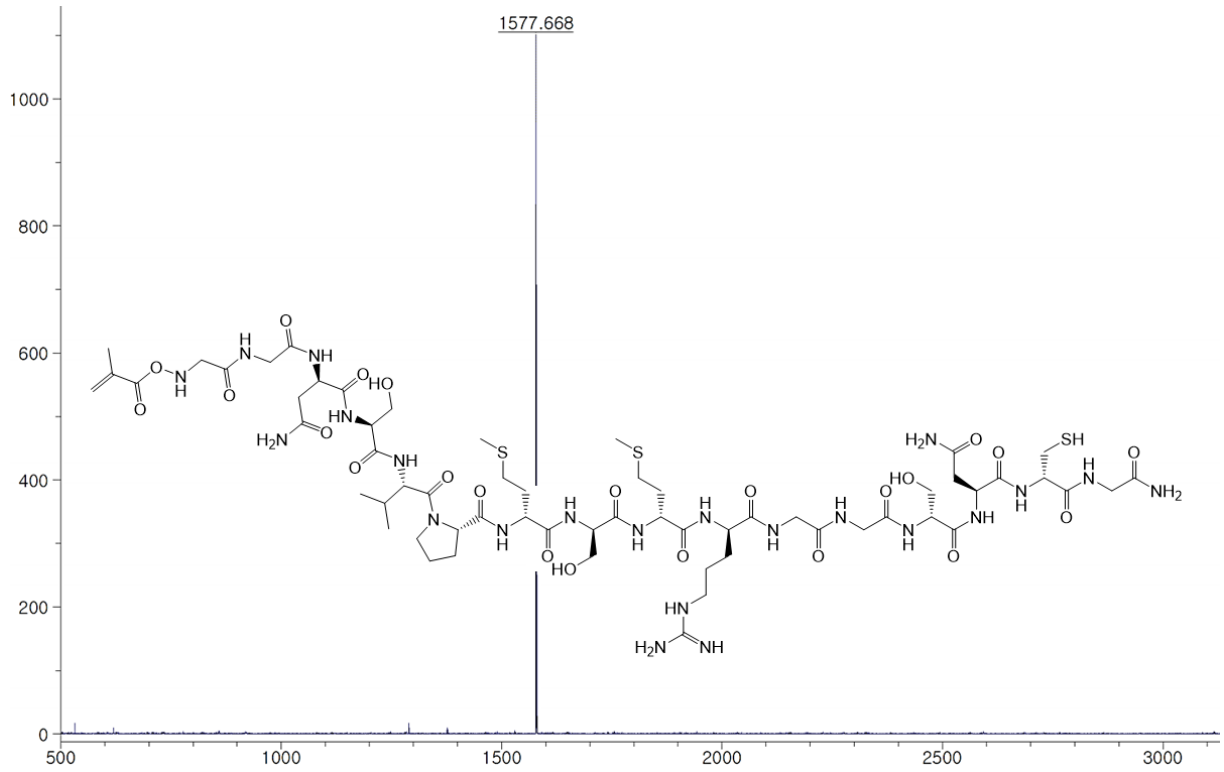

Figure S4.3. MALDI spectrum of methacrylated MMP-degradable peptide (MeP). Degradable peptide with sequence methacrylate-GGNS-VPMS↓MRGG-GNCG. Expected mass: 1578 g/mol. Actual mass: 1577.6 g/mol.

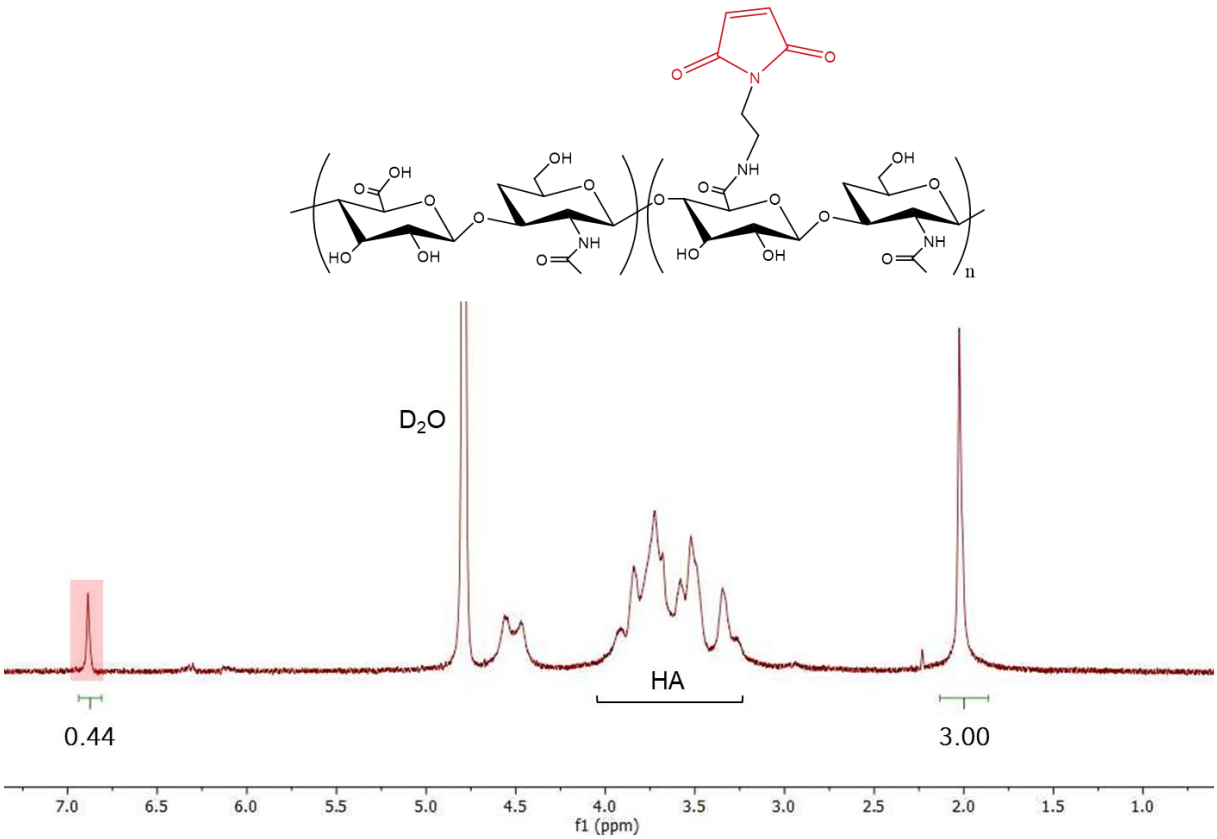

Figure S4.4. ^{1}H NMR spectrum of maleimide-modified hyaluronic acid (MaHA). Maleimide functionalization was determined to be 22% from integration of the doublet δ=6.92, 2 H (highlighted red) relative to the methyl singlet of HA (δ=2.1, 3 H).

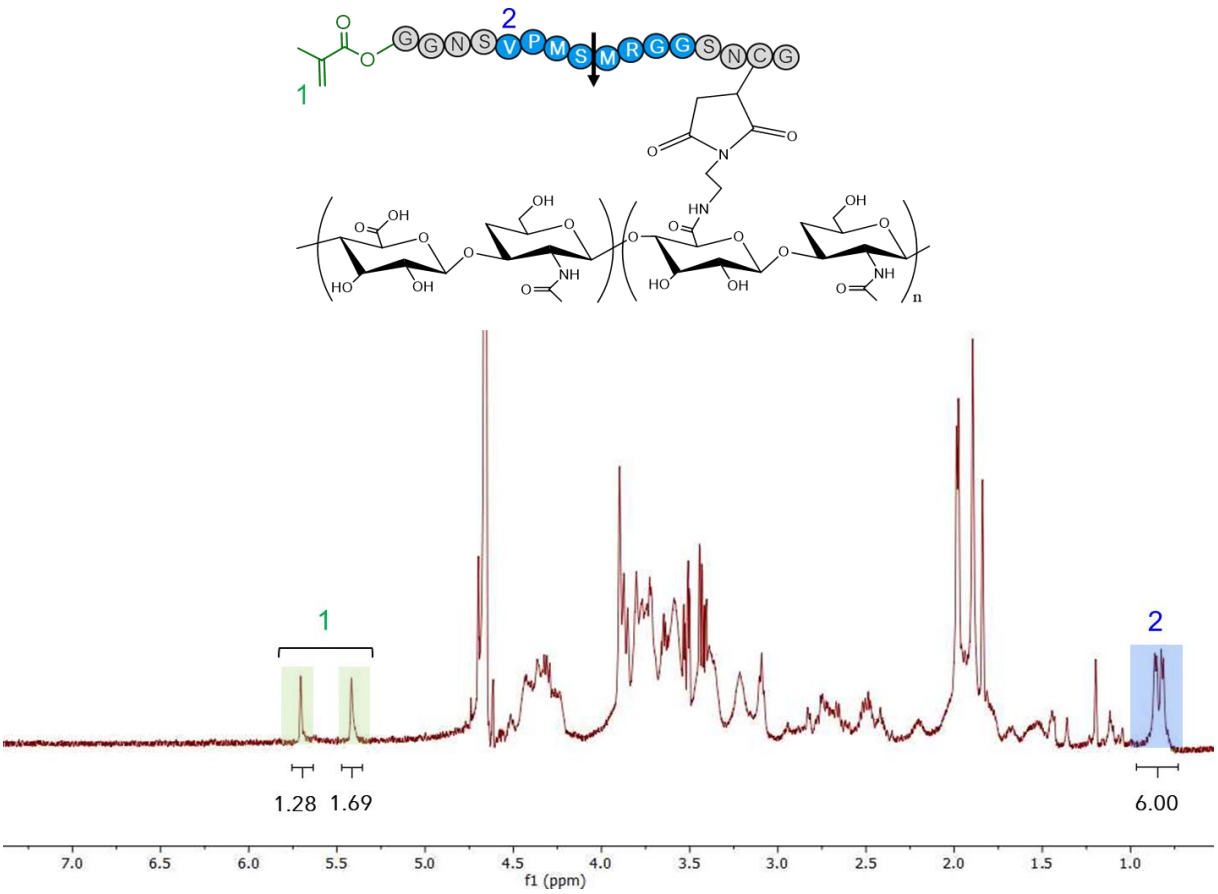

Figure S4.5. ^{1}H NMR spectrum of methacrylated peptide modified hyaluronic acid (MePHA). When the degradable peptide (MeP) is mixed with maleimide modified HA (MaHA), the maleimide doublet is consumed by the available thiol on the peptide (cysteine). Loss of the maleimide peak, and the corresponding introduction of methacrylate peaks, indicates successful peptide conjugation. The modification of the HA backbone is assumed to stay constant at 22%. Methacrylate peaks (δ=5.82, 1 H and δ=6.25, 1 H; highlighted green) are calibrated to the valine peak of the peptide sequence (δ=1.02, 6 H; highlighted blue).

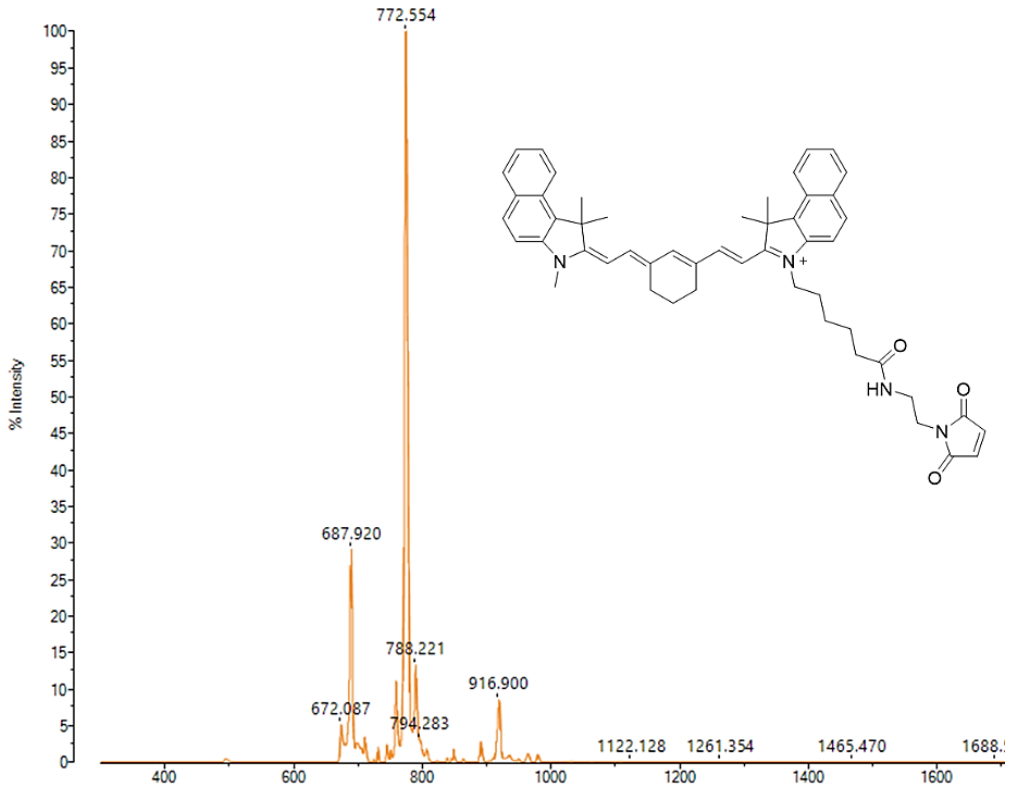

Figure S4.6. MALDI spectrum of maleimide Cyanine 7.5 fluorophore. Purchased from Lumiprobe Corporation. Expected mass: 771.4 g/mol. Actual mass: 772.5 g/mol.

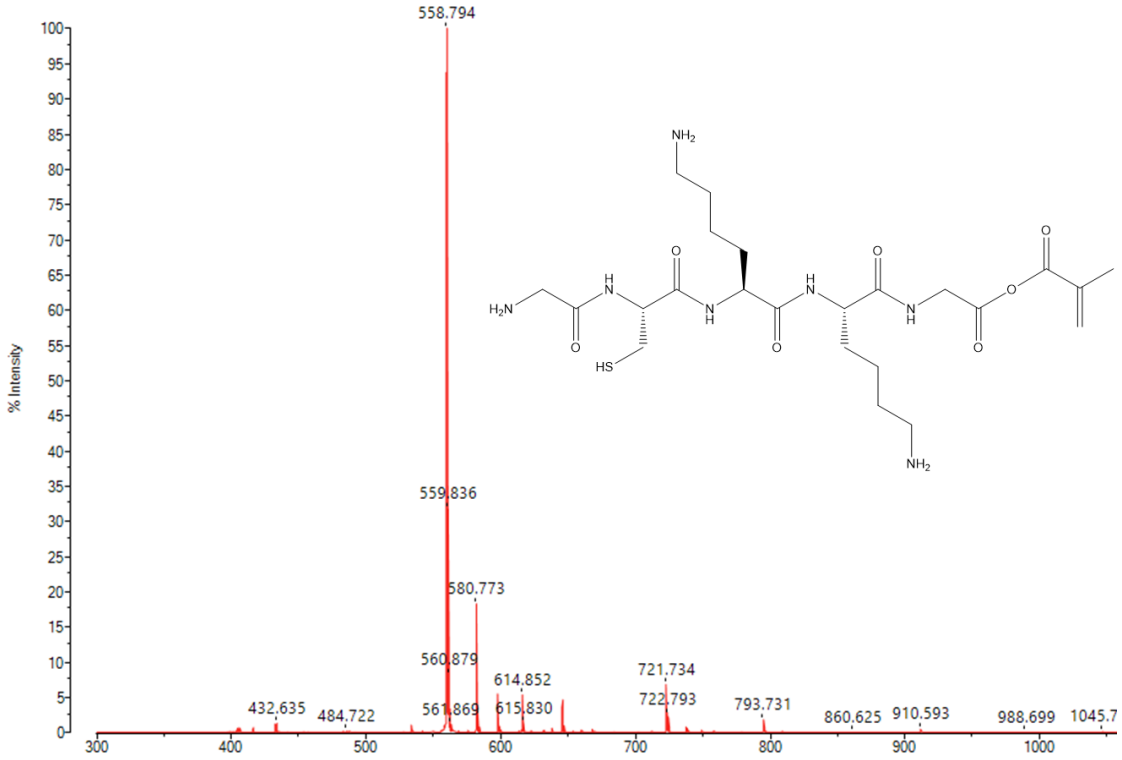

Figure S4.7. MALDI spectrum of methacrylated carrier peptide. Methacrylated peptide with sequence methacrylate-GKKCG synthesized for conjugation with maleimide Cyanine 7.5 fluorophore. Expected mass: 559.2 g/mol. Actual mass: 558.8 g/mol.

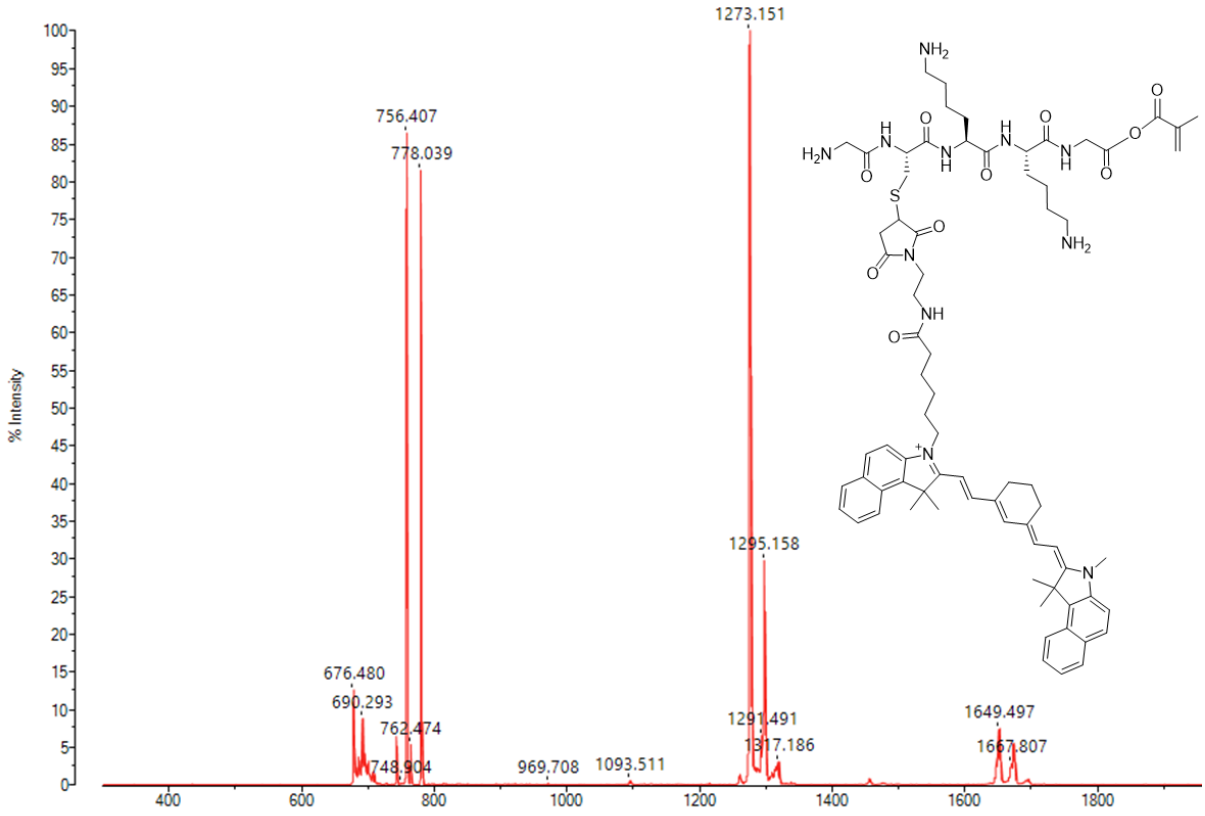

Figure S4.8. MALDI spectrum of the Cy7.5 labeled methacrylated peptide. Methacrylated peptide conjugated with maleimide Cy7.5 fluorophore to enable covalent conjugation to the HA backbone via UV light mediated radical cross-linking of methacrylates. Expected mass: 1273.6 g/mol. Actual mass: 1273.1 g/mol.

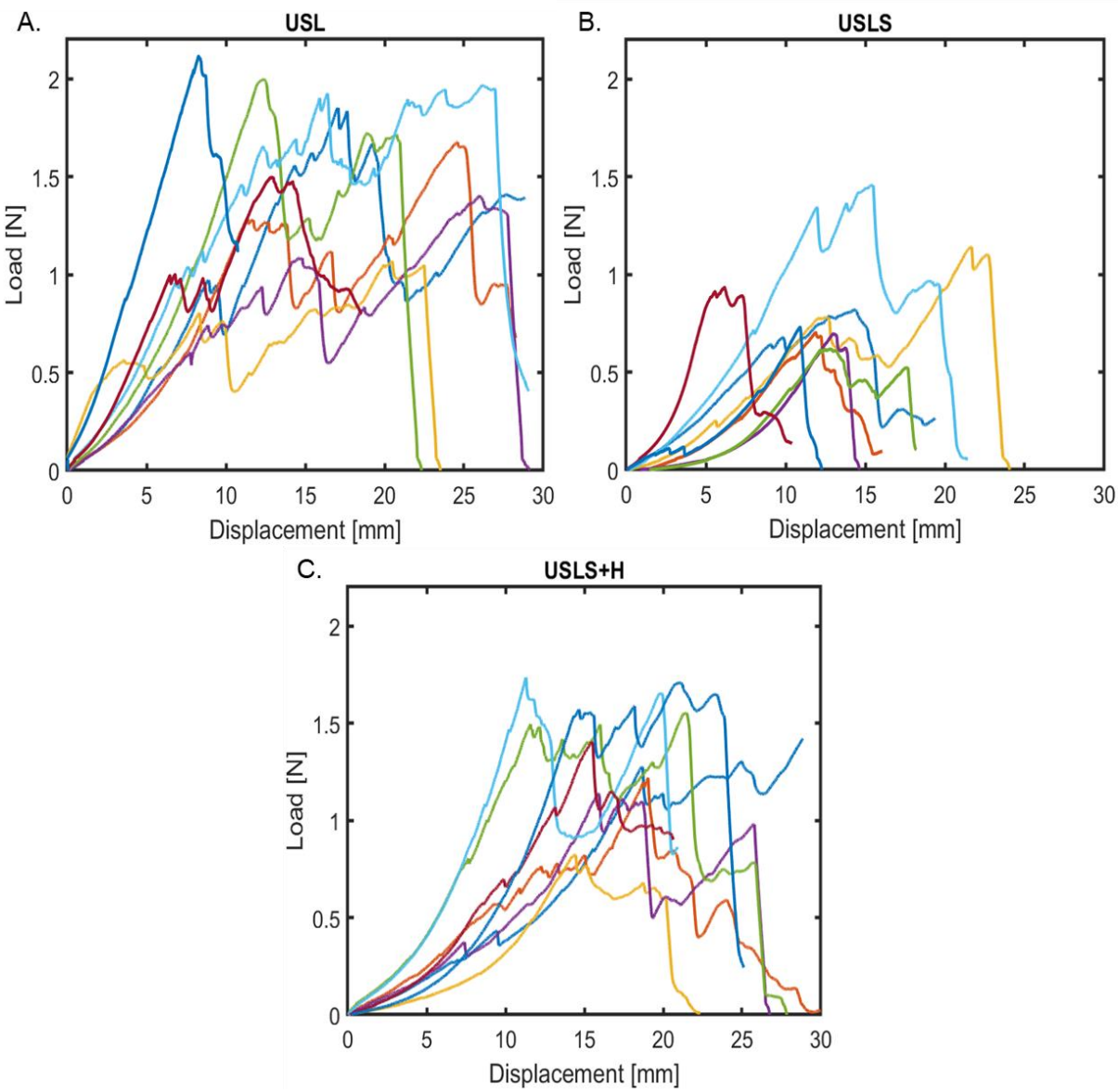

Figure S4.9. Load-displacement collected from n = 8 samples per experimental group up to failure. Data are separated by experimental groups A) intact USL, B) USLS and C) USLS with the hydrogel augmentation (USLS+H).

CHAPTER 5: Fibrous Hyaluronic Acid Hydrogel Influences Functional Repair of Volumetric Muscle Loss

Miller B., Boudreau R., Gentry J., Bandara G., Christ G.J., Caliari S. R.

5.1. Abstract

Volumetric muscle loss (VML) is a devastating orthopedic injury characterized by permanent loss of muscle mass, structure, and function. While skeletal muscle tissue possesses an innate ability to heal from most injuries, VML injuries compromise the wound healing response resulting in loss of joint range of motion, persistent functional deficits, pathologic fibrotic deposition, and lifelong disability. Biomaterials, such as hydrogels, can enhance 3D cell migration and proliferation by providing a tissue-like cellular microenvironment. Current standards-of-care for VML fail to fully recover functional muscle recovery. To address these limitations, our laboratory has developed a hydrogel with muscle mimicking fibrous topography for the treatment of VML. The hyaluronic acid (HA) based hydrogel system includes two components: HA functionalized with chemically reactive norbornene groups for light-mediated thiol-ene click chemistry and electrospun HA nanofibers functionalized with methacrylate groups which stabilize the hydrogel fibers. Mechanical properties were controlled by modulating amounts of matrix metalloproteinase (MMP)-degradable crosslinker to produce gels with a storage modulus of 1.0 kPa. Functional recovery was assessed following implantation of the HA hydrogels via *in situ* polymerization into rat tibialis anterior (TA) VML defects at 4-, 8-, and 12-weeks post injury. After 12 weeks, the muscles treated with the fibrous hydrogel produced maximum isometric torque that was statistically higher than non-treated tissues. This finding show that scaffolds with native fibrillar architecture can facilitate improved skeletal muscle function thus highlighting their potential as a therapeutic for VML injuries.

5.2. Introduction

Skeletal muscle is a dynamic tissue capable of adapting and remodeling in response to external stimuli and to maintain homeostasis. However, in the case of congenital and acquired diseases or traumatic injuries, damage to a large portion of muscle fibers and surrounding tissues results in a permanent loss of muscle mass, function, and poor cosmetic outcomes. Injuries of this nature have been termed volumetric muscle loss (VML). Current treatments, such as autologous tissue transfer, result in poor levels of functional recovery (H. B. Baker et al., 2017). As a result, there is a clear need to improve medical therapies for VML that better restore the functional movements important for daily activities and improve quality of life for patients.

To address limitations of VML, researchers have focused on the use of tissue engineering and biomaterials systems to support repair mechanisms. A wide variety of materials have been investigated for skeletal muscle tissue engineering and have been reviewed extensively elsewhere (Cunniffe et al., 2019; Gilbert-Honick et al., 2018; Kwee & Mooney, 2017). Previous studies have indicated the success of softer scaffolds (~3 kPa Elastic modulus) (Basurto et al., 2022) while others cite the fibrous architecture of native muscle to be a critical feature for biomaterials design (Rao et al., 2018). In an effort to recapitulate these key biophysical features, we have previously developed a 3D fibrous hydrogel for fibrous tissue engineering (B. Miller et al., 2021). Scaffold design includes the use of hyaluronic acid (HA) as the main polymeric component along with electrospinning to create the fibrous architecture desired for fibrous tissue applications. As a logical extension of our previous work, we aimed to explore how our 3D fibrous hydrogel scaffolds influence skeletal muscle repair in a biologically relevant VML injury model.

5.3. Materials and methods

Materials: Sodium hyaluronate (sodium HA, 64 kDa) was purchased from Lifecore Biosciences. β-cyclodextrin (CD), hexamethylenediamine (HDA), ammonium chloride, and p-Toluenesulfonyl chloride were purchased from TCI America. Tetrabutylammonium hydroxide (TBA-OH) was purchased from Acros Organics. All other materials were purchased from Sigma-Aldrich.

Synthesis of NorHA/MeHA: Hyaluronic acid (HA) was functionalized with chemically reactive norbornene groups as previously described. Briefly, sodium hyaluronate (Lifecore, 62 kDa) was first converted to hyaluronic acid tert-butyl ammonium salt (HA-TBA) using Dowex 50W proton exchange resin. HA-TBA was subsequently filtered, titrated to a pH of 7.05, frozen and lyophilized. Norbornene groups were then added by a reaction with 5-norbornene-2-methylamine and benzotriazole-1-yloxytris-(dimethylamino) (BOP) in dimethylsulfoxide (DMSO). The reaction was conducted at 25°C for 2 hours prior to being quenched with cold deionized (DI) water and transferred to dialysis tubing. Finally, NorHA was dialyzed for 5 days, filtered, dialyzed for an additional 5 days, frozen and lyophilized. The degree of HA modification with norbornene was calculated at 20% determined via proton nuclear magnetic resonance (^{1}H NMR). Methacrylate modification of the HA backbone was achieved via methacrylate esterification with the primary hydroxyl group of sodium HA at basic pH. The degree of methacrylate modification was controlled by the amount of methacrylic anhydride introduced during synthesis and was determined to be 28% of the HA disaccharides via ^{1}H NMR.

Electrospinning MeHA fibers: MeHA was dissolved at 2% (w/v) in DI water along with 3.5% (w/v) poly(ethylene oxide) (PEO, 900 kDa) and 0.05% (w/v) Irgacure 2959 (I2959) for 24-48 h prior to electrospinning. The polymer solutions were electrospun using an Elmarco NanoSpider (NS Lab) with the following collection parameters: applied voltage: ~ 45 kV, electrode distance: 22 cm, orifice diameter: 0.7, substrate: Teflon paper, substrate speed: 20 mm/min, carriage speed: 100 mm/sec. Hydrogel nanofibers were deposited onto Teflon paper, placed into a container which was purged with nitrogen, and crosslinked with UV light (254 nm) for 10 minutes.

Hydrogel formulation: NorHA hydrogels were fabricated via an UV light mediated thiol−ene click reaction between norbornene groups and terminal thiols. A hydrogel precursor solution was prepared by incorporating a thiolated RGD peptide (GCGYGRGDSPG, 1mM, Genscript), to act as a cell adhesive and lithium acylphosphinate (LAP, 1mM) to serve as the photo initiator, into a 6 wt% NorHA stock solution. Hydrogel mechanical properties were then modulated by adjusting the concentration of dithiol containing MMP-degradable peptides in the precursor solution and photopolymerized using 365 nm UV light at an intensity of 10 mW/ cm^2.

Rheology: All rheological measurements were performed on an Anton Paar MCR 302 rheometer with the plate temperature set at 37°C. Hydrogel formulations were characterized using a cone-plate geometry (25 mm diameter, 0.5°, 25 μm gap). Mechanical properties of the hydrogels were tested using a time sweep (1 Hz, 0.5% strain) with UV crosslinking (365 nm, 10 mW cm^{-2}, 2 min).

Animal care: This study was conducted in compliance with the Animal Welfare Act, the Implementing Animal Welfare Regulations, and in accordance with the principles of the Guide for the Care and Use of Laboratory Animals. The University of Virginia Animal Care and Use Committee approved all animal procedures. A total of 24 male Lewis Rats (Charles River Laboratories) age matched to 12 weeks weighing 299.9 ± 20.4 g were purchased and individually housed in a vivarium accredited by the American Association for the Accreditation of Laboratory Animal Care and provided with food and water *ad libitum*.

Surgical procedure: The VML injury model was created using a previously established tibialis anterior (TA) injury model (Corona et al., 2013; Gillies & Lieber, 2011). A total of 24 male Lewis Rats, weighing approximately 300 g were randomly designated to three different experimental groups: no repair (NR; n = 8), non-fibrous NorHA hydrogel scaffold (GEL; n = 8), and NorHA with MeHA fiber scaffold (GEL+F; n = 8). To create the surgical defect, rats were anesthetized via isoflurane and the surgical site was aseptically prepared by repeated washes with alcohol and iodine. A longitudinal skin incision was made on the anterior side of the lower left leg to expose the anterior crural muscles. The skin was then separated from the underlying fascia using surgical scissors. The fascia was then separated to expose the underlying musculature. Next, the extensor digitorum longus (EDL) and extensor hallucis longus (EHL) muscles was surgically ablated to avoid compensatory hypertrophy of synergistic muscles involved in dorsiflexion during later in vivo functional assessment (Corona et al., 2013). The VML defect size was approximated from a validated linear regression to estimate TA muscle mass from rat body weight. TA muscle corresponds to approximately 0.17% of the total body weight, as previously determined. Excision of 20% of the TA muscle mass at the middle third of the muscle characterized the VML injury. Following creation of the injury, the fascia was then sutured back in place using 6-0 Vicryl sutures, and the skin was closed using 5-0 polydioxanone subcuticular sutures. Skin glue was applied over top of the closed skin to avoid reopening of the injury. For the first three days following surgery, animal health was monitored daily. Afterwards, animal health was monitored weekly.

In vivo *hydrogel degradation analysis:* To evaluate *in vivo* degradation of the non-fibrous and the fibrous hydrogels, scaffolds conjugated with the GCKKG-Cyanine7.5 fluorophore (NIR) were imaged post injury. Serial images were taken during a 5-week period using a LagoX live imaging system (ex:770 nm, em: 810 nm) and signal intensity was measured by integrating equivalent areas over the region-of-interest. Signal was normalized to peak intensity for individual scaffolds following surgery and then averaged to obtain degradation profiles for each group (n = 3).

In vivo *functional testing:* Isometric force testing was performed on animals prior to surgery and at 4-, 8-, and 12-weeks post-surgery. These results were used to quantify the deficit created by the surgical defect and track functional recovery. *In vivo* force testing was conducted using an established protocol in which isometric torque is produced as a function of stimulation frequency (1-200 Hz) (Mintz et al., 2016). Lewis rats were anesthetized (2% isoflurane) during testing and the left hind limb was aseptically prepared by 3x washes with alcohol and iodine. The foot was secured against a force transducer foot plate, with care to ensure that the heel was flush against the

bottom of the plate. After, the knee joint was positioned so the foot and tibia were at a 90° angle. Force testing was evaluated by stimulation of the peroneal nerve with needle electrodes (21 G). These platinum electrodes were placed in the posterior compartment of the lower leg along either side of the peroneal nerve. The muscle length was adjusted until maximal twitch force was achieved. The contractile force of the anterior crural muscles was then assessed using measurements of peak isometric tetanic force as dorsiflexion occurred. Torque outputs at all timepoints were normalized to the body weight of the animal at the time of testing.

Statistical Analysis: All data are presented as means and their standard deviations (SDs). NorHA/MePHA hydrogel mechanical properties were analyzed for n = 3 hydrogels per group. Cell viability and shape data were statistically analyzed using one-way analysis of variance (ANOVA). These statistical analyses were conducted using GraphPad Prism 9.0 and R. *P* values < 0.05 were considered statistically significant.

5.4. Results and discussion

5.4.1. Fibrous degradable hydrogel scaffold fabrication

We chose HA as the polymeric backbone of our hydrogel design due to its role in supporting skeletal muscle development and tissue repair (Juhas et al., 2014; L. Wang et al., 2018). In addition, HA is amenable to chemical modification with reactive crosslinking groups (**Figure 5.1A,B**) to enable tunability of material biophysical properties such as stiffness and degradability (Caliari et al., 2016; Gramlich et al., 2013). Both the non-fibrous NorHA hydrogels and the NorHA with MeHA fiber composite hydrogels were formed by UV photopolymerization in the presence of photoinitiator. The resulting hydrogel demonstrated a storage modulus of ~ 1 kPa via oscillatory shear rheology (**Figure 5.1C**). With pendant cysteine residues and a sequence shown to degrade *in vivo* (GCNSVPMSMRGGNCG, degradation occurs between the serine and methionine residues), a peptide was used as a di-thiol crosslinker (Wade, Bassin, Rodell, et al., 2015). Amount of the degradable peptide crosslinker was used to control stiffness and obtain the desired modulus.

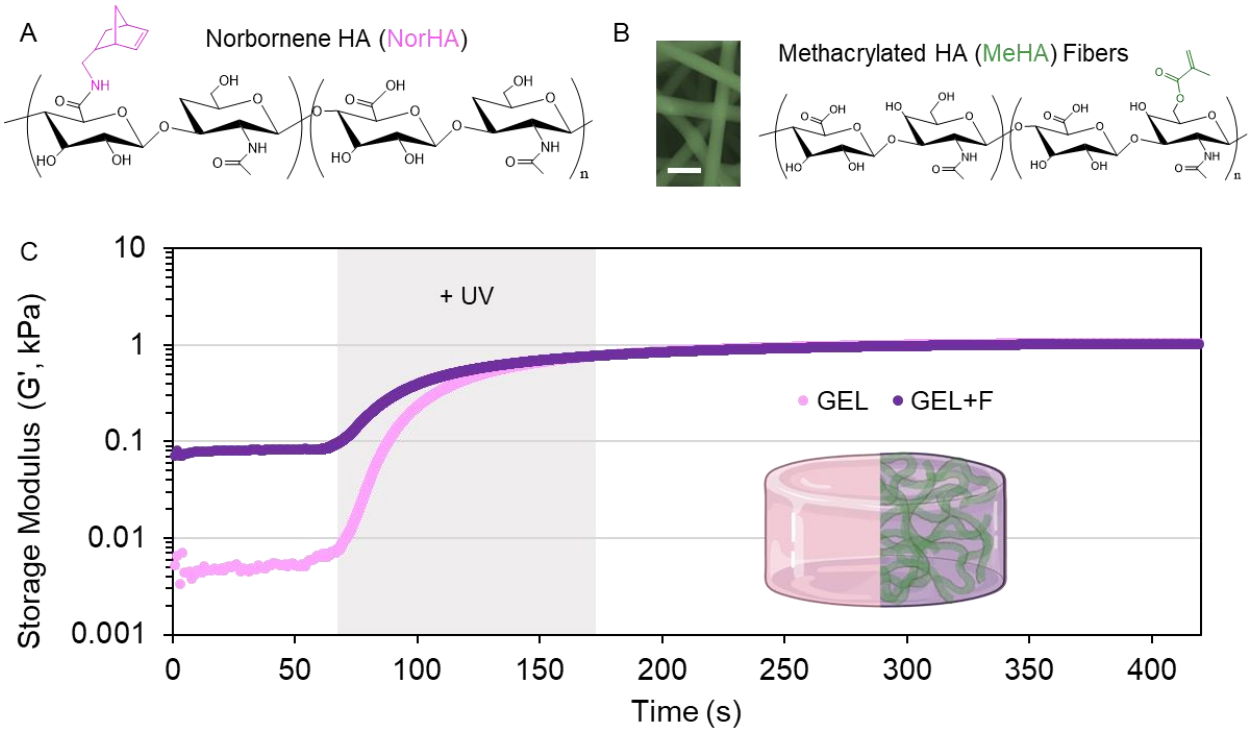

Figure 5.1. Hydrogel mechanical characterization. A) Chemical structure of NorHA. B) Electrospinning was used to fabricate MeHA hydrogel nanofibers. Fiber structure was verified using scanning electron microscopy (SEM) prior to hydration and composite hydrogel formation. Scale bar = 500 nm. C) Oscillatory shear rheology showed that following photopolymerization in the presence of LAP photoinitiator (2 min, 365 nm, 10 mW cm^{-2}), the storage moduli (G') of the two formulations were both ~ 1 kPa (shear modulus). Fibrous hydrogel composite contained 10 w/w % MeHA fibers. All tests were performed at 37°C, n = 3 hydrogels per experimental group

5.4.2. Creation of rat TA VML injury and hydrogel delivery

Fibrous and non-fibrous NorHA scaffolds were delivered and photocrosslinked in situ into an established rat tibialis anterior (TA) model of VML. Prior to delivery, the hydrogel scaffolds were prepared using sterile technique. There were no post-implantation mortalities recorded in either of the hydrogel groups. A total of three experimental groups were investigated: no repair (NR; n = 8), non-fibrous NorHA hydrogel scaffold (GEL; n = 8), and NorHA with MeHA fiber scaffold (GEL+F; n = 8). As expected, animals demonstrated healthy weight gain over the course of the study (Passipieri et al., 2017) (Figure 5.2A) with data normalized to body weight at each time interval. Weight normalization is important when reporting in vivo torque production values as there is a linear correlation between muscle mass and force production (Mintz et al., 2016). Prior to surgery, functional muscle contraction was assessed to establish baseline maximal isometric torque in response to peroneal nerve stimulation (Figure 5.2B). Baseline values were statistically indistinguishable between groups (NR: 104.1 ± 3.3, GEL: 103.1 ± 2.7, and GEL+F: 100.5 ± 5.7 $N \cdot mm \cdot kg^{-1}$). The weight of the TA muscle excised from the animals were statistically similar across experimental groups (NR: 104.6 ± 4.4 mg; GEL: 106.9 ± 7.0 mg; GEL+F: 107.8 ± 8.0 mg) indicating reproducible creation of the VML injuries (Figure 5.2C). Following creation of the injury, hydrogel solutions were delivered within the defect area and photopolymerized. Wound closure (e.g. suturing the fascia and then the skin) secured scaffold placement.

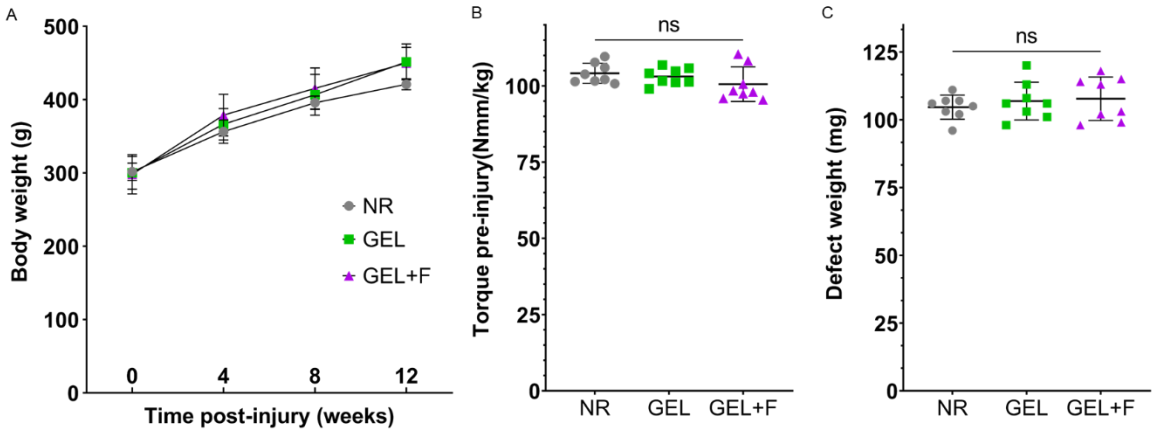

Figure 5.2. Comparison of the body weight, injury, and functional baseline parameters among treatment groups. A) Body weights of study animals reveal normal healthy weight gain in all treatment groups over the course of 12 weeks. B) Graphical comparison illustrating the equivalence of the mean baseline contraction force resulting from peroneal nerve stimulation and measured with a footplate force transducer in all treatment groups. C) Surgical dissections resulted in reproducible injuries of 106.4 ± 6.5 mg. In all cases, individual responses are normalized to their body weight. No statistical differences were observed between experimental groups following two-way and one-way ANOVA. Data are presented as mean ± SEM. *n* = 8 animals per experimental group. NR, no repair; GEL, NorHA hydrogel; GEL+F, NorHA hydrogel with 10 w/w % MeHA fibers; ns, not significant.

5.4.3. In vivo assessment of hydrogel degradation

While several materials and scaffolds have been investigated as potential therapeutics for VML, very few have looked at degradation of the implanted material. *In vivo* degradation of the non-fibrous and fibrous hydrogel scaffolds were tracked using a near-infrared (NIR) fluorophore dye (Cyanine7.5, Cy7.5) covalently bound to the HA chemical backbone prior to scaffold formation. Following implantation of the fluorescently labeled hydrogels within the TA defect area, erosion of the scaffolds was quantified via Cy7.5 signal decay over the course of 35 days, or 5 weeks. Both scaffolds demonstrated faster erosion over the first week (losing nearly 60% of the NIR signal) with slower erosion thereafter (**Figure 5.3A**). Representative serial *in vivo* optical images are shown for the non-fibrous NorHA hydrogel (GEL, **Figure 5.3B**) and fibrous NorHA hydrogel (GEL+F, **Figure 5.3C**) at days 5, 14, and 28. While the fibrous hydrogel is seen to exhibit a slightly slower degradation profile, there is no statistical significance between the two groups. The similar degradation rate is hypothesized to be due to the relatively low fiber density used in this study to achieve comparable material stiffness between the two groups. Interestingly, both of these scaffolds eroded at a more linear rate expected, a feature seen in non-degradable scaffolds (Wade, Bassin, Rodell, et al., 2015), potentially due to the bolus delivery of the scaffold that slowed tissue clearance after the initial week of observed degradation. While only a qualitative assessment of degradation, these results demonstrate the degradability of the two hydrogel formulations and provide context when discussing material influence on functional outcomes.

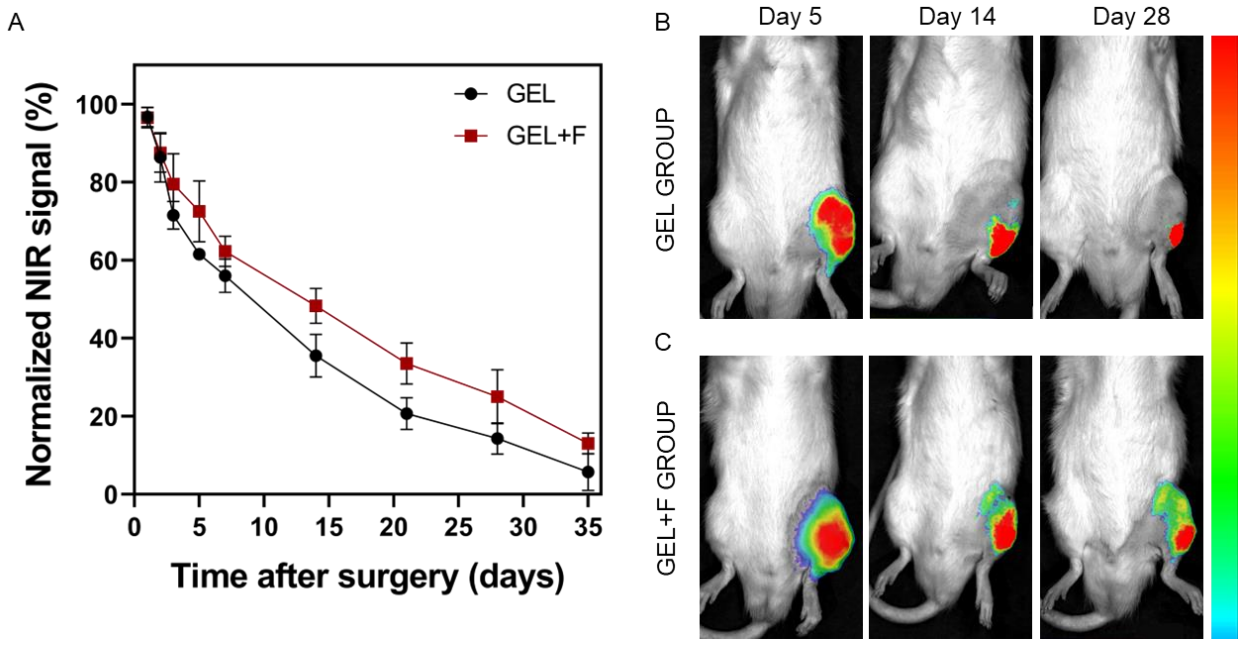

Figure 5.3. In vivo hydrogel degradation. A) Erosion of the hydrogel scaffolds quantified by signal decay of Cyanine7.5 dye covalently bonded to HA before scaffold formation. Data are presented as mean ± SEM. (n = 4). Representative serial in vivo optical images used to quantify degradation of B) NorHA hydrogel (GEL) and C) NorHA with MeHA fibers (GEL+F) composite.

5.4.4. Evaluation of TA functional recovery

Functional muscle contraction was assessed *in vivo* prior to surgery (baseline) and then at 4, 8, and 12 weeks post-surgery (Corona et al., 2013; Passipieri et al., 2017). Briefly, the animal's injured (left) hindlimb was affixed to a force transducer and thin electrodes were inserted on the proximal end of the TA along the peroneal nerve. The resulting isometric torque values were normalized to preinjury baseline force and body weight at the time of testing. Baseline values align with the published studies using the TA model and similar methods of testing isometric contractile force (Christensen et al., 2022; Dienes et al., 2021; Mintz et al., 2020). As illustrated, postsurgical isometric torque testing at 8 weeks showed a statistically significant increase in the torque generated by the GEL+F group compared to both the NR and GEL groups. At 12 weeks, the significance was only seen between the GEL+F group compared to the NR group. Figure 5.4 shows the maximal isometric torque values, normalized as a percentage of the original baseline responses. These values were 48.2 ± 4.4, 48.1 ± 3.7 and 52.8 ± 4.8 % at 4 weeks, 52.4 ± 4.3, 53.0 ± 1.6 and 58.1 ± 4.0 % at 8 weeks, and 55.6 ± 7.6, 58.0 ± 3.6 and 64.1 ± 3.9 % at 12 weeks for NR, GEL, and GEL+F respectively. There was no evidence of the hydrogels remaining in the injury site when the muscles were explanted and weighed at the 12 week time point, leaving *de novo* muscle regeneration as a plausible explanation for the increased TA mass in the GEL+F group relative to the untreated (NR) and non-fibrous NorHA hydrogel (GEL) animals.

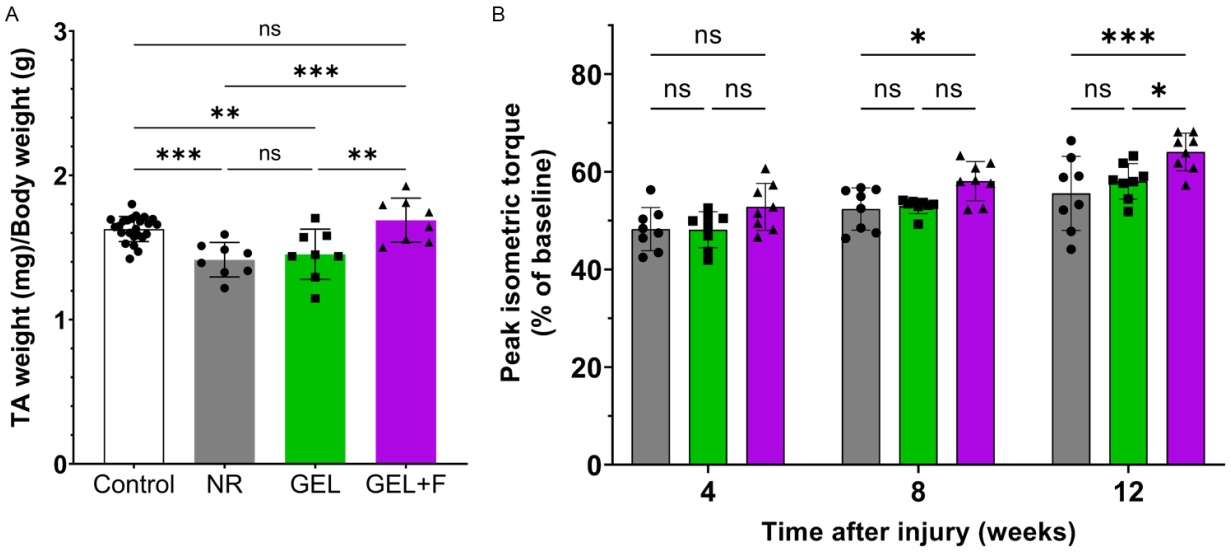

Figure 5.4. Comparison of maximal functional recovery over time as well as the normalized TA weight at 12 weeks post injury. A) TA weight/body weight at 12 weeks postinjury. Notably, TA muscles treated with the fibrous hydrogel displayed a statistically significant gain of mass compared to both untreated and non-fiber hydrogel treated TA muscles. The "control" group on this graph represents the contralateral control TA muscles collected from each animal (n = 24). B) Values for peak isometric torque production for each of the treatment groups as a percentage of the respective initial maximum preinjury isometric torque response. n = 8 for each experimental group; ns, not significant; * P < 0.05, ** P < 0.01, *** P < 0.001.

5.5. Conclusions

In summary, this work aimed to inform biomaterial design to improve the treatment of VML injuries by designing a biomaterial system that mimics biophysical features critical to healthy function, including a fibrous architecture and stiffness. We have shown that fibrous HA hydrogels can promote a significant functional recovery of severely damaged skeletal muscle in an established and a biologically relevant rodent model of TA VML injury. Notably, the measurements showing recovery of isometric torque was achieved in the absence of both cells and growth factors. Although further studies are required to better understand the mechanisms that are responsible for the improved isometric torque, these data have important implications for improved therapeutics for VML injuries. Future work will quantify histological outcomes following fibrous hydrogel implantation to better understand regenerative outcomes alluded to here.

5.6. Acknowledgements

The authors thank Luna Innovations for the use of their NanoSpider for hydrogel nanofiber production and Prof. George Christ for use of his surgical space. This work was supported by the DoD (W81XWH-19-1-0157).

CHAPTER 6: CONCLUSIONS AND FUTURE DIRECTIONS

6.1 Summary

The work presented in this dissertation focused on 1) the design and development of a biomaterial platform for fibrous tissue repair 2) the development of a pelvic organ prolapse (POP) rodent model, and 3) the augmentation of POP repair using the hydrogel biomaterial. This dissertation explored the use of a fibrous and injectable hyaluronic acid (HA) hydrogel with independent control over mechanical stability, ligand presentation, and fiber content. These properties allowed for the investigation of various hydrogel formulations to determine how these factors affected degradation and repair capabilities *in vivo*. While this material was demonstrated in application of pelvic floor ligamental augmentation, it could potentially be cross-applied to tendons and ligament in other areas of the body, as well as other soft yet robust fibrous tissues such as skeletal muscle.

In Chapter 2, we describe the development of an injectable hyaluronic acid (HA)-based fibrous hydrogel that recreated key biophysical features of fibrous tissue including the fibrous architecture. Viscoelastic hydrogels (G' ~ 7 kPa, G" ~ 1 kPa) were fabricated that demonstrated shear-thinning and self-healing properties, mechanics representing healthy fibrous tissue, and minimally invasive delivery potential, respectively. This was provided by hydrogel fibers assembled with supramolecular guest-host interactions that were then investigated for how they would impact cell viability and cell shape metrics following injection. Currently, much of what is known about how material properties influence cell behavior is confined to 2D substrates that do not accurately reflect the complex tissue microenvironment. To address this knowledge gap, we electrospun HA modified with reactive methacrylate groups and supramolecular molecules adamantane (Ad, guest) and β-cyclodextrin (CD, host) to produce 3D fibrous hydrogels. Encapsulated hMSCs demonstrated satisfactory viability following injection (~ 90%) and were more spread and elongated within the guest-host fibrous hydrogel compared to nonfibrous controls. With the supramolecular guest-host interactions on the surface of the fibers, the final hydrogel formulation exhibited mechanical integrity, shear-thinning behavior, rapid self-healing, and cytocompatibility. Together, these data highlight the potential of this injectable fibrous hydrogel platform for cell and tissue engineering applications. Moreover, these data add to the growing body of work encapsulating cells in 3D hydrogels to investigate cell behavior.

Chapter 3 describes the development of a new rodent model for uterosacral ligament suspension (USLS). This small animal model is the first published description of USLS in a rat. Creation of this method addresses the urgent need to develop accessible animal models that can assist in the investigation of new materials for POP treatment. In addition, since the model was developed using multiparous female rats, a major risk factor in pelvic organ prolapse (POP), researchers now have a reference to move beyond using nulliparous rats for investigations. Aside from the surgical method, the developed model describes a tensile testing technique that allows investigation of uterosacral ligament and repair mechanical properties *in situ* for the first time. We expect this

animal model to greatly impact the field of engineering for women's health as it has laid the foundation for further models and for improvements in mechanical testing to standardize the measurement of pelvic floor soft tissue properties *in situ*. Overall, the animal model developed in chapter 3 will be a useful tool for future tissue engineers to investigate new therapeutics for POP within the pelvic floor tissue structures.

As an extension of our work in Chapter 2 and 3, in Chapter 4 we aimed to assess the *in vivo* efficacy of the supramolecular fibrous hydrogel to augment USLS repair in our newly developed animal model. Given the postsurgical complications associated with mesh-based augmentation and the 40% failure rate of the USLS native tissue repair, there is an urgent need to explore alternative biomaterials with properties that are more compatible with the vagina and pelvic floor. This work describes the first hydrogel augmentation of USLS in rodents demonstrating the usefulness of the USLS rat model in the investigation of therapeutics for prolapse treatment. With a carrier hydrogel to encapsulate the guest-host fibers, the material was used to augment the USL-vaginal vault interface created during the USLS procedure. Applying an *in situ* tensile testing method, the repair with hydrogel augmentation significantly increased the pull-out load (~ 1.4 N) compared to the USLS procedure with sutures alone (~ 0.9 N). This demonstrated that the hydrogel assisted in recovery of mechanical properties to be closer to the intact USL tissue (pull-out force ~ 1.7 N). *In vivo* hydrogel degradation tracking demonstrated exponential decay of fluorescent signal resulting in near dissolution of the hydrogel at 6-weeks post-surgery (~ 94% degraded), further supporting the tissue healing to account for the recovery of tensile resistance. Together, these results are encouraging as to the potential of this hydrogel platform to augment USLS procedures.

In Chapter 5 we sought to explore how the fibrous hydrogel influenced *in vivo* skeletal muscle regeneration following VML injury. Formulation of the fibrous hydrogel was simplified with methacrylate-modified HA (MeHA) fibers (~ 10% v/v) encapsulated in a norbornene-modified HA (NorHA) hydrogel. This NorHA-fiber composite allowed for a more direct comparison between this and previous work with non-fibrous hydrogels. The reactive norbornene groups allowed for stiffness and ligand tunability using UV radical crosslinking, an enzymatically degradable dithiol crosslinker, RGD cell binding ligand, and photoinitiator. Mechanical properties were controlled by modulating amounts of the peptide crosslinker and fibers to produce gels with a storage modulus shown in previous studies to promote *de novo* tissue formation in skeletal muscle wound healing (G' ~ 1 kPa, equivalent to E ~ 3 kPa). To assess how material mechanical properties influenced skeletal muscle wound healing, hydrogels were *in situ* photopolymerized into the tibialis anterior (TA) model of VML. *In vivo* degradation tracking demonstrated exponential decay of fluorescent signal by 5 weeks post-injury, indicating that the wound healing niche was able to adequately degrade the fibrous NorHA hydrogel. At 12-weeks post-injury, muscles treated with the fibrous hydrogel produced maximal isometric contraction resembling native muscle (~ 64% recovery) and significantly higher than the non-repaired control (~ 55% recovery) or non-fibrous hydrogel (~ 58% recovery) groups. Together, these data show that careful design of material composition can support improved functional VML recovery.

6.2 Future directions

6.2.1. Sex as a variable in fibrous tissue engineering

The urgent clinical need for advanced fibrous biomaterials reaching far beyond the fibrous tissue injuries discussed in this dissertation. While the growing body of literature around nanofibrous scaffolds is encouraging, the lack of successful treatment options for complex fibrous tissue injuries (such as those seen in the rotator cuff or pelvis) highlights the need for translational research. Even aside from the subpar treatment options currently available for fibrous tissue injuries, healing processes are limited by the hypocellularity and avascular nature of the ECM (Mauck et al., 2009). Adding to these challenges, when healing does occur in these dense tissues, the ordered structure of the native tissue is replaced with a disorganized fibrous scar exhibiting poor mechanical properties (Gonzalez-Fernandez et al., 2019). Tissue engineering strategies are vast and progress for fibrous tissues are being made, but there is a glaring gap in knowledge. The field has largely been naïve to "sex as a variable" in designing potential treatment strategies.

Gender differences in therapeutics outside of reproductive health have historically been willfully ignored, if not aggressively avoided. Before 2016, even studies specifically investigating therapeutics or interventions specifically for females were not required to use a female animal model (*History of women's participation in clinical research*, n.d.). Recently, there has been a push within biomedical research to acknowledge these sex differences and studies are being done that highlight the differences of cardiac muscle cells between men and women (Walker et al., 2021) and the differences in how women experience healing post-surgery (S. D. Daniels et al., 2019). The mechanisms behind these differences are still unknown and require further study. When it comes to fibrous tissues specifically, studies have shown that the sex differences in tendon and ligament biomechanical properties are significant in the period of life where the sex hormonal profiles are markedly different between men and women (Magnusson et al., 2016). However, as of 2016, clinicians lack effective interventions for the treatment of tendon disorders as researchers are just beginning to look at how sex differences in biomechanical properties may be related to structural differences. Owing to an increase in female sports participation, sports medicine studies have lead investigations focused on sex-based differences thereby providing useful context.

Women are at substantially greater risk for anterior cruciate ligament (ACL) injuries than men (Y. Liu et al., 2022), with literature suggesting that there is an association between hormone fluctuation and ACL injury. Recently, a female sports company decided to track player injuries, recording menstrual cycle information at the time of incident. Data collected over a 4-year period showed that women were twice as likely to incur muscle and tendon injuries in the late follicular phase of their menstrual cycles (Martin et al., 2021). Additionally, the last few years have brought an increased understanding of the crucial sex differences seen in skeletal muscle homeostasis and exercise capacity (Ikeda et al., 2019). Altogether, these studies highlight the need for sex as a variable to be taken into consideration when designing biomaterials for fibrous tissue injuries.

6.2.2. Translational gynecological tissue engineering

The need for studies to consider sex-based differences affects more than fibrous tissue repair. Gender bias has been an ongoing issue in health care with underrepresentation of women in health studies, trivialization of women's physical complaints, and discrimination in the awarding of research grants. It has been almost three decades since the first requirements to include women in clinical trials, yet the inequitable distribution of funds has hampered progress (Mazure & Jones, 2015). A recent study found that the NIH applies a disproportionate share of its funding resources to diseases that primarily affect men (Mirin, 2021). This is significant since the NIH is the largest funding organization for health research in the world, contributing $26.1 billion in 2013. The next largest is the European commission contributing $3.7 billion (Viergever & Hendriks, 2016). Aside from funding, the perceived benign nature of many gynecological disorders is a disservice to the 15 – 30% of women who experience debilitating chronic pelvic pain due to endometriosis, dysmenorrhea, or other pelvic disorders (Kuligowska et al., 2005; Kutch & Tu, 2016; Laganà et al., 2017; Najimudeen et al., 2020). There is a strong need to develop this underserved field, thus tissue engineering strategies are being leveraged to design biomimetic materials for ovarian, endometrial, pelvic organ prolapse, placental, and cervical insufficiently (Fogg et al., 2022).

Within the broad topic of women's health research, gynecological disorders (e.g. cancers, pelvic organ prolapse, and uterine and ovarian diseases) are especially underfunded and under researched (Gregersen et al., 2020; Spencer et al., 2019). Many of these disorders predominantly rely on invasive exploratory surgery for diagnosis since the non-invasive options are unreliable (Yoeli-Bik et al., 2022). For cancers specifically, alternative screening methods are being explored (Cook et al., 2022) but the disparity in funding prevents prompt clinical translation. Meanwhile, pelvic organ prolapse prevention and treatment is limited by poorly understood underlying etiologies (Orlicky et al., 2021). As discussed in previous chapters, the lack of biomechanical or disease mechanistic information severely handicaps treatment advancement efforts and leads to disappointing clinical outcomes. Last, uterine and ovarian diseases exhibit chronic inflammatory conditions that result in poor reproductive outcomes and suggest interconnectivity between the various disorders. Notably, the chronic inflammation reported with polycystic ovary syndrome (Velez et al., 2021) may be contributing to endometrial inflammation, or vice versa, resulting in reproductive dysfunction (Palomba & Giudice, 2020). Studies have shown that the native ECM is a dynamic regulator of ovarian follicle development (Kreeger et al., 2006) and uterine leiomyoma (fibroid development) has been associated with the excess deposition of ECM (Fujisawa & Castellot, 2014). However, a greater understanding of the female reproductive organs and their "normal" attributes are essential to designing suitable treatments for ovarian and uterine diseases.

Women's health is a broad category encompassing gynecologic, reproductive and sexual health care, all associated with many challenges and unsolved problems for researchers (De Vita & Munson, 2021; K. S. Miller et al., 2019). Progress in the last decade highlights the interdisciplinary nature of the work, requiring engineers, clinicians, and reproductive scientists to develop techniques reimaged for the application of studying women's health. Ultimately, continued

innovation in gynecological tissue engineering, along with an increase in women's health funding, has the potential to greatly impact the lives of women worldwide.

6.2.3. Medical equity and the future of biomedical engineering

There are currently major gaps in knowledge regarding women's health in tissue engineering design, yet this knowledge gap is even more profound when including additional understudied factors such as ethnicity and ancestral background (Oh et al., 2015). For example, the incidence of clinically symptomatic fibroids in reproductive-age women is ~ 20%, with that number jumping to nearly 80% in black women (Fujisawa & Castellot, 2014). As scientist and engineers, it is imperative to include diverse populations in our experimental design, both in terms of scientific integrity but also as a matter of social justice. Further, diverse populations of young scientists are more likely to stay in academia if they feel represented both within their community and their research topics (Godbole et al., n.d.; Lambert et al., 2020). Moreover, ensuring equal access to funding for young investigators (R. J. Daniels, 2015), regardless of geographical location (Wahls, 2016), will help curb the mass exodus of young scientists choosing to leave their positions in academic research. Shaping a diverse and equitable next generation of science and biomedical engineering researchers demands nothing less.

REFERENCES

Aachmann, F. L., Larsen, K. L., & Wimmer, R. (2012). Interactions of cyclodextrins with aromatic amino acids: A basis for protein interactions. *Journal of Inclusion Phenomena and Macrocyclic Chemistry*, *73*(1–4), 349–357. https://doi.org/10.1007/s10847-011-0071-y

Abramowitch, S. D., Feola, A., Jallah, Z., & Moalli, P. A. (2009). Tissue mechanics, animal models, and pelvic organ prolapse: A review. *European Journal of Obstetrics and Gynecology and Reproductive Biology*, *144*(SUPPL 1), 146–158. https://doi.org/10.1016/j.ejogrb.2009.02.022

Abramowitch, S., & Easley, D. (2016). Biomechanical Characterization of Native Pelvic Floor Organs and Tissues. In L. Hoyte & M. Damaser (Eds.), *Biomechanics of the Female Pelvic Floor* (1st ed., pp. 109–130). Elsevier Inc. https://doi.org/10.1016/B978-0-12-803228-2.00005-2

Abrams, G. A., Goodman, S. L., Nealey, P. F., Franco, M., & Murphy, C. J. (2000). Nanoscale topography of the basement membrane underlying the corneal epithelium of the rhesus macaque. *Cell and Tissue Research*, *299*(1), 39–46. https://doi.org/10.1007/s004410050004

Aguado, B. A., Mulyasasmita, W., Su, J., Ph, D., Lampe, K. J., Ph, D., Heilshorn, S. C., & Ph, D. (2012). Improving Viability of Stem Cells During Syringe Needle Flow Through the Design of Hydrogel Cell Carriers. *Tissue Engineering Part A*, *18*, 806–815. https://doi.org/10.1089/ten.tea.2011.0391

Alberts, B., Johnson, A., Lewis, J., Raff, M., & Roberts, K. (2002). *Molecular Biology of the Cell , 4th edition*. Garland Science.

Alshomer, F., Chaves, C., & Kalaskar, D. M. (2018). Advances in Tendon and Ligament Tissue Engineering: Materials Perspective. *Journal of Materials*, *2018*, 1–17. https://doi.org/10.1155/2018/9868151

Ashton-Miller, J. A., & DeLancey, J. O. L. (2007). Functional anatomy of the female pelvic floor. *Annals of the New York Academy of Sciences*, *1101*, 266–296. https://doi.org/10.1196/annals.1389.034

Aubé, M., & Tu, L. M. (2018). Current trends and future perspectives in pelvic reconstructive surgery. *Women's Health (London, England)*, *14*. https://doi.org/10.1177/1745506518776498

Ayubi, F. S., Armstrong, P. J., Mattia, M. S., & Parker, D. M. (2008). Abdominal wall hernia repair: A comparison of Permacol® and Surgisis® grafts in a rat hernia model. *Hernia*, *12*(4), 373–378. https://doi.org/10.1007/s10029-008-0359-z

Baah-Dwomoh, A., McGuire, J., Tan, T., & De Vita, R. (2016). Mechanical Properties of Female Reproductive Organs and Supporting Connective Tissues: A Review of the Current State of Knowledge. *Applied Mechanics Reviews*, *68*(6), 1–12. https://doi.org/10.1115/1.4034442

Baker, B. M., & Chen, C. S. (2012). Deconstructing the third dimension-how 3D culture microenvironments alter cellular cues. *Journal of Cell Science*, *125*(13), 3015–3024. https://doi.org/10.1242/jcs.079509

Baker, B. M., Trappmann, B., Wang, W. Y., Sakar, M. S., Kim, I. L., Shenoy, V. B., Burdick, J. A., & Chen, C. S. (2015). Cell-mediated fibre recruitment drives extracellular matrix mechanosensing in engineered fibrillar microenvironments. *Nature Materials*, *14*(12), 1262–1268. https://doi.org/10.1038/nmat4444

Baker, H. B., Passipieri, J. A., Siriwardane, M., Ellenburg, M. D., Vadhavkar, M., Bergman, C. R., Saul, J. M., Tomblyn, S., Burnett, L., & Christ, G. J. (2017). Cell and Growth Factor-Loaded Keratin Hydrogels for Treatment of Volumetric Muscle Loss in a Mouse Model. *Tissue Engineering Part A*, *23*(11–12), 572–584. https://doi.org/10.1089/ten.tea.2016.0457

Bancelin, S., Aimé, C., Gusachenko, I., Kowalczuk, L., Latour, G., Coradin, T., & Schanne-Klein, M. C. (2014). Determination of collagen fibril size via absolute measurements of second-harmonic generation signals. *Nature Communications*, *5*, 1–8. https://doi.org/10.1038/ncomms5920

Basurto, I. M., Mora, M. T., Gardner, G. M., Christ, G. J., & Caliari, S. R. (2021). Aligned and electrically conductive 3D collagen scaffolds for skeletal muscle tissue engineering. *Biomaterials Science*, *9*(11), 4040–4053. https://doi.org/10.1039/d1bm00147g

Basurto, I. M., Passipieri, J. A., Gardner, G. M., Smith, K. K., Amacher, A. R., Hansrisuk, A. I., Christ, G. J., & Caliari, S. R. (2022). Photoreactive Hydrogel Stiffness Influences Volumetric Muscle Loss Repair. *Tissue Engineering Part A*, *00*(00), 1–18. https://doi.org/10.1089/ten.tea.2021.0137

Becker, W. R., & De Vita, R. (2015). Biaxial mechanical properties of swine uterosacral and cardinal ligaments. *Biomechanics and Modeling in Mechanobiology*, *14*(3), 549–560. https://doi.org/10.1007/s10237-014-0621-5

Bélanger, M. C., & Marois, Y. (2001). Hemocompatibility, biocompatibility, inflammatory and in vivo studies of primary reference materials low-density polyethylene and polydimethylsiloxane: A review. *Journal of Biomedical Materials Research*, *58*, 467–477. https://doi.org/10.1002/jbm.1043

Beldjilali-Labro, M., Garcia, A. G., Farhat, F., Bedoui, F., Grosset, J. F., Dufresne, M., & Legallais, C. (2018). Biomaterials in tendon and skeletal muscle tissue engineering: Current trends and challenges. *Materials*, *11*(7). https://doi.org/10.3390/ma11071116

Bickhaus, J. A., Fraser, M. O., Weidner, A. C., Jayes, F. L., Amundsen, C. L., Gall, K., Miller, A. T., Marini, F. C., Robboy, S. J., & Siddiqui, N. Y. (2021). Polycarbonate Urethan Mesh: a New Material for Pelvic Reconstruction. *Female Pelvic Medicine & Reconstructive Surgery*, *27*(2). https://doi.org/10.1097/SPV

Bradley, M. S., Bickhaus, J. A., Amundsen, C. L., Newcomb, L. K., Truong, T., Weidner, A. C., & Siddiqui, N. Y. (2020). Vaginal Uterosacral Ligament Suspension: A Retrospective Cohort of Absorbable and Permanent Suture Groups. *Female Pelvic Medicine & Reconstructive Surgery*, *26*(5), 287–298. https://doi.org/10.1097/SPV

Brincat, C. A. (2019). Pelvic Organ Prolapse Reconsidering Treatment, Innovation, and Failure. *JAMA - Journal of the American Medical Association*, *322*(11), 1054–1065. https://doi.org/10.1001/jama.2019.12812

Burdick, J. A., Chung, C., Jia, X., Randolph, M. A., & Langer, R. (2005). Controlled degradation and mechanical behavior of photopolymerized hyaluronic acid networks. *Biomacromolecules*, *6*(1), 386–391. https://doi.org/10.1021/bm049508a

Burdick, J. A., & Prestwich, G. D. (2011). Hyaluronic acid hydrogels for biomedical applications. *Advanced Materials*, *23*(12), 41–56. https://doi.org/10.1002/adma.201003963

Bursac, N., Juhas, M., & Rando, T. A. (2015). Synergizing Engineering and Biology to Treat and Model Skeletal Muscle Injury and Disease. *Annual Review of Biomedical Engineering*, *17*, 217–242. https://doi.org/10.1146/annurev-bioeng-071114-040640

Cadena, I., Chen, A., Arvidson, A., & Fogg, K. C. (2020). Biomaterial strategies to replicate gynecological tissue. *Biomaterials Science*, 26–28. https://doi.org/10.1039/d0bm01240h

Caliari, S. R., & Burdick, J. A. (2016). A practical guide to hydrogels for cell culture. *Nature Methods*, *13*(5), 405–414. https://doi.org/10.1038/nmeth.3839

Caliari, S. R., Vega, S. L. S. L., Kwon, M., Soulas, E. M., & Burdick, J. A. (2016). Dimensionality and spreading influence MSC YAP/TAZ signaling in hydrogel environments. *Biomaterials*, *103*(6188), 314–323. https://doi.org/10.1016/j.biomaterials.2016.06.061

Campbell, R. M. (1950). The anatomy and histology of the sacrouterine ligaments. *American Journal of Obstetrics and Gynecology*, *59*(1), 1–12. https://doi.org/10.1016/0002-9378(50)90334-6

Chainani, A., Hippensteel, K. J., Kishan, A., Garrigues, N. W., Ruch, D. S., Guilak, F., & Little, D. (2013). Multilayered electrospun scaffolds for tendon tissue engineering. *Tissue Engineering - Part A*, *19*(23–24), 2594–2604. https://doi.org/10.1089/ten.tea.2013.0165

Chang, Y., Sun, X., Li, Q., Ding, X., Liu, H., & Wang, J. (2017). Silk fibroin scaffold as a potential choice for female pelvic reconstruction: A study on the biocompatibility in abdominal wall, pelvic, and vagina. *Microscopy Research and Technique*, *80*(3), 291–297. https://doi.org/10.1002/jemt.22653

Chapple, C. R., Osman, N. I., Mangera, A., Hillary, C., Roman, S., Bullock, A., & Macneil, S. (2015). Application of Tissue Engineering to Pelvic Organ Prolapse and Stress Urinary Incontinence. *Lower Urinary Tract Symptoms (LUTS)*, *7*, 63–70. https://doi.org/10.1111/luts.12098

Chaudhuri, O., Gu, L., Klumpers, D., Darnell, M., Bencherif, S. A., Weaver, J. C., Huebsch, N., Lee, H. P., Lippens, E., Duda, G. N., & Mooney, D. J. (2016). Hydrogels with tunable stress relaxation regulate stem cell fate and activity. *Nature Materials*, *15*(3), 326–334. https://doi.org/10.1038/nmat4489

Chen, G., & Jiang, M. (2011). Cyclodextrin-based inclusion complexation bridging supramolecular chemistry and macromolecular self-assembly. *Chemical Society Reviews*, *40*(5), 2254–2266. https://doi.org/10.1039/c0cs00153h

Chen, M. H., Wang, L. L., Chung, J. J., Kim, Y. H., Atluri, P., & Burdick, J. A. (2017). Methods to Assess Shear-Thinning Hydrogels for Application As Injectable Biomaterials. *ACS Biomaterials Science and Engineering*, *3*(12), 3146–3160.

https://doi.org/10.1021/acsbiomaterials.7b00734

Chopin-Doroteo, M., Mandujano-Tinoco, E. A., & Krötzsch, E. (2021). Tailoring of the rheological properties of bioinks to improve bioprinting and bioassembly for tissue replacement. *Biochimica et Biophysica Acta - General Subjects*, *1865*(2). https://doi.org/10.1016/j.bbagen.2020.129782

Christ, G. J., Sharma, P., Hess, W., & Bour, R. (2021). *Modular biofabrication platform for diverse tissue engineering applications and related method thereof* (Patent No. US 2021/0369917 A1).

Christensen, K. W., Turner, J., Coughenour, K., Maghdouri-White, Y., Bulysheva, A. A., Sergeant, O., Rariden, M., Randazzo, A., Sheean, A. J., Christ, G. J., & Francis, M. P. (2022). Assembled Cell-Decorated Collagen (AC-DC) Fiber Bioprinted Implants with Musculoskeletal Tissue Properties Promote Functional Recovery in Volumetric Muscle Loss. *Advanced Healthcare Materials*, *11*(3), 1–15. https://doi.org/10.1002/adhm.202101357

Christman, K., Alperin, M., & Duran, P. (2022). *Extracellular Matrix for Treating Pelvic Floor Disorders and Skeletal Muscle Degeneration* (Patent No. US 2022/0296776 A1).

Christopherson, G. T., Song, H., & Mao, H. Q. (2009). The influence of fiber diameter of electrospun substrates on neural stem cell differentiation and proliferation. *Biomaterials*, *30*(4), 556–564. https://doi.org/10.1016/j.biomaterials.2008.10.004

Cola, A., Marino, G., Milani, R., Barba, M., Volontè, S., Spelzini, F., Manodoro, S., & Frigerio, M. (2022). Native-tissue prolapse repair: Efficacy and adverse effects of uterosacral ligaments suspension at 10-year follow up. *International Journal of Gynecology and Obstetrics*, *September 2021*, 1–6. https://doi.org/10.1002/ijgo.14096

Cook, C. J., Miller, A. E., Barker, T. H., Di, Y., & Fogg, K. C. (2022). Characterizing the extracellular matrix transcriptome of cervical, endometrial, and uterine cancers. *Matrix Biology Plus*, *15*, 100117. https://doi.org/10.1016/j.mbplus.2022.100117

Corona, B. T., Rivera, J. C., Owens, J. G., Wenke, J. C., & Rathbone, C. R. (2015). Volumetric muscle loss leads to permanent disability following extremity trauma. *Journal of Rehabilitation Research and Development*, *52*(7), 785–792. https://doi.org/10.1682/JRRD.2014.07.0165

Corona, B. T., Ward, C. L., Baker, H. B., Walters, T. J., & Christ, G. J. (2013). Implantation of *In Vitro* Tissue Engineered Muscle Repair Constructs and Bladder Acellular Matrices Partially Restore *In Vivo* Skeletal Muscle Function in a Rat Model of Volumetric Muscle Loss Injury. *Tissue Engineering Part A*, *20*, 131219054609007. https://doi.org/10.1089/ten.tea.2012.0761

Cosgrove, B. D., Mui, K. L., Driscoll, T. P., Caliari, S. R., Mehta, K. D., Assoian, R. K., Burdick, J. A., & Mauck, R. L. (2016). N-cadherin adhesive interactions modulate matrix mechanosensing and fate commitment of mesenchymal stem cells. *Nature Materials*, *15*(12), 1297–1306. https://doi.org/10.1038/nmat4725

Couri, B. M., Lenis, A. T., Borazjani, A., Paraiso, M. F. R., & Damaser, M. S. (2012). Animal

models of female pelvic organ prolapse: Lessons learned. *Expert Review of Obstetrics and Gynecology*, *7*(3), 249–260. https://doi.org/10.1586/eog.12.24

Courtney, T., Sacks, M. S., Stankus, J., Guan, J., & Wagner, W. R. (2006). Design and analysis of tissue engineering scaffolds that mimic soft tissue mechanical anisotropy. *Biomaterials*, *27*(19), 3631–3638. https://doi.org/10.1016/j.biomaterials.2006.02.024

Cundiff, Geoffrey W. MD, FACOG, FACS, F. (2020). Surgical Innovation and the US Food and Drug Administration. *Female Pelvic Medicine & Reconstructive Surgery*, *25*(4), 263–264. https://doi.org/10.1097/SPV

Cunniffe, G. M., Díaz-Payno, P. J., Sheehy, E. J., Critchley, S. E., Almeida, H. V., Pitacco, P., Carroll, S. F., Mahon, O. R., Dunne, A., Levingstone, T. J., Moran, C. J., Brady, R. T., O'Brien, F. J., Brama, P. A. J., & Kelly, D. J. (2019). Tissue-specific extracellular matrix scaffolds for the regeneration of spatially complex musculoskeletal tissues. *Biomaterials*, *188*(September 2018), 63–73. https://doi.org/10.1016/j.biomaterials.2018.09.044

Daghma, D. E. S., Malhan, D., Simon, P., Stötzel, S., Kern, S., Hassan, F., Lips, K. S., Heiss, C., & El Khassawna, T. (2018). Computational segmentation of collagen fibers in bone matrix indicates bone quality in ovariectomized rat spine. *Journal of Bone and Mineral Metabolism*, *36*(3), 297–306. https://doi.org/10.1007/s00774-017-0844-5

Daniels, R. J. (2015). A generation at risk : Young investigators and the future of the biomedical workforce. *PNAS*, *112*(2), 313–318. https://doi.org/10.1073/pnas.1418761112

Daniels, S. D., Stewart, C. M., Garvey, K. D., Brook, E. M., Higgins, L. D., & Matzkin, E. G. (2019). Sex-Based Differences in Patient-Reported Outcomes After Arthroscopic Rotator Cuff Repair. *Orthopaedic Journal of Sports Medicine*, *7*(11), 1–10. https://doi.org/10.1177/2325967119881959

Davidson, M. D., Song, K. H., Lee, M. H., Llewellyn, J., Du, Y., Baker, B. M., Wells, R. G., & Burdick, J. A. (2019). Engineered Fibrous Networks to Investigate the Influence of Fiber Mechanics on Myofibroblast Differentiation. *ACS Biomaterials Science and Engineering*, *5*(8), 3899–3908. https://doi.org/10.1021/acsbiomaterials.8b01276

De Vita, R., & Munson, J. (2021). Special Issue on the Advances in Engineering for Women's Health. *Annals of Biomedical Engineering*, *49*, 1785–1787. https://doi.org/10.1007/s10439-021-02837-5

De Witte, T.-M., Fratila-Apachitei, L. E., Zadpoor, A. A., & Peppas, N. A. (2018). Bone tissue engineering via growth factor delivery: from scaffolds to complex matrices. *Regenerative Biomaterials*, *5*(4), 197–211. https://doi.org/10.1093/rb/rby013

Dienes, J., Browne, S., Farjun, B., Amaral Passipieri, J., Mintz, E. L., Killian, G., Healy, K. E., & Christ, G. J. (2021). Semisynthetic Hyaluronic Acid-Based Hydrogel Promotes Recovery of the Injured Tibialis Anterior Skeletal Muscle Form and Function. *ACS Biomaterials Science and Engineering*, *7*(4), 1587–1599. https://doi.org/10.1021/acsbiomaterials.0c01751

Dimatteo, R., Darling, N. J., & Segura, T. (2018). In situ forming injectable hydrogels for drug delivery and wound repair. *Advanced Drug Delivery Reviews*, *127*, 167–184.

https://doi.org/10.1016/j.addr.2018.03.007

Disney, C. M., Lee, P. D., Hoyland, J. A., Sherratt, M. J., & Bay, B. K. (2018). A review of techniques for visualising soft tissue microstructure deformation and quantifying strain Ex Vivo. *Journal of Microscopy*, *272*(3), 165–179. https://doi.org/10.1111/jmi.12701

Donaldson, K., & De Vita, R. (2022). Ex vivo uniaxial tensile properties of rat utero-sacral ligaments. *Under Review*.

Donaldson, K., Huntington, A., & De Vita, R. (2021). Mechanics of Uterosacral Ligaments: Current Knowledge, Existing Gaps, and Future Directions. *Annals of Biomedical Engineering*, *49*, 1788–1804. https://doi.org/10.1007/s10439-021-02755-6

Doostmohammadi, M., Forootanfar, H., & Ramakrishna, S. (2020). Regenerative medicine and drug delivery: Progress via electrospun biomaterials. *Materials Science and Engineering C*, *109*(April 2019), 110521. https://doi.org/10.1016/j.msec.2019.110521

Drury, J. L., & Mooney, D. J. (2003). Hydrogels for tissue engineering: Scaffold design variables and applications. *Biomaterials*, *24*(24), 4337–4351. https://doi.org/10.1016/S0142-9612(03)00340-5

Eder, C., Schmidt-Bleek, K., Geissler, S., Sass, F. A., Maleitzke, T., Pumberger, M., Perka, C., Duda, G. N., & Winkler, T. (2020). Mesenchymal stromal cell and bone marrow concentrate therapies for musculoskeletal indications: a concise review of current literature. *Molecular Biology Reports*, *47*(6), 4789–4814. https://doi.org/10.1007/s11033-020-05428-0

Engler, A. J., Sen, S., Sweeney, H. L., & Discher, D. E. (2006). Matrix elasticity directs stem cell lineage specification. *Cell*, *126*(4), 677–689. https://doi.org/10.1016/j.cell.2006.06.044

Eskandari, S., Guerin, T., Toth, I., & Stephenson, R. J. (2017). Recent advances in self-assembled peptides: Implications for targeted drug delivery and vaccine engineering. *Advanced Drug Delivery Reviews*, *110–111*, 169–187. https://doi.org/10.1016/j.addr.2016.06.013

Fairbanks, B. D., Schwartz, M. P., Bowman, C. N., & Anseth, K. S. (2009). Photoinitiated polymerization of PEG-diacrylate with lithium phenyl-2,4,6-trimethylbenzoylphosphinate: polymerization rate and cytocompatibility. *Biomaterials*, *30*(35), 6702–6707. https://doi.org/10.1016/j.biomaterials.2009.08.055

FDA takes action to protect women's health, orders manufacturers of surgical mesh intended for transvaginal repair of pelvic organ prolapse to stop selling all devices. (2019). Food and Drug Administration (FDA). https://www.fda.gov/news-events/press-announcements/fda-takes-action-protect-womens-health-orders-manufacturers-surgical-mesh-intended-transvaginal

Feola, A., Abramowitch, S., Jallah, Z., Stein, S., Barone, W., Palcsey, S., & Moalli, P. (2013). Deterioration in biomechanical properties of the vagina following implantation of a high-stiffness prolapse mesh. *BJOG: An International Journal of Obstetrics and Gynaecology*, *120*(2), 224–232. https://doi.org/10.1111/1471-0528.12077

Feola, Andrew, Abramowitch, S., Jones, K., Stein, S., & Moalli, P. (2010). Parity negatively impacts vaginal mechanical properties and collagen structure in rhesus macaques. *American*

Journal of Obstetrics and Gynecology, *203*(6), 595.e1-595.e8. https://doi.org/10.1016/j.ajog.2010.06.035

Feola, Andrew, Moalli, P., Alperin, M., Duerr, R., Gandley, R. E., & Abramowitch, S. (2011). Impact of pregnancy and vaginal delivery on the passive and active mechanics of the rat vagina. *Annals of Biomedical Engineering*, *39*(1), 549–558. https://doi.org/10.1007/s10439-010-0153-9

Fogg, K., Tseng, N.-H., Peyton, S. R., Holeman, P., McLoughlin, S., Fisher, J. P., Sutton, A., Shikanov, A., Hashemi, N. N., Zhang, Y., House, M. D., Vogt, B. J., Aguado, B. A., Bradford, J., Robinson, J. L., Thomas, P. K., Lau, A. G., & Oyen, M. (2022). Roadmap on Biomaterials for Women's Health To. *Journal of Physical Materials*. https://doi.org/10.1088/2515-7639/ac90ee%0AManuscript

Frantz, C., Stewart, K. M., Weaver, V. M., Frantz, C., Stewart, K. M., & Weaver, V. M. (2010). *The Extracellular Matrix at a Glance*. *2010*, 4195–4200. https://doi.org/10.1242/jcs.023820

Frontera, W. R., & Ochala, J. (2015). Skeletal Muscle: A Brief Review of Structure and Function. *Behavior Genetics*, *45*(2), 183–195. https://doi.org/10.1007/s00223-014-9915-y

Fu, Q., Duan, C., Yan, Z., Li, Y., Si, Y., Liu, L., Yu, J., & Ding, B. (2018). *Nanofiber-Based Hydrogels : Controllable Synthesis and Multifunctional Applications*. *1800058*, 1–19. https://doi.org/10.1002/marc.201800058

Fujisawa, C., & Castellot, J. J. (2014). Matrix production and remodeling as therapeutic targets for uterine leiomyoma. *Journal of Cell Communication and Signaling*, *8*(3), 179–194. https://doi.org/10.1007/s12079-014-0234-x

Gaffey, A. C., Chen, M. H., Venkataraman, C. M., Trubelja, A., Rodell, C. B., Dinh, P. V, Hung, G., MacArthur, J. W., Soopan, R. V, Burdick, J. A., & Atluri, P. (2015). Injectable shear-thinning hydrogels used to deliver endothelial progenitor cells, enhance cell engraftment, and improve ischemic myocardium. *The Journal of THoracic and Cardiovascular Surgery*, *150*(5), 1268–1277. https://doi.org/10.1016/j.jtcvs.2015.07.035

Gent, A. N., & Kaang, S. (1986). Pull-off forces for adhesive tapes. *Journal of Applied Polymer Science*, *32*(4), 4689–4700. https://doi.org/10.1002/app.1986.070320433

Gigliobianco, G., Regueros, S. R., Osman, N. I., Bissoli, J., Bullock, A. J., Chapple, C. R., & MacNeil, S. (2015). Biomaterials for pelvic floor reconstructive surgery: How can we do better? *BioMed Research International*, *2015*. https://doi.org/10.1155/2015/968087

Gilbert-Honick, J., Iyer, S. R., Somers, S. M., Lovering, R. M., Wagner, K., Mao, H. Q., & Grayson, W. L. (2018). Engineering functional and histological regeneration of vascularized skeletal muscle. *Biomaterials*, *164*, 70–79. https://doi.org/10.1016/j.biomaterials.2018.02.006

Gilbert, P. M., Havenstrite, K. L., Magnusson, K. E. G., Sacco, A., Leonardi, N. A., Kraft, P., Nguyen, N. K., Thrun, S., Lutolf, M. P., & Blau, H. M. (2010). Substrate elasticity regulates skeletal muscle stem cell self-renewal in culture. *Science*, *329*(5995), 1078–1081. https://doi.org/10.1126/science.1191035

Gillies, A. R., & Lieber, R. L. (2011). Structure and function of the skeletal muscle extracellular

matrix. *Muscle and Nerve*, *44*(3), 318–331. https://doi.org/10.1002/mus.22094

Gnecco, J. S., Brown, A. T., Kan, E. L., Baugh, L., Ives, C., Loring, M., & Griffith, L. G. (2020). Physiomimetic Models of Adenomyosis. *Seminars in Reproductive Medicine*, *38*(2–3), 179–196. https://doi.org/10.1055/s-0040-1719084

Godbole, A., Miller, B., Bothwell, M. K., Montfort, D., & Davis, S. C. (n.d.). Engineering students' perceptions of belonging through the lens of social identity. *CoNECD 2018 - Collaborative Network for Engineering and Computing Diversity Conference*. https://peer.asee.org/29530

Gonzalez-Fernandez, T., Sikorski, P., & Leach, J. K. (2019). Bio-instructive materials for musculoskeletal regeneration. *Acta Biomaterialia*, *96*, 20–34. https://doi.org/10.1016/j.actbio.2019.07.014

Gramlich, W. M., Kim, I. L., & Burdick, J. A. (2013). Synthesis and orthogonal photopatterning of hyaluronic acid hydrogels with thiol-norbornene chemistry. *Biomaterials*, *34*(38), 9803–9811. https://doi.org/10.1016/j.biomaterials.2013.08.089

Gregersen, P. K., Kilcoyne, A., Kim, J. J., Lavender, M., Marsh, E. E., Matteson, K. A., Maybin, J. A., Metz, C. N., Moreno, I., Silk, K., Sommer, M., Simon, C., Wagner, P., Griffith, L. G., Tariyal, R., & Taylor, H. S. (2020). Expert Reviews Menstruation : science and society. *American Journal of Obstetrics & Gynecology*, *2019*(November), 624–664.

Greiner, A., & Wendorff, J. H. (2007). Electrospinning: A fascinating method for the preparation of ultrathin fibers. *Angew. Chem. Int. Ed.*, *46*(30), 5670–5703. https://doi.org/10.1002/anie.200604646

Grewal, M. G., & Highley, C. B. (2021). Electrospun hydrogels for dynamic culture systems: advantages, progress, and opportunities. *Biomaterials Science*. https://doi.org/10.1039/d0bm01588a

Griffin, M., Premakumar, Y., Seifalian, A., Butler, P. E., & Szarko, M. (2016). Biomechanical characterization of human soft tissues using indentation and tensile testing. *Journal of Visualized Experiments*, *2016*(118), 1–8. https://doi.org/10.3791/54872

Grimm, M. J. (2019). Engineering and women's health: A slow start, but gaining momentum. *Interface Focus*, *9*(4). https://doi.org/10.1098/rsfs.2019.0017

Hansen, S. G., Taskin, M. B., Chen, M., Wogensen, L., Vinge Nygaard, J., & Axelsen, S. M. (2019). Electrospun nanofiber mesh with fibroblast growth factor and stem cells for pelvic floor repair. *Journal of Biomedical Materials Research Part B: Applied Biomaterials*, jbm.b.34364. https://doi.org/10.1002/jbm.b.34364

Haylen, B. T., Maher, C. F., Barber, M. D., Camargo, S., Dandolu, V., Digesu, A., Goldman, H. B., Huser, M., Milani, A. L., Moran, P. A., Schaer, G. N., & Withagen, M. I. J. (2016). An International Urogynecological Association (IUGA) / International Continence Society (ICS) Joint Report on the Terminology for Female Pelvic Organ Prolapse (POP). *Neurourology and Urodynamics*, *35*, 137–168. https://doi.org/10.1002/nau.22922

Herschorn, S. (2004). Female Pelvic Floor Anatomy : The Pelvic Floor , Supporting Structures , and Pelvic Organs. *Reviews in Urology*, *6*, S2–S10.

https://www.ncbi.nlm.nih.gov/pmc/articles/PMC1472875/

Highley, C. B., Prestwich, G. D., & Burdick, J. A. (2016). Recent advances in hyaluronic acid hydrogels for biomedical applications. *Current Opinion in Biotechnology*, *40*, 35–40. https://doi.org/10.1016/j.copbio.2016.02.008

Highley, C. B., Rodell, C. B., Burdick, J. A., Highley, C. B., Rodell, C. B., & Burdick, J. A. (2015). Direct 3D Printing of Shear-Thinning Hydrogels into Self- Healing Hydrogels. *Advanced Materials*, *27*, 5057–5079. https://doi.org/10.1002/adma.201501234

Highley, C. B., Rodell, C. B., Kim, I. L., Wade, R. J., & Burdick, J. A. (2014). Ordered, adherent layers of nanofibers enabled by supramolecular interactions. *J. Mater. Chem. B*, *2*, 8110–8115. https://doi.org/10.1039/c4tb00724g

Highley, C. B., Song, K. H., Daly, A. C., & Burdick, J. A. (2019). Jammed Microgel Inks for 3D Printing Applications. *Advanced Science*, *6*(1). https://doi.org/10.1002/advs.201801076

Hilderbrand, A. M., Ford, E. M., Guo, C., Sloppy, J. D., & Kloxin, A. M. (2020). Hierarchically structured hydrogels utilizing multifunctional assembling peptides for 3D cell culture. *Biomaterials Science*, *8*(5), 1256–1269. https://doi.org/10.1039/c9bm01894h

Hinderer, S., Layland, S. L., & Schenke-Layland, K. (2016). ECM and ECM-like materials - Biomaterials for applications in regenerative medicine and cancer therapy. *Advanced Drug Delivery Reviews*, *97*, 260–269. https://doi.org/10.1016/j.addr.2015.11.019

History of women's participation in clinical research. (n.d.). National Institutes of Health. https://orwh.od.nih.gov/toolkit/recruitment/history

Hu, C., Zhang, F., Long, L., Kong, Q., Luo, R., & Wang, Y. (2020). Dual-responsive injectable hydrogels encapsulating drug-loaded micelles for on-demand antimicrobial activity and accelerated wound healing. *Journal of Controlled Release*, *324*(May), 204–217. https://doi.org/10.1016/j.jconrel.2020.05.010

Hui, E., Gimeno, K. I., Guan, G., & Caliari, S. R. (2019). Spatiotemporal Control of Viscoelasticity in Phototunable Hyaluronic Acid Hydrogels. *Biomacromolecules*, *20*(11), 4126–4134. https://doi.org/10.1021/acs.biomac.9b00965

Hympanova, L., Mori da Cunha, M. G. M. C., Rynkevic, R., Zündel, M., Gallego, M. R., Vange, J., Callewaert, G., Urbankova, I., Van der Aa, F., Mazza, E., & Deprest, J. (2017). Physiologic musculofascial compliance following reinforcement with electrospun polycaprolactone-ureidopyrimidinone mesh in a rat model. *Journal of the Mechanical Behavior of Biomedical Materials*, *74*(June), 349–357. https://doi.org/10.1016/j.jmbbm.2017.06.032

Hynes, R. O. (2009). The extracellular matrix: Not just pretty fibrils. *Science*, *326*(5957), 1216–1219. https://doi.org/10.1126/science.1176009

Ik, S. L., Oh, H. K., Meng, W., Kang, I. K., & Ito, Y. (2004). Nanofabrication of microbial polyester by electrospinning promotes cell attachment. *Macromolecular Research*, *12*(4), 374–378. https://doi.org/10.1007/bf03218414

Ikeda, K., Horie-Inoue, K., & Inoue, S. (2019). Functions of estrogen and estrogen receptor

signaling on skeletal muscle. *Journal of Steroid Biochemistry and Molecular Biology*, *191*(March), 105375. https://doi.org/10.1016/j.jsbmb.2019.105375

Iwanaga, R., Orlicky, D. J., Arnett, J., Guess, M. K., Hurt, K. J., & Connell, K. A. (2016). Comparative histology of mouse, rat, and human pelvic ligaments. *International Urogynecology Journal*, *27*(11), 1697–1704. https://doi.org/10.1007/s00192-016-3008-6

Jammalamadaka, U., & Tappa, K. (2018). Recent advances in biomaterials for 3D printing and tissue engineering. *Journal of Functional Biomaterials*, *9*(1). https://doi.org/10.3390/jfb9010022

Järvinen, T. A. H., Järvinen, T. L. N., Kääriäinen, M., Kalimo, H., & Järvinen, M. (2005). Muscle injuries: Biology and treatment. *American Journal of Sports Medicine*, *33*(5), 745–764. https://doi.org/10.1177/0363546505274714

Jelovsek, J. E., Barber, M. D., Norton, P., Brubaker, L., Gantz, M., Richter, H. E., Weidner, A., Menefee, S., Schaffer, J., Pugh, N., & Meikle, S. (2018). Effect of uterosacral ligament suspension vs sacrospinous ligament fixation with or without perioperative behavioral therapy for pelvic organ vaginal prolapse on surgical outcomes and prolapse symptoms at 5 years in the OPTIMAL randomized clinical trial. *JAMA - Journal of the American Medical Association*, *319*(15), 1554–1565. https://doi.org/10.1001/jama.2018.2827

Jelovsek, J. E., Maher, C., & Barber, M. D. (2007). Pelvic organ prolapse. *Lancet*, *369*(9566), 1027–1038. https://doi.org/10.1016/S0140-6736(07)60462-0

Ji, Y., Ghosh, K., Shu, X. Z., Li, B., Sokolov, J. C., Prestwich, G. D., Clark, R. A. F., & Rafailovich, M. H. (2006). Electrospun three-dimensional hyaluronic acid nanofibrous scaffolds. *Biomaterials*, *27*(20), 3782–3792. https://doi.org/10.1016/j.biomaterials.2006.02.037

Johannesson, L., Enskog, A., Mölne, J., Diaz-Garcia, C., Hanafy, A., Dahm-Kähler, P., Tekin, A., Tryphonopoulos, P., Morales, P., Rivas, K., Ruiz, P., Tzakis, A., Olausson, M., & Brännström, M. (2013). Preclinical report on allogeneic uterus transplantation in non-human primates. *Human Reproduction*, *28*(1), 189–198. https://doi.org/10.1093/humrep/des381

Juhas, M., Engelmayr, G. C., Fontanella, A. N., Palmer, G. M., & Bursac, N. (2014). Biomimetic engineered muscle with capacity for vascular integration and functional maturation in vivo. *Proceedings of the National Academy of Sciences of the United States of America*, *111*(15), 5508–5513. https://doi.org/10.1073/pnas.1402723111

Jun, I., Han, H. S., Edwards, J. R., & Jeon, H. (2018). Electrospun fibrous scaffolds for tissue engineering: Viewpoints on architecture and fabrication. *International Journal of Molecular Sciences*, *19*(3). https://doi.org/10.3390/ijms19030745

Kafantari, H., Kounadi, E., Fatouros, M., Milonakis, M., & Tzaphlidou, M. (2000). Structural alterations in rat skin and bone collagen fibrils induced by ovariectomy. *Bone*, *26*(4), 349–353. https://doi.org/10.1016/S8756-3282(99)00279-3

Kakuta, T., Takashima, Y., & Harada, A. (2013). Highly elastic supramolecular hydrogels using host-guest inclusion complexes with cyclodextrins. *Macromolecules*, *46*(11), 4575–4579.

https://doi.org/10.1021/ma400695p

Kasabwala, K., Goueli, R., & Culligan, P. J. (2019). A live porcine model for robotic sacrocolpopexy training. *International Urogynecology Journal*, *30*(8), 1371–1375. https://doi.org/10.1007/s00192-019-03936-7

Katti, D., Vasita, R., & Shanmugam, K. (2008). Improved Biomaterials for Tissue Engineering Applications: Surface Modification of Polymers. *Current Topics in Medicinal Chemistry*, *8*(4), 341–353. https://doi.org/10.2174/156802608783790893

Kenton, Kimberyly; Mueller, E. R. (2006). The global burden of female pelvic floor disorders. *BJU International*, *98*(s1), 6–7. https://doi.org/10.1111/j.1464-410x.2006.06300.x

Khademhosseini, A., Vacanti, J. P., & Langer, R. (2009). Progress in tissue. *Scientific American*, *300*(5), 64–71. https://doi.org/10.1038/scientificamerican0509-64

Khorshidi, S., Solouk, A., Mirzadeh, H., Mazinani, S., Lagaron, J. M., Sharifi, S., & Ramakrishna, S. (2016). A review of key challenges of electrospun scaffolds for tissue-engineering applications. *J Tissue Eng Regen Med*, *10*, 715–738. https://doi.org/10.1002/term

Kim, I. L., Khetan, S., Baker, B. M., Chen, C. S., & Burdick, J. A. (2013). Fibrous hyaluronic acid hydrogels that direct MSC chondrogenesis through mechanical and adhesive cues. *Biomaterials*, *34*(22), 5571–5580. https://doi.org/10.1016/j.biomaterials.2013.04.004

Klinge, U., Klosterhalfen, B., Conze, J., Limberg, W., Obolenski, B., Öttinger, A. P., & Schumpelick, V. (1998). Modified mesh for hernia repair that is adapted to the physiology of the abdominal wall. *European Journal of Surgery*, *164*(12), 951–960. https://doi.org/10.1080/110241598750005138

Knapp, D. M., Barocas, V. H., Moon, A. G., Yoo, K., Petzold, L. R., & Tranquillo, R. T. (1997). Rheology of reconstituted type I collagen gel in confined compression. *Journal of Rheology*, *41*(5), 971–993. https://doi.org/10.1122/1.550817

Koebele, S. V., Palmer, J. M., Hadder, B., Melikian, R., Fox, C., Strouse, I. M., Denardo, D. F., George, C., Daunis, E., Nimer, A., Mayer, L. P., Dyer, C. A., & Bimonte-Nelson, H. A. (2019). Hysterectomy Uniquely Impacts Spatial Memory in a Rat Model: A Role for the Nonpregnant Uterus in Cognitive Processes. *Endocrinology*, *160*(1), 1–19. https://doi.org/10.1210/en.2018-00709

Krause, H. G., & Goh, J. T. (2009). Biomechanical properties of graft materials employed for pelvic floor reconstructive surgeries. *Current Opinion in Obstetrics and Gynecology*, *21*(5), 419–423. https://doi.org/10.1097/GCO.0b013e32832fd27c

Kreeger, P. K., Deck, J. W., Woodruff, T. K., & Shea, L. D. (2006). The in vitro regulation of ovarian follicle development using alginate-extracellular matrix gels. *Biomaterials*, *27*(5), 714–723. https://doi.org/10.1016/j.biomaterials.2005.06.016

Kuligowska, E., Deeds, L., & Lu, K. (2005). Pelvic Pain : Overlooked and Underdiagnosed Gynecologic. *RadioGraphics*, *25*(1), 3–20. http://radiographics.rsna.org/content/25/1/3.full

Kuo, C. K., Marturano, J. E., & Tuan, R. S. (2010). Novel strategies in tendon and ligament

tissue engineering: Advanced biomaterials and regeneration motifs. *BMC Sports Science, Medicine and Rehabilitation*, *2*(1), 1–14. https://doi.org/10.1186/1758-2555-2-20

Kuo, C. K., & Tuan, R. S. (2003). Tissue Engineering with Mesenchymal Stem Cells. *IEEE Engineering in Medicine and Biology Magazine*, *22*(5), 51–56. https://doi.org/10.1109/MEMB.2003.1256272

Kurniawan, N. A., & Bouten, C. V. C. (2018). Mechanobiology of the cell–matrix interplay: Catching a glimpse of complexity via minimalistic models. *Extreme Mechanics Letters*, *20*, 59–64. https://doi.org/10.1016/j.eml.2018.01.004

Kurtaliaj, I., Golman, M., Abraham, A. C., & Thomopoulos, S. (2019). Biomechanical testing of murine tendons. *Journal of Visualized Experiments*, *2019*(152), 1–12. https://doi.org/10.3791/60280

Kutch, J. J., & Tu, F. F. (2016). Altered brain connectivity in dysmenorrhea: pain modulation and the motor cortex. *Pain*, *157*(1), 5–6. https://doi.org/10.1097/j.pain.0000000000000364

Kwee, B. J., & Mooney, D. J. (2017). Biomaterials for skeletal muscle tissue engineering. *Current Opinion in Biotechnology*, *47*, 16–22. https://doi.org/10.1016/j.copbio.2017.05.003

Kyburz, K. A., & Anseth, K. S. (2015). *Synthetic Mimics of the Extracellular Matrix : How Simple is Complex Enough ? 43*(3), 489–500. https://doi.org/10.1007/s10439-015-1297-4

Laganà, A. S., La Rosa, V. L., Rapisarda, A. M. C., Valenti, G., Sapia, F., Chiofalo, B., Rossetti, D., Frangež, H. B., Bokal, E. V., & Vitale, S. G. (2017). Anxiety and depression in patients with pulmonary hypertension: Impact and management challenges. *International Journal of Women's Health*, *9*, 323–330. https://doi.org/10.2147/IJWH.S119729

Lambert, W. M., Wells, M. T., Cipriano, M. F., Sneva, J. N., Morris, J. A., & Golightly, L. M. (2020). Career choices of underrepresented and female postdocs in the biomedical sciences. *ELife*, *9*, e48774. https://doi.org/10.7554/eLife.48774

Lavelle, R. S., Christie, A. L., Alhalabi, F., & Zimmern, P. E. (2016). Risk of Prolapse Recurrence after Native Tissue Anterior Vaginal Suspension Procedure with Intermediate to Long-Term Followup. *Journal of Urology*, *195*(4), 1014–1020. https://doi.org/10.1016/j.juro.2015.10.138

Lee, C. H., Shin, H. J., Cho, I. H., Kang, Y. M., Kim, I. A., Park, K. D., & Shin, J. W. (2005). Nanofiber alignment and direction of mechanical strain affect the ECM production of human ACL fibroblast. *Biomaterials*, *26*(11), 1261–1270. https://doi.org/10.1016/j.biomaterials.2004.04.037

Lee, H., Gu, L., Mooney, D. J., Levenston, M. E., & Chaudhuri, O. (2017). Mechanical confinement regulates cartilage matrix formation by chondrocytes. *Nature Materials*, *16*(December). https://doi.org/10.1038/nmat4993

Lee, K. Y., & Mooney, D. J. (2001). Hydrogels for tissue engineering. *Chemical Reviews*, *101*(7), 1869–1879. https://doi.org/10.1021/cr000108x

Li, J., & Mooney, D. J. (2016). Designing hydrogels for controlled drug delivery. *Nature Reviews Materials*. https://doi.org/10.1097/IOP.0b013e31819ac7c5

Li, W.-J., Mauck, R. L., & Tuan, R. S. (2006). Electrospun Nanofibrous Scaffolds: Production, Characterization, and Applications for Tissue Engineering and Drug Delivery. *Journal of Biomedical Nanotechnology*, *1*(3), 259–275. https://doi.org/10.1166/jbn.2005.032

Liang, R., Knight, K., Easley, D., Palcsey, S., Abramowitch, S., & Moalli, P. A. (2017). Towards rebuilding vaginal support utilizing an extracellular matrix bioscaffold. *Acta Biomaterialia*, *57*, 324–333. https://doi.org/10.1016/j.actbio.2017.05.015

Liang, R., Zong, W., Palcsey, S., Abramowitch, S., & Moalli, P. A. (2015). Impact of prolapse meshes on the metabolism of vaginal extracellular matrix in rhesus macaque. *American Journal of Obstetrics and Gynecology*, *212*(2), 174.e1-174.e7. https://doi.org/10.1016/j.ajog.2014.08.008

Lim, W. L., Liau, L. L., Ng, M. H., Chowdhury, S. R., & Law, J. X. (2019). Current Progress in Tendon and Ligament Tissue Engineering. *Tissue Engineering and Regenerative Medicine*, *16*(6), 549–571. https://doi.org/10.1007/s13770-019-00196-w

Liu, J., Saul, D., Böker, K. O., Ernst, J., Lehman, W., & Schilling, A. F. (2018). Current Methods for Skeletal Muscle Tissue Repair and Regeneration. *BioMed Research International*, *2018*, 1–11. https://doi.org/10.1155/2018/1984879

Liu, Y., Rodeo, S. A., Deng, X. H., Song, Z., Chen, D., & Casey, E. (2022). Evaluation of sex differences in rodent anterior cruciate ligament injury. *Journal of Orthopaedic Research*, 1–12. https://doi.org/10.1002/jor.25346

Loebel, C., Mauck, R. L., & Burdick, J. A. (2019). Local nascent protein deposition and remodelling guide mesenchymal stromal cell mechanosensing and fate in three-dimensional hydrogels. *Nature Materials*, *18*(8), 883–891. https://doi.org/10.1038/s41563-019-0307-6

Loebel, C., Rodell, C. B., Chen, M. H., & Burdick, J. A. (2017). Shear-thinning and self-healing hydrogels as injectable therapeutics and for 3D-printing. *Nature Protocols*, *12*(8), 1521–1541. https://doi.org/10.1038/nprot.2017.053

Loftsson, T., Saokham, P., & Sá Couto, A. R. (2019). Self-association of cyclodextrins and cyclodextrin complexes in aqueous solutions. *International Journal of Pharmaceutics*, *560*(January), 228–234. https://doi.org/10.1016/j.ijpharm.2019.02.004

Lou, J., Stowers, R., Nam, S., Xia, Y., & Chaudhuri, O. (2018). Stress relaxing hyaluronic acid-collagen hydrogels promote cell spreading, fiber remodeling, and focal adhesion formation in 3D cell culture. *Biomaterials*, *154*, 213–222. https://doi.org/10.1016/j.biomaterials.2017.11.004

Lowder, J. L., Debes, K., Moon, D. K., Howden, N., Abramowitch, S. D., & Moalli, P. A. (2007). Adaptations of the rat vagina in pregnancy to accommodate delivery. *Obstetrics and Gynecology*, *109*(1), 128–135. https://doi.org/10.1097/01.AOG.0000246798.78839.62

Luchristt, D., Weidner, A. C., & Siddiqui, N. Y. (2022). Urinary basement membrane graft-augmented sacrospinous ligament suspension: a description of technique and short-term outcomes. *International Urogynecology Journal*, *33*(5), 1347–1350. https://doi.org/10.1007/s00192-022-05159-9

Lutolf, M. P., & Hubbell, J. A. (2005). Synthetic biomaterials as instructive extracellular

microenvironments for morphogenesis in tissue engineering. *Nature Biotechnology*, *23*(1), 47–55. https://doi.org/10.1038/nbt1055

Ma, Y., Guess, M., Datar, A., Hennessey, A., Cardenas, I., Johnson, J., & Connell, K. A. (2012). Knockdown of Hoxa11 In Vivo in the Uterosacral Ligament and Uterus of Mice Results in Altered Collagen and Matrix Metalloproteinase Activity1. *Biology of Reproduction*, *86*(4), 1–8. https://doi.org/10.1095/biolreprod.111.093245

Madl, A. C., Madl, C. M., & Myung, D. (2020). Injectable Cucurbit[8]uril-Based Supramolecular Gelatin Hydrogels for Cell Encapsulation. *ACS Macro Letters*, *9*, 0–7. https://doi.org/10.1021/acsmacrolett.0c00184

Magnusson, S. P., Heinemeier, K. M., & Kjaer, M. (2016). Metabolic Influences on Risk for Tendon Disorders. In *Advances in Experimental Medicine and Biology* (Vol. 920). https://doi.org/10.1007/978-3-319-33943-6_2

Mahdy, M. A. A. (2019). Skeletal muscle fibrosis: an overview. *Cell and Tissue Research*, *375*(3), 575–588. https://doi.org/10.1007/s00441-018-2955-2

Mann, C. J., Perdiguero, E., Kharraz, Y., Aguilar, S., Pessina, P., Serrano, A. L., & Muñoz-Cánoves, P. (2011). Aberrant repair and fibrosis development in skeletal muscle. *Skeletal Muscle*, *1*(21). https://doi.org/10.1186/2044-5040-1-21

Mann, J. L., Yu, A. C., Agmon, G., & Appel, E. (2017). Supramolecular Polymeric Biomaterials. *Biomaterials Science*. https://doi.org/10.1039/C7BM00780A

Manodoro, S., Frigerio, M., Milani, R., & Spelzini, F. (2018). Tips and tricks for uterosacral ligament suspension: how to avoid ureteral injury. *International Urogynecology Journal*, *29*(1), 161–163. https://doi.org/10.1007/s00192-017-3497-y

Mansoor, A., Curinier, S., Campagne-Loiseau, S., Platteeuw, L., Jacquetin, B., & Rabischong, B. (2017). Development of an ovine model for training in vaginal surgery for pelvic organ prolapse. *International Urogynecology Journal*, *28*(10), 1595–1597. https://doi.org/10.1007/s00192-017-3292-9

Mao, A. S., & Mooney, D. J. (2015). Regenerative medicine: Current therapies and future directions. *Proceedings of the National Academy of Sciences*, *112*(47), 14452–14459. https://doi.org/10.1073/pnas.1508520112

Martin, D., Timmins, K., Cowie, C., Alty, J., Mehta, R., Tang, A., & Varley, I. (2021). Injury Incidence Across the Menstrual Cycle in International Footballers. *Frontiers in Sports and Active Living*, *3*(March), 1–7. https://doi.org/10.3389/fspor.2021.616999

Martins, P., Lopes Silva-Filho, A., Rodrigues Maciel Da Fonseca, A. M., Santos, A., Santos, L., Mascarenhas, T., Natal Jorge, R. M., & Ferreira, A. J. M. (2013). Biomechanical properties of vaginal tissue in women with pelvic organ prolapse. *Gynecologic and Obstetric Investigation*, *75*(2), 85–92. https://doi.org/10.1159/000343230

Matellan, C., & del Rıó Hernández, A. E. (2019). Engineering the cellular mechanical microenvironment – From bulk mechanics to the nanoscale. *Journal of Cell Science*, *132*(9). https://doi.org/10.1242/jcs.229013

Matera, D. L., Wang, W. Y., Smith, M. R., Shikanov, A., & Baker, B. M. (2019). Fiber Density Modulates Cell Spreading in 3D Interstitial Matrix Mimetics. *ACS Biomaterials Science and Engineering*, *5*(6), 2965–2975. https://doi.org/10.1021/acsbiomaterials.9b00141

Mauck, R. L., Baker, B. M., Nerurkar, N. L., Burdick, J. A., Li, W. J., Tuan, R. S., & Elliott, D. M. (2009). Engineering on the straight and narrow: The mechanics of nanofibrous assemblies for fiber-reinforced tissue regeneration. *Tissue Engineering - Part B: Reviews*, *15*(2), 171–193. https://doi.org/10.1089/ten.teb.2008.0652

Mazure, C. M., & Jones, D. P. (2015). Twenty years and still counting : including women as participants and studying sex and gender in biomedical research. *BMC Women's Health*, *15*(94). https://doi.org/10.1186/s12905-015-0251-9

Mertens, J. P., Sugg, K. B., Lee, J. D., & Larkin, L. M. (2013). Engineering muscle constructs for the creation of functional engineered musculoskeletal tissue. *Regenerative Medicine*, *9*(1), 89–100. https://doi.org/10.2217/rme.13.81

Messner, M., Kurkov, S. V., Jansook, P., & Loftsson, T. (2010). Self-assembled cyclodextrin aggregates and nanoparticles. *International Journal of Pharmaceutics*, *387*(1–2), 199–208. https://doi.org/10.1016/j.ijpharm.2009.11.035

Miller, B., Hansrisuk, A., Highley, C. B., & Caliari, S. R. (2021). Guest–Host Supramolecular Assembly of Injectable Hydrogel Nanofibers for Cell Encapsulation. *ACS Biomaterials Science & Engineering*. https://doi.org/10.1021/acsbiomaterials.1c00275

Miller, B. J., Jones, B. K., Turner, J. S., Caliari, S. R., & Vaughan, M. H. (2022). Development of a Uterosacral Ligament Suspension Rat Model. *Journal of Visualized Experiments*, *186*. https://doi.org/10.3791/64311

Miller, K. S., Myers, K., & Oyen, M. (2019). Bioengineering in women's health: part I. *Interface Focus*, *9*. https://doi.org/10.1098/rsfs.2019.0017

Mintz, E. L., Passipieri, J. A., Franklin, I. R., Toscano, V. M., Afferton, E. C., Sharma, P. R., & Christ, G. J. (2020). Long-Term Evaluation of Functional Outcomes Following Rat Volumetric Muscle Loss Injury and Repair. *Tissue Engineering - Part A*, *26*(3–4), 140–156. https://doi.org/10.1089/ten.tea.2019.0126

Mintz, E. L., Passipieri, J. A., Lovell, D. Y., & Christ, G. J. (2016). Applications of In Vivo Functional Testing of the Rat Tibialis Anterior for Evaluating Tissue Engineered Skeletal Muscle Repair. *Journal of Visualized Experiments*, *116*, 1–9. https://doi.org/10.3791/54487

Mirin, A. A. (2021). Gender Disparity in the Funding of Diseases by the U.S. National Institutes of Health. *Journal of Women's Health*, *30*(7), 956–963. https://doi.org/10.1089/jwh.2020.8682

Moalli, P. A., Howden, N. S., Lowder, J. L., Navarro, J., Debes, K. M., Abramowitch, S. D., & Woo, S. L. Y. (2005). A rat model to study the structural properties of the vagina and its supportive tissues. *American Journal of Obstetrics and Gynecology*, *192*(1), 80–88. https://doi.org/10.1016/j.ajog.2004.07.008

Molloy, T., Wang, Y., & Murrell, G. A. C. (2003). The roles of growth factors in tendon and ligament healing. *Sports Medicine*, *33*(5), 381–394. https://doi.org/10.2165/00007256-

200333050-00004

Mori da Cunha, M. G. M. C., Mackova, K., Hympanova, L. H., Bortolini, M. A. T., & Deprest, J. (2021). Animal models for pelvic organ prolapse: systematic review. *International Urogynecology Journal*, *32*(6), 1331–1344. https://doi.org/10.1007/s00192-020-04638-1

Mukherjee, S., Darzi, S., Paul, K., Werkmeister, J. A., & Gargett, C. E. (2019). Mesenchymal stem cell-based bioengineered constructs: Foreign body response, cross-talk with macrophages and impact of biomaterial design strategies for pelvic floor disorders. *Interface Focus*, *9*(4). https://doi.org/10.1098/rsfs.2018.0089

Murphy, A. R., Campo, H., & Kim, J. J. (2022). Strategies for modelling endometrial diseases. *Nature Reviews Endocrinology*. https://doi.org/10.1038/s41574-022-00725-z

Najimudeen, M., Myint, M. H., & Masharudin, A. W. (2020). Reappraisal on the Management of Primary Dysmenorrhoea in Adolescents. *Scholars International Journal of Obstetrics and Gynecology*, *3*(9), 192–199. https://doi.org/10.36348/sijog.2020.v03i09.001

National Archives. (2022). *Federal Animal Welfare Regulations*. https://www.ecfr.gov/current/title-9/chapter-I/subchapter-A/part-2/subpart-C/section-2.31

National Research Council. (2011). Guide for the Care and Use of Laboratory Animals: Eighth Edition. In N. R. Council (Ed.), *National Academies Press*. The National Academies Press. https://doi.org/10.17226/12910

NIH Office of Women's Health. (2016). *Pelvic Organ Prolapse Fact Sheet*.

Ning, L., Gil, C. J., Hwang, B., Theus, A. S., Perez, L., Tomov, M. L., Bauser-Heaton, H., & Serpooshan, V. (2020). Biomechanical factors in three-dimensional tissue bioprinting. *Applied Physics Reviews*, *7*(4). https://doi.org/10.1063/5.0023206

Oh, S. S., Galanter, J., Thakur, N., Pino-yanes, M., Barcelo, N. E., White, M. J., Bruin, D. M. De, Greenblatt, R. M., Bibbins-, K., Wu, A. H. B., Borrell, L. N., Gunter, C., Powe, N. R., & Burchard, E. G. (2015). Diversity in Clinical and Biomedical Research : A Promise Yet to Be Fulfilled. *PLoS Med*, *12*(12), e1001918. https://doi.org/10.1371/journal.pmed.1001918

Olsen, A. L., Smith, V. J., Bergstrom, J. O., Colling, J. C., & Clark, A. L. (1997). Epidemiology of surgically managed pelvic organ prolapse and urinary incontinence. *Obstetrics and Gynecology*, *89*(4), 501–506. https://doi.org/10.1016/S0029-7844(97)00058-6

Orlicky, D. J., Guess, M. K., Bales, E. S., Rascoff, L. G., Arruda, J. S., Hutchinson-Colas, J. A., Johnson, J., & Connell, K. A. (2021). Using the novel pelvic organ prolapse histologic quantification system to identify phenotypes in uterosacral ligaments in women with pelvic organ prolapse. *American Journal of Obstetrics and Gynecology*, *224*(1), 67.e1-67.e18. https://doi.org/10.1016/j.ajog.2020.10.040

Osman, S. K., Brandl, F. P., Zayed, G. M., Teßmar, J. K., & Göpferich, A. M. (2011). Cyclodextrin based hydrogels: Inclusion complex formation and micellization of adamantane and cholesterol grafted polymers. *Polymer*, *52*(21), 4806–4812. https://doi.org/10.1016/j.polymer.2011.07.059

Ouyang, L., Highley, C. B., Rodell, C. B., Sun, W., & Burdick, J. A. (2016). 3D Printing of Shear-Thinning Hyaluronic Acid Hydrogels with Secondary Cross-Linking. *ACS Biomaterials Science and Engineering*, *2*(10), 1743–1751. https://doi.org/10.1021/acsbiomaterials.6b00158

Owens, B. D., Kragh, J. F., Macaitis, J., Svoboda, S. J., & Wenke, J. C. (2007). Characterization of extremity wounds in operation Iraqi freedom and operation enduring freedom. *Journal of Orthopaedic Trauma*, *21*(4), 254–257. https://doi.org/10.1097/BOT.0b013e31802f78fb

Palmerola, R., & Rosenblum, N. (2019). Prolapse Repair Using Non-synthetic Material: What is the Current Standard? *Current Urology Reports*, *20*(11). https://doi.org/10.1007/s11934-019-0939-8

Palomba, S., & Giudice, L. C. (2020). Endometrial function in women with polycystic ovary syndrome: a comprehensive review. *Human Reproduction Update*, *00*(0), 1–35. https://doi.org/10.1093/humupd/dmaa051

Park, H., Woo, E. K., & Lee, K. Y. (2014). Ionically cross-linkable hyaluronate-based hydrogels for injectable cell delivery. *Journal of Controlled Release*, *196*, 146–153. https://doi.org/10.1016/j.jconrel.2014.10.008

Passipieri, J. A., Baker, H. B., Siriwardane, M., Ellenburg, M. D., Vadhavkar, M., Saul, J. M., Tomblyn, S., Burnett, L., & Christ, G. J. (2017). Keratin Hydrogel Enhances *In Vivo* Skeletal Muscle Function in a Rat Model of Volumetric Muscle Loss. *Tissue Engineering Part A*, *23*(11–12), 556–571. https://doi.org/10.1089/ten.tea.2016.0458

Pathak, A., & Kumar, S. (2011). Biophysical regulation of tumor cell invasion: Moving beyond matrix stiffness. *Integrative Biology*, *3*(4), 267–278. https://doi.org/10.1039/c0ib00095g

Patterson, J., & Hubbell, J. A. (2010). Enhanced proteolytic degradation of molecularly engineered PEG hydrogels in response to MMP-1 and MMP-2. *Biomaterials*, *31*(30), 7836–7845. https://doi.org/10.1016/j.biomaterials.2010.06.061

Paul, K., Darzi, S., McPhee, G., Del Borgo, M. P., Werkmeister, J. A., Gargett, C. E., & Mukherjee, S. (2019). 3D bioprinted endometrial stem cells on melt electrospun poly ε-caprolactone mesh for pelvic floor application promote anti-inflammatory responses in mice. *Acta Biomaterialia*, *97*, 162–176. https://doi.org/10.1016/j.actbio.2019.08.003

Paul, K., Darzi, S., Werkmeister, J. A., Gargett, C. E., & Mukherjee, S. (2020). Emerging nano/micro-structured degradable polymeric meshes for pelvic floor reconstruction. *Nanomaterials*, *10*(6). https://doi.org/10.3390/nano10061120

Pedersen, J. A., & Swartz, M. A. (2005). Mechanobiology in the third dimension. *Annals of Biomedical Engineering*, *33*(11), 1469–1490. https://doi.org/10.1007/s10439-005-8159-4

Peña, E., Calvo, B., Martínez, M. A., Martins, P., Mascarenhas, T., Jorge, R. M. N., Ferreira, A., & Doblaré, M. (2010). Experimental study and constitutive modeling of the viscoelastic mechanical properties of the human prolapsed vaginal tissue. *Biomechanics and Modeling in Mechanobiology*, *9*(1), 35–44. https://doi.org/10.1007/s10237-009-0157-2

Place, E. S., Evans, N. D., & Stevens, M. M. (2009). Complexity in biomaterials for tissue engineering. *Nature Materials*, *8*(6), 457–470. https://doi.org/10.1038/nmat2441

Pollot, B. E., & Corona, B. T. (2016). Volumetric Muscle Loss. In M. Kyba (Ed.), *Skeletal Muscle Regeneration in the Mouse: Methods and Protocols* (Vol. 1460, pp. 19–31). Springer. https://doi.org/10.1007/978-1-4939-3810-0

Prestwich, G. D., Luo, Y., Ziebell, M. R., Vercruysse, K. P., Kirker, K. R., & MacMaster, J. S. (2000). Chemically modified hyaluronan: new biomaterials and probes for cell biology. *New Frontiers in Medical Sciences Redefining Hyaluronan*, *1196*, 181-194 372.

Rajagopal, K., & Schneider, J. P. (2004). Self-assembling peptides and proteins for nanotechnological applications. *Current Opinion in Structural Biology*, *14*(4), 480–486. https://doi.org/10.1016/j.sbi.2004.06.006

Rao, L., Qian, Y., Khodabukus, A., Ribar, T., & Bursac, N. (2018). Engineering human pluripotent stem cells into a functional skeletal muscle tissue. *Nature Communications*, *9*(1), 1–12. https://doi.org/10.1038/s41467-017-02636-4

Raucci, M. G., D'Amora, U., Ronca, A., & Ambrosio, L. (2020). Injectable Functional Biomaterials for Minimally Invasive Surgery. *Advanced Healthcare Materials*, *9*(13), 1–20. https://doi.org/10.1002/adhm.202000349

Reisenauer, C., Shiozawa, T., Oppitz, M., Busch, C., Kirschniak, A., Fehm, T., & Drews, U. (2008). The role of smooth muscle in the pathogenesis of pelvic organ prolapse - An immunohistochemical and morphometric analysis of the cervical third of the uterosacral ligament. *International Urogynecology Journal*, *19*(3), 383–389. https://doi.org/10.1007/s00192-007-0447-0

Riley, L., Schirmer, L., & Segura, T. (2019). Granular hydrogels: emergent properties of jammed hydrogel microparticles and their applications in tissue repair and regeneration. *Current Opinion in Biotechnology*, *60*, 1–8. https://doi.org/10.1016/j.copbio.2018.11.001

Robinson, J., Shikanov, A., & Harley, B. (2020). Special Issue on Tissue Engineering for Women's Health. *Tissue Engineering - Part A*, *26*(13 and 14), 685–687. https://doi.org/10.1089/ten.tea.2020.29017.jro

Rodell, C. B., Kaminski, A. L., & Burdick, J. A. (2013). Rational design of network properties in guest-host assembled and shear-thinning hyaluronic acid hydrogels. *Biomacromolecules*, *14*(11), 4125–4134. https://doi.org/10.1021/bm401280z

Rodell, C. B., MacArthur, J. W., Dorsey, S. M., Wade, R. J., Wang, L. L., Woo, Y. J., & Burdick, J. A. (2015). Shear-thinning supramolecular hydrogels with secondary autonomous covalent crosslinking to modulate viscoelastic properties in vivo. *Advanced Functional Materials*, *25*(4), 636–644. https://doi.org/10.1002/adfm.201403550

Rose, J. C., & De Laporte, L. (2018). Hierarchical Design of Tissue Regenerative Constructs. *Advanced Healthcare Materials*, *7*(6), 1–31. https://doi.org/10.1002/adhm.201701067

Rosso, F., Giordano, A., Barbarisi, M., & Barbarisi, A. (2004). From Cell-ECM Interactions to Tissue Engineering. *Journal of Cellular Physiology*, *199*(2), 174–180. https://doi.org/10.1002/jcp.10471

Samuelsson, E. C., Victor, F. T. A., Tibblin, G., & Svardsudd, K. F. (1999). Signs of genital prolapse in a Swedish population of women 20 to 59 years of age and possible related

factors. *American Journal of Obstetrics and Gynecology*, *180*(2), 299–305. https://doi.org/10.1016/S0002-9378(99)70203-6

Scott, J. E. (1995). Extracellular matrix, supramolecular organisation and shape. *J. Anat*, *187*, 259–269. https://doi.org/10.1016/0277-9536(83)90357-x

Shikanov, A., Xu, M., Woodruff, T. K., & Shea, L. D. (2009). Interpenetrating fibrin-alginate matrices for in vitro ovarian follicle development. *Biomaterials*, *30*(29), 5476–5485. https://doi.org/10.1016/j.biomaterials.2009.06.054

Shynlova, O., Bortolini, M. A. T., & Alarab, M. (2013). Genes responsible for vaginal extracellular matrix metabolism are modulated by women's reproductive cycle and menopause. *International Braz j Urol : Official Journal of the Brazilian Society of Urology*, *39*(2), 257–267. https://doi.org/10.1590/s1677-5538.ibju.2013.02.15

Siddiqui, N. Y., Grimes, C. L., Casiano, E. R., Abed, H. T., Jeppson, P. C., Olivera, C. K., Sanses, T. V., Steinberg, A. C., South, M. M., Balk, E. M., & Sung, V. W. (2015). Mesh Sacrocolpopexy Compared With Native Tissue Vaginal Repair. *Obstetrics & Gynecology*, *125*(1), 44–55. https://doi.org/10.1097/aog.0000000000000570

Sisso, A. M., Boit, M. O., & DeForest, C. A. (2020). Self-healing injectable gelatin hydrogels for localized therapeutic cell delivery. *Journal of Biomedical Materials Research - Part A*, *108*(5), 1112–1121. https://doi.org/10.1002/jbm.a.36886

Slaughter, B. V., Khurshid, S. S., Fisher, O. Z., Khademhosseini, A., & Peppas, N. A. (2009). Hydrogels in Regenerative Medicine. *Handbook of Polymer Applications in Medicine and Medical Devices*, 279–302. https://doi.org/10.1016/B978-0-323-22805-3.00012-8

Smeds, K. A., & Grinstaff, M. W. (2001). Photocrosslinkable polysaccharides for in situ hydrogel formation. *Journal of Biomedical Materials Research*, *54*(1), 115–121. https://doi.org/10.1002/1097-4636(200101)54:1<115::AID-JBM14>3.0.CO;2-Q

Smith, K., & Christ, G. J. (2019). *Incorporation of In Vitro Double Seeding for Enhanced Development of Tissue Engineered Skeletal Muscle Implants* (Issue December) [University of Virginia]. https://libraetd.lib.virginia.edu/public_view/tt44pn43m

Spencer, R. J., Rice, L. W., Ye, C., Woo, K., & Uppal, S. (2019). Disparities in the allocation of research funding to gynecologic cancers by Funding to Lethality scores. *Gynecologic Oncology*, *152*(1), 106–111. https://doi.org/10.1016/j.ygyno.2018.10.021

Spicer, C. D. (2020). Hydrogel scaffolds for tissue engineering: The importance of polymer choice. *Polymer Chemistry*, *11*(2), 184–219. https://doi.org/10.1039/c9py01021a

Subak, L. L., Waetjen, L. E., Van Den Eeden, S., Thom, D. H., Vittinghoff, E., & Brown, J. S. (2001). Cost of pelvic organ prolapse surgery in the United States. *Obstetrics and Gynecology*, *98*(4), 646–651. https://doi.org/10.1016/S0029-7844(01)01472-7

Sundararaghavan, H. G., & Burdick, J. A. (2011). Gradients with depth in electrospun fibrous scaffolds for directed cell behavior. *Biomacromolecules*, *12*(6), 2344–2350. https://doi.org/10.1021/bm200415g

Sung, V. W., Washington, B., & Raker, C. A. (2010). Costs of ambulatory care related to female

pelvic floor disorders in the United States. *American Journal of Obstetrics and Gynecology*, *202*(5), 483.e1-483.e4. https://doi.org/10.1016/j.ajog.2010.01.015

Tamayol, A., Akbari, M., Annabi, N., Paul, A., Khademhosseini, A., & Juncker, D. (2013). Fiber-based tissue engineering: Progress, challenges, and opportunities. *Biotechnology Advances*, *31*(5), 669–687. https://doi.org/10.1016/j.biotechadv.2012.11.007

Tan, A. R., Ifkovits, J. L., Baker, B. M., Brey, D. M., Mauck, R. L., & Burdick, J. A. (2008). Electrospinning of photocrosslinked and degradable fibrous scaffolds. *Journal of Biomedical Materials Research - Part A*, *87*(4), 1034–1043. https://doi.org/10.1002/jbm.a.31853

Tan, T., Cholewa, N. M., Case, S. W., & De Vita, R. (2016). Micro-structural and Biaxial Creep Properties of the Swine Uterosacral–Cardinal Ligament Complex. *Annals of Biomedical Engineering*, *44*(11), 3225–3237. https://doi.org/10.1007/s10439-016-1661-z

Tan, T., Davis, F. M., Gruber, D. D., Massengill, J. C., Robertson, J. L., & De Vita, R. (2015). Histo-mechanical properties of the swine cardinal and uterosacral ligaments. *Journal of the Mechanical Behavior of Biomedical Materials*, *42*, 129–137. https://doi.org/10.1016/j.jmbbm.2014.11.018

Tang, J. D., Roloson, E. B., Amelung, C. D., & Lampe, K. J. (2019). Rapidly Assembling Pentapeptides for Injectable Delivery (RAPID) Hydrogels as Cytoprotective Cell Carriers. *ACS Biomaterials Science and Engineering*, *5*(5), 2117–2121. https://doi.org/10.1021/acsbiomaterials.9b00389

Teo, W. E., & Ramakrishna, S. (2006). A review on electrospinning design and nanofibre assemblies. *Nanotechnology*, *17*(14). https://doi.org/10.1088/0957-4484/17/14/R01

Theocharis, A. D., Skandalis, S. S., Gialeli, C., & Karamanos, N. K. (2016). Extracellular matrix structure. *Advanced Drug Delivery Reviews*, *97*, 4–27. https://doi.org/10.1016/j.addr.2015.11.001

Tibbitt, M. W., & Anseth, K. S. (2009). Hydrogels as extracellular matrix mimics for 3D cell culture. *Biotechnology and Bioengineering*, *103*(4), 655–663. https://doi.org/10.1002/bit.22361

Tomasek, J. J., Gabbiani, G., Hinz, B., Chaponnier, C., & Brown, R. A. (2002). Myofibroblasts and mechano-regulation of connective tissue remodelling. *Nature Reviews Molecular Cell Biology*, *3*(5), 349–363. https://doi.org/10.1038/nrm809

Ushiki, T. (2002). Collagen Fibers, Reticular Fibers and Elastic Fibers. A Comprehensive Understanding from a Morphological Viewpoint. *Arch. Histol. Cytol.*, *65*(2), 109–126. https://doi.org/10.1679/aohc.65.109

Vashaghian, M., Zaat, S. J., Smit, T. H., & Roovers, J. P. (2018). Biomimetic implants for pelvic floor repair. *Neurourology and Urodynamics*, *37*(2), 566–580. https://doi.org/10.1002/nau.23367

Vasita, R., & Katti, D. S. (2006). Nanofibers and their applications in tissue engineering. *International Journal of Nanomedicine*, *1*(1), 15–30. https://doi.org/10.2147/nano.2006.1.1.15

Velez, L. M., Seldin, M., & Motta, A. B. (2021). Inflammation and reproductive function in women with polycystic ovary syndrome. *Biology of Reproduction*, *104*(6), 1205–1217. https://doi.org/10.1093/biolre/ioab050

Viergever, R. F., & Hendriks, T. C. C. (2016). The 10 largest public and philanthropic funders of health research in the world : what they fund and how they distribute their funds. *Health Research Policy and Systems*, *14*(12). https://doi.org/10.1186/s12961-015-0074-z

Vodegel, E. V., Kastelein, A. W., Jansen, C. H. J. R., Limpens, J., Zwolsman, S. E., Roovers, J. P. W. R., Hooijmans, C. R., & Guler, Z. (2022). The effects of oestrogen on vaginal wound healing: A systematic review and meta-analysis. *Neurourology and Urodynamics*, *41*(1), 115–126. https://doi.org/10.1002/nau.24819

Wade, R. J., Bassin, E. J., Gramlich, W. M., & Burdick, J. A. (2015). Nanofibrous hydrogels with spatially patterned biochemical signals to control cell behavior. *Advanced Materials*, *27*(8), 1356–1362. https://doi.org/10.1002/adma.201404993

Wade, R. J., Bassin, E. J., Rodell, C. B., & Burdick, J. A. (2015). Protease-degradable electrospun fibrous hydrogels. *Nature Communications*, *6*, 6639. https://doi.org/10.1038/ncomms7639

Wade, R. J., & Burdick, J. A. (2012). Engineering ECM signals into biomaterials. *Materials Today*, *15*(10), 454–459. https://doi.org/10.1016/S1369-7021(12)70197-9

Wahls, W. P. (2016). Biases in grant proposal success rates , funding rates and award sizes affect the geographical distribution of funding for biomedical research. *PeerJ*, *4*, e1917. https://doi.org/10.7717/peerj.1917

Walker, C. J., Schroeder, M. E., Aguado, B. A., Anseth, K. S., & Leinwand, L. A. (2021). Anseth - Review Article: Matters of the heart : Cellular sex differences. *Journal of Molecular and Cellular Cardiology*, *160*, 42–55. https://doi.org/10.1016/j.yjmcc.2021.04.010

Wang, L., Neumann, M., Fu, T., Li, W., Cheng, X., & Su, B. L. (2018). Porous and responsive hydrogels for cell therapy. *Current Opinion in Colloid and Interface Science*, *38*, 135–157. https://doi.org/10.1016/j.cocis.2018.10.010

Wang, Y., Cao, Z., Cheng, R., Qin, M., Zhang, D., Deng, L., Chen, X., & Cui, W. (2019). Immunomodulated electrospun fibrous scaffolds via bFGF camouflage for pelvic regeneration. *Applied Materials Today*, *15*, 570–581. https://doi.org/10.1016/j.apmt.2019.04.005

Whooley, J., Cunnane, E. M., Do Amaral, R., Joyce, M., MacCraith, E., Flood, H. D., O'Brien, F. J., & Davis, N. F. (2020). Stress urinary incontinence and pelvic organ prolapse: Biologic graft materials revisited. *Tissue Engineering - Part B: Reviews*, *26*(5), 475–483. https://doi.org/10.1089/ten.teb.2020.0024

Wolf, K. J., & Kumar, S. (2019). Hyaluronic Acid: Incorporating the Bio into the Material. *ACS Biomaterials Science and Engineering*, *5*(8), 3753–3765. https://doi.org/10.1021/acsbiomaterials.8b01268

Woo, S. L., Almarza, A. J., Karaoglu, S., & Abramowitch, S. D. (2007). Functional Tissue

Engineering of Ligament and Tendon Injuries. In A. Atala, R. Lanza, J. Thomson, & R. Nerem (Eds.), *Principles of Regenerative Medicine* (3rd ed., pp. 1206–1231). Elsevier Science & Technology.

Wu, J. M., Kawasaki, A., Hundley, A. F., Dieter, A. A., Myers, E. R., & Sung, V. W. (2011). Predicting the number of women who will undergo incontinence and prolapse surgery, 2010 to 2050. *American Journal of Obstetrics and Gynecology*, *205*(3), 230.e1-230.e5. https://doi.org/10.1016/j.ajog.2011.03.046

Wu, J. M., Matthews, C. A., Conover, M. M., Pate, V., & Jonsson Funk, M. (2014). Lifetime risk of stress urinary incontinence or pelvic organ prolapse surgery. *Obstetrics and Gynecology*, *123*(6), 1201–1206. https://doi.org/10.1097/AOG.0000000000000286

Wu, X., Jia, Y. Y., Sun, X., & Wang, J. (2020). Tissue engineering in female pelvic floor reconstruction. *Engineering in Life Sciences*, *20*(7), 275–286. https://doi.org/10.1002/elsc.202000003

Xie, J., Bao, M., Bruekers, S. M. C., & Huck, W. T. S. (2017). Collagen Gels with Different Fibrillar Microarchitectures Elicit Different Cellular Responses. *ACS Applied Materials and Interfaces*, *9*(23), 19630–19637. https://doi.org/10.1021/acsami.7b03883

Yoeli-Bik, R., Lengyel, E., Mills, K. A., & Abramowicz, J. S. (2022). Ovarian Masses: The Value of Acoustic Shadowing on Ultrasound Examination. *Journal of Ultrasound in Medicine*, 1–11. https://doi.org/10.1002/jum.16100

Yoshida, K., Jayyosi, C., Lee, N., Mahendroo, M., & Myers, K. M. (2019). Mechanics of cervical remodelling: Insights from rodent models of pregnancy. *Interface Focus*, *9*(5). https://doi.org/10.1098/rsfs.2019.0026

Yu, L., & Ding, J. (2008). Injectable hydrogels as unique biomedical materials. *Chem. Soc. Rev.*, 1473–1481. https://doi.org/10.1039/b713009k

Yuan, M., Hu, M., Dai, F., Fan, Y., Deng, Z., Deng, H., & Cheng, Y. (2021). Application of synthetic and natural polymers in surgical mesh for pelvic floor reconstruction. *Materials and Design*, *209*, 109984. https://doi.org/10.1016/j.matdes.2021.109984

Zhang, J., & Ma, P. X. (2013). Cyclodextrin-based supramolecular systems for drug delivery: Recent progress and future perspective. *Advanced Drug Delivery Reviews*, *65*(9), 1215–1233. https://doi.org/10.1016/j.addr.2013.05.001

Zhang, X., Shi, X., Gautrot, J. E., & Peijs, T. (2021). Nanoengineered electrospun fibers and their biomedical applications: a review. *Nanocomposites*, *7*(1), 1–34. https://doi.org/10.1080/20550324.2020.1857121